DESIGN OF A QUANTITATIVE MICROSCOPE FOR IMAGE CYTOMETRY USING A SOLID STATE DETECTOR IN THE PRIMARY IMAGE PLANE

by

Bruno Jaggi, P.Eng.

B.A.Sc. University of British Columbia

A THESIS SUBMITTED IN PARTIAL FULFILLMENT

OF THE REQUIREMENTS FOR THE DEGREE OF

MASTER OF APPLIED SCIENCE

in the School

of

Engineering Science

SIMON FRASER UNIVERSITY

June 1989

APPROVAL

Name: Bruno Jaggi, P.Eng.

Degree: Master of Applied Science

Title of Thesis:

Design of a Quantitative Microscope for Image Cytometry using a Solid State Detector in the Primary Image Plane

Examining Committee:

Chairman: Dr. Vladimir Cuperman

Dr. Jamal Deen
Assistant Professor, Senior Supervisor

Dr. Branko Palcic
Head, Cancer Imaging, Cancer Control Agency of B.C.

Associate Professor, Pathology and Physics,
University of British Columbia

Adjunct Professor, School of Engineering Science
Simon Fraser University

Dr. Jim Cavers, P.Eng.
Professor

Dr. Andrew Rawicz
Associate Professor, External Examiner

Date Approved: 3 Aug. 93

PARTIAL COPYRIGHT LICENSE

I hereby grant to Simon Fraser University the right to lend my thesis, project or extended essay (the title of which is shown below) to users of the Simon Fraser University Library, and to make partial or single copies only for such users or in response to a request from the library of any other university, or other educational institution, on its own behalf or for one of its users. I further agree that permission for multiple copying of this work for scholarly purposes may be granted by me or the Dean of Graduate Studies. It is understood that copying or publication of this work for financial gain shall not be allowed without my written permission.

Title of Thesis/Project/Extended Essay

Design of a Quantitative Microscope for Image Cytometry Using a Solid State Detector in the Primary Image Plane

Author: _____
(signature)

Bruno Jaggi
(name)

9 Aug. 99
(date)

ABSTRACT

The acquisition of accurate, high resolution microscopic images with a wide field of view is a crucial aspect in image cytometry applications. An example of this is the detection of early cancers and premalignant cells such as dysplasia of the cervix. For that purpose, a unique, visible light, quantitative microscope was developed that uses a high density solid state detector positioned in the primary image plane of an objective lens. The essence of this design is the elimination of multiple lens systems used in compound visible light microscopes, as well as the use of a large area, charge-coupled device (CCD). The CCD, together with the objective lens and electronic circuits, optimizes conditions for quantitative measurements in image cytometry.

Using Koehler illumination, light is transmitted through the specimen and focussed by a single diffraction-limited, ultrawide, flat field objective lens. The objective magnifies and projects the image onto a 1320 x 1035 picture element CCD with individual detector size of 6.8 μm x 6.8 μm. The signals are directly digitized to 10 bits and mapped 1:1 into a large frame memory at a rate of up to 10 Mbytes/s. The full digital image is continuously displayed at a rate of 80 Mbytes/s on a grey scale monitor. The image can also be accessed by a workstation for quantitative measurements and analysis.

The rationale for these specificiations and other design parameters as well as how the CCD characteristics relate to the optics and image display are discussed. Theoretical derivations and experimental data are presented. Of particular importance is the sampling density and resolving power of the detector which was

experimentally verified. A mathematical model to calculate the point-spread function of the optics and the detector as well as of the system is derived. These considerations and subsequent preliminary measurements on the implemented prototype of the microscope showed that a spatial resolution of 0.43 μm with a field of view of 150 μm x 120 μm and a photometric resolution of 500:1 was achieved. These performances are significantly better than that of the best quantitative microscopes available to date.

ACKNOWLEDGEMENT

This project could not have been carried out without the support and assistance of the engineering group of Cancer Imaging at the B.C. Cancer Research Centre. They all helped to create an environment that allowed me to design and develop the Solid State Microscope. In particular, I wish to acknowledge Mr. Steven Poon, P.Eng., for the software and Mr. Brian Pontifex, EIT, for the hardware support.

I also would like to acknowledge the work by the supervisory committee, Dr. Vladimir Cuperman, chairman of the examining committee; Dr. Jamal Deen, senior supervisor; Dr. Branko Palcic, supervisor; Dr. Jim Cavers, supervisor; Dr. Andrew Rawicz, external examiner; and Dr. Donald George, director of the School of Engineering Science at Simon Fraser University. A warm thank you goes to Dr. Branko Palcic who has been an excellent mentor. His unselfish effort during the conception, the design and development of the microscope is much appreciated.

The funding for this project was provided by Microscan Imaging & Instrumentation Inc., the National Research Council of Canada, National Cancer Institute of Canada, Medical Research Council of Canada, and by the Cancer Control Agency of British Columbia.

TABLE OF CONTENTS

LIST OF TABLES

LIST OF FIGURES

CHAPTER I: INTRODUCTION

1.1 Outline

This thesis concerns quantitative microscopy within the context of image cytometry. In particular, the thesis addresses the design of a new type of quantitative, visible light microscope, and its underlying theory. The new microscope will be referred to as the Solid State Microscope or the SSM. First, modern microscopy and image cytometry are discussed since they provide the frame of this work and since they define the requirements and limitations of the design. In Chapter 2, the concept of the SSM is presented; for that purpose the conventional compound microscope is described in some detail, followed by two chapters dealing with the design. Chapter 3 derives theoretical aspects and describes experimental data necessary to define and validate the design. Using system analysis based on the Fourier theory for optical and electrical systems, the SSM is mathematically described. In Chapter 4, technical aspects are discussed and a prototype implementation is presented. In the last Chapter critical aspects of the design are discussed, the status of the project is reviewed, future implications of this work are considered and the author's contribution is summarized.

The thesis is based on a patent entitled "Quantitative light microscope using a solid state detector in the primary image plane" (Jaggi, Deen, and Palcic 1989a), on a paper published in Optical Engineering entitled "The design of a solid state microscope" (Jaggi, Deen, and Palcic 1989b), on a SPIE Proceeding paper entitled "Development of a solid state microscope" (Jaggi and Palcic 1989a) and on an invited presentation on "Charge-coupled device requirements in the

design of the quantitative microscope for image cytometry" at the Electronic Imaging Conference (Jaggi and Palcic 1989b).

1.2 Background

The microscope is a tool used in science, engineering and medicine to image small objects not directly discernible by the human eye. The visualization of microscopic objects has brought about an immense contribution to the scientific knowledge and consequently, much effort has been spent in understanding and improving microscopy. Indeed, over the last four hundred years, the microscope has evolved from the first visible light, multiple lens, compound microscope developed by Zaccharias Janssen of Middleburg, The Netherlands (Bradbury 1968; Johnson 1983) to a mature technology as manifested by modern quantitative microscopes (Teague 1988; Pluta 1988). These microscopes make use of a large range of wavelengths and a number of image acquisition techniques. Despite this highly developed technology, microscopy continues to evolve as new scientific needs arise for the discovery of new structures in cell biology, medicine and material science. In fact, since the introduction of semiconductor technology, image processing computers and lasers, to name only the more important ones, a large number of investigations have focused on new approaches to microscopy. These include laser scanning, confocal, quantum limited, continuous-motion scanning, video-enhanced, near-field optical, acoustic, x-ray, electron, scanning tunneling and atomic force microscopy. The new developments aim to increase resolution, enlarge the microscope field, and speed up the acquisition of the microscope image data. However, most importantly, all of the new developments aim at quantitative microscopy which measures structures rather than simply

observe them. These improvements can be achieved using new image scanning techniques such as in confocal microscopy, by decreasing wavelength such as in x-ray microscopy, or through technological improvements in optics and transducers as is the case in video-enhanced microscopy. Despite much excitement in fundamentally new approaches such as scanning tunneling or near field optical microscopy which promise a spatial resolution improvement over conventional visible light microscopes of 1000 and 30 fold respectively, the visible light microscope is still one of the most used instruments in science. As a consequence, further research and development is being undertaken to improve this device in many laboratories. The demand for the visible light microscope stems from its ease of use, its flexibility, and non-obstructive imaging.

An interesting way to study modern microscopy is by considering the variables that limit its performance, i.e. its resolution, the field of view, the acquisition rate and the distortions. Based on wave theory, a fundamental limitation is the illuminating wavelength. It determines, together with the parameters of the microscope components, the highest spatial resolution. Spatial resolution is an important performance parameter and is defined as the resolving power to distinguish closely spaced objects (Royal Microscopical Society 1989). Another more technology related limitation is the scanning mechanism used to illuminate and/or acquire the image. There are three basic scanners: i) point by point scanners, ii) line scanners and iii) area scanners. Point by point scanners are more accurate, because of the elimination of stray light and isoplanatic non-uniformities (no change occurs in an object's shape within the imaging plane) in the optical system, but generally they are slower than line or area scanners. Yet

another major limitation is the imaging optics and transducer technology since these components, each with its own point spread function, distort the acquired image. Hence, illumination wavelength, together with the scanning mechanism, optics, and detector technology are the variables that are being explored in the new approaches to image acquisition in microscopy. The other performance parameters that requires definition is photometric resolution. Photometry in general evaluates the quantity of light measured by the eye or physical receptors. Photometric resolution is defined as the photometric contrast i.e. max (I_2/I_1) where I is intensity in lumen and the subscripts refer to different imaging areas (Royal Microscopical Society 1989). Photometric reduction is also defined as a measure of the signal-to-noise ratio at a low spatial frequency object and the degree of linearity between light intensity and signal output (Young 1983). Together with these definitions of resolution the limiting variables lend themselves to the description and the classification of modern microscopes.

1.3 Overview of New Approaches to Microscopy

The different approaches of the modern microscopy together with the underlying principles and limitations are discussed in this section. A summary of the state-of-the-art microscopes and their typical system parameters are shown in Table Ia/b. The conventional visible light microscope will be discussed separately in Sections 1.4, 1.5 and 2.1.

The Laser Scanning Microscope (LSM) is a single spot scanner, i.e. an image is formed by scanning the sample with a single laser illumination spot and by capturing its response. The scanning is either mechanical and is achieved by a precision microscope stage for scanning the sample (Van der Voort 1985; Brakenhoff, Blom and Barends 1979) or by

TYPICAL SYSTEM PARAMETERS / *TYPE OF MICROSCOPE*	spatial resolution	photometric resolution	field of view (typical)	wavelength, range, illumination mode	acquisition speed	applications, particularities	sample preparation, system flexibility, medium
Laser Scanning &Confocal Microscopy	x,y 0.25μm (1.4 x increase) z 0.5 μm	10 bits	512x512 pixels laser	400 nm to 700 nm	2 s/frame	-fluorescence, -sectioning, -high contrast	- non-destructive - flexible - air, oil
Quantum-Limited Imaging	x,y 3μm	6 bits	512x512 pixels	400 to 700 nm band limited epi-fluorescence	$^1/_{30}$ s/frame	-fluorescence, -real time, -high sensitivity	- non-destructive - flexible - air
Continuous-Motion Scanning	x,y 1 μm	8 bits	2000 pixels wide bands	400 to 700 nm bright field	> 1 ms/line	-screening, -fast scanning	- non-destructive - flexible
Video-enhanced Microscopy	25 nm single point	6 bits	512x512 pixels	400 to 700 nm DIC bright field	$^1/_{30}$ s/frame	-optimized contrast	- non-destructive - flexible - oil
X-Ray Microscope	x,y 10 nm	6 bits	256 by 256 pixels	2 GHz	5 min/frame	-experimental	- destructive - flexible
Acoustic Microscope	x,y 0.5 μm	10 bits	512x512 pixels	3 GHz	2.6 s/frame 10 μs/pixel	-penetration of opaque material, -high contrast, -experimental	- non-destructive - flexible - water, cryogenic

Table Ia: Overview and Specifications of Modern Microscopes (continued)

TYPICAL SYSTEM PARAMETERS / *TYPE OF MICROSCOPE*	spatial resolution	photometric resolution	field of view (typical)	wavelength, range, illumination mode	acquisition speed	applications, particularities	sample preparation, system flexibility, medium
Electron Microscope	x,y 3 Å (poor vertical resolution)	6 bits	512x512 pixels (CRT, film)	300 GHz	1 to 10 sec/ frame	high spatial resolution	- destructive - difficult - vacuum operated
Scanning Tunnelling Microscope (STM)	x,y 2.5 Å z 0.1 Å	gray scale corresponds to changes in tunnelling current	800x600 pixels (piezoelectric range)	10 Å	10 min/frame	-conductive surfaces required, -experimental	- non-destructive - difficult
Atomic Force Microscope (AFM)	x,y 5 Å	corresponds to changes in tunnelling current	800x600 pixels piezoelectric range	N/A	10 min/frame	-non-conductive surfaces possible -experimental	- non-destructive - difficult
Near Field Microscopy	x,y 50 nm theoretical 10 nm		512x512 pixel stage travel 7.5x7.5 μm	visible light	10 min/frame projected - 6 s/frame	- biological structures - semiconductors - experimental	- non-destructive - difficult

Table Ib: Overview and Specifications of Modern Microscopes

deflecting surfaces such as galvanometers (Ploem 1987; Wilke 1985). The image acquisition in such systems is slow, more than 2 s/frame, except in the case of the ultrafast laser scanner (Shoemaker et al. 1982) where a 24,000 to 48,000 rpm polygon scanner is used to deflect the beam resulting in image acquisition rate of 100 frames/s. The laser beam spot can be variable in size and adjusted to a minimum diameter of 0.5 μm. The resolution and the dimensions of the microscope field of view are equivalent to a conventional visible light microscope, i.e. a spatial resolution of 0.3 μm and a 512 x 512 picture element (pixel) frame. LSM is ideally suited for quantitative fluorescence measurements, since its high intensity point by point scanning laser minimizes fading and quenching of the fluorochromes, lowers the level of autofluorescence from the objective and sample, and achieves a photometric resolution of 10 bits. Three-dimensional structures can also be imaged as the LSM can be easily used in a confocal mode.

The principles of <u>Confocal Scanning Microscopes</u> (CSM) is that the specimen is illuminated one point at a time, as in LSM, and this same point is imaged precisely onto the transducer which acquires only light emitting from that same point (Kino, Corle and Xiao 1988; Amos, White and Fordham 1987; Wilson and Sheppard 1984). This principle where illumination and detection are confocal with each other is shown in figure 1. One point illumination and detection is achieved by placing a spatial filter in front of the light source (illumination pinhole) and the transducer (detector pinhole), respectively. The result is an image of high lateral resolution and with a very pronounced focal depth discrimination. The confocal mode eliminates most of the out-of-focus light and glare from other parts of the image. This is indicated in

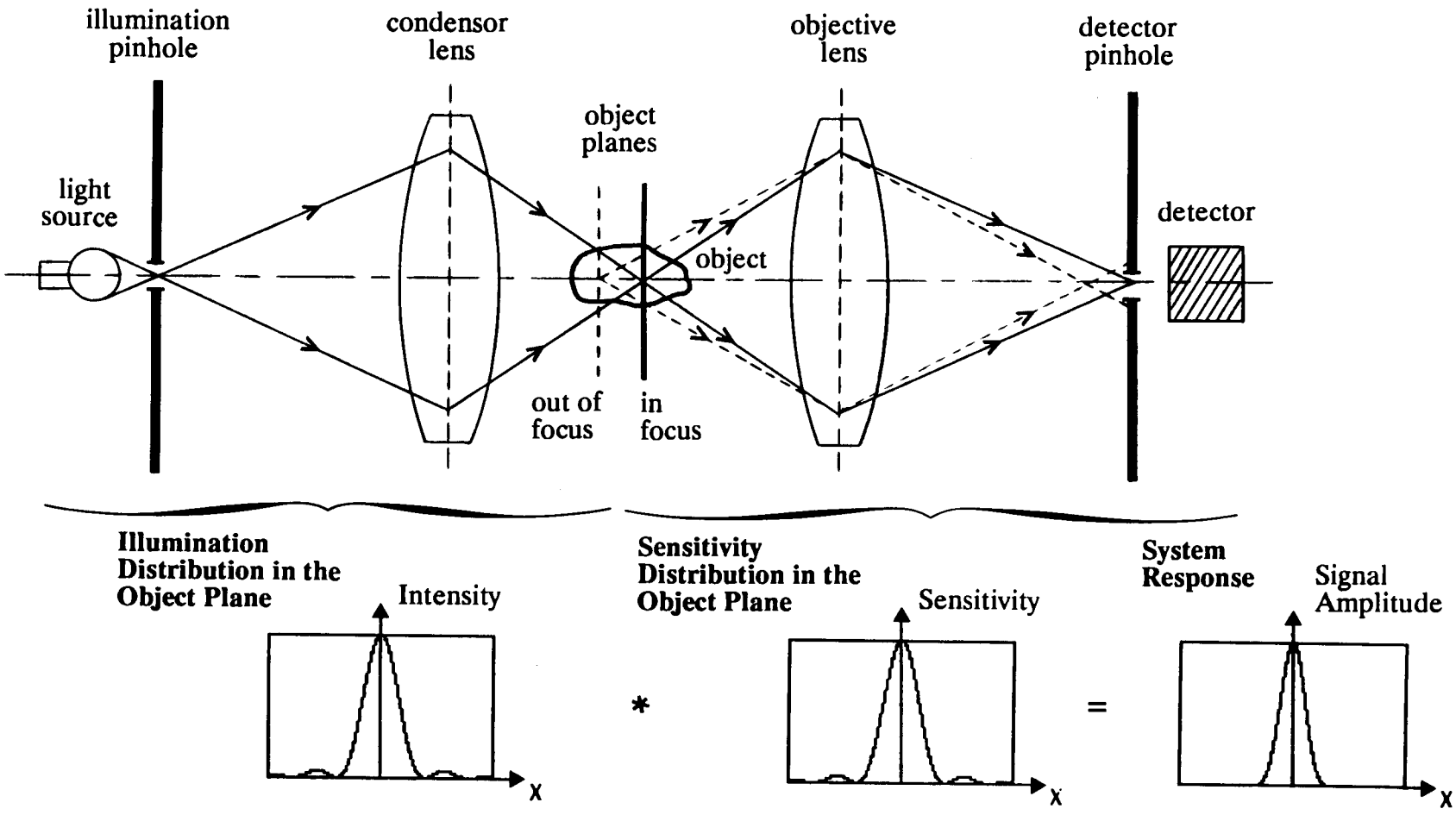

Figure 1: Principle of Confocal Microscopy.

figure 1 with the dashed line rays of light emanating from an out-of-focus plane. The high lateral resolution is improved because the side lobes of the diffraction pattern are eliminated. Expressed in mathematical terms, the system response is the product of the diffraction pattern due to the illumination system and the diffraction pattern due of the detection optics. These diffraction patterns can be represented as point spread functions (psf) shown for a rectangular aperture in figure 1 as intensity versus the spatial dimension x. If both point spread functions are approximated by a $\text{sinc}^2(x)$ function, then the system response is a $\text{sinc}^4(x)$ function resulting in a lateral resolution improvement of 1.4. Although improved by a factor 1.4, the maximum lateral resolution of 0.25 μm is limited; it is proportional to the wavelength and inversely proportional to the numerical aperture of the objective as in visible light microscopy. The illumination source is usually a laser, and is generally restricted to UV, visible light and near IR wavelength range. Since the diffraction side lobes are eliminated and one works with a single point, both coherent and incoherent light can be used. While in a conventional microscope there is no light fall-off when an object is defocused, the CSM has a marked fall-off and hence three-dimensional imaging is feasible. Its focal plane resolution (depth of focus) is inversely proportional to the square of the numerical aperture and is typically 0.5 μm. A field of view of 512 x 512 pixels with a photometric resolution of 10 bits can be achieved. Similar to LSM, the field is limited by the scanning mechanism which is in the form of a precision stage scanner facilitating acquisitions of larger fields. However, this scanning mechanism implies a possible registration error due to inaccuracies of the position of the illumination beam and detector plane scanning.

A number of different CSMs have been developed to scan confocal images by either moving the light source by means of scanning beam (Lasersharp MRC-500, Bio-Rad, England; Confocal Laser Scan Microscope, Carl Zeiss Inc., West Germany), moving the sample (e.g. Juang, Finzi and Bustamante 1988), or moving the pinholes. Yet another approach was developed in the tandem scanning microscope (TSM) where a large number of spatially separated points are illuminated and transduced simultaneously, making it possible to build a direct view, real-time confocal microscope image (Petran 1985).

The next three microscope technologies are based on conventional visible light microscopes, each optimizing a particular parameter, namely sensitivity, speed, and contrast. In Quantum-Limited Imaging (QLI), light sensitivity is maximized to detect low light level images (10^{-2} to 10^{-8} lux face plate illumination) which is necessary for fluorescence studies. The fluorescence light intensity (Section 1.4.1, equation 2 to 4) is limited by the excitation energy, the quantum efficiency of the fluorochrome, the concentration of the fluorochrome and the light loss in the optical system. These parameters generally cannot be controlled by the experimenter since an increase in excitation energy results in bleaching, the quantum efficiency is given by the compound whose type and concentration is limited by quenching and the experimental procedures. As for light losses, they depend on the microscope set-up which is determined by other considerations such as the required magnification and microscopy mode.

Traditionally, photomultipliers are used to detect fluorescence as they possess high sensitivity, excellent linearity, a high SNR and a short response time. However, the photomultiplier is a one pixel detector and does not provide spatial information. To acquire a low

light level two dimensional image, an image intensifier can be used. The principle underlying the operation of an image intensifier is based on the photo-electric effect. This conversion of photons into electrons is followed by a high gain of amplification and subsequent re-conversion of the photon-electron image into an optical image. If such a device has a photocathode as an input and a phosphor screen as an output then it is referred to as a GEN 1 type device. These devices have a typical gain of 45,000 for a single stage. An example of such a device is the widely used S20 extended red photocathode and P20 green output phosphor screen. The image of a GEN 1 can be captured by a video-based camera for further processing and display from the phosphor screen. For higher end devices, the image intensifier and video detector are optically coupled with an optical fibre.

A further development of the image intensifier is the second generation (GEN 2) microchannel plate (MCP), which provides electronic amplification (typical gain of 10,000 to 30,000 for a single stage) within the image intensifier. The MCP is a secondary electron multiplier like the photomultiplier, but consists of several million glass capillaries (channels) within a thin silicon-based wafer. Each channel acts as an independent electron multiplier since the inner walls of these channels are coated with a resistant secondary electron-emission material which is electrically coupled to the input and output electrodes of the channel. The GEN 2 image intensifiers achieve a spatial resolution of approximately 18 lp/mm (line pairs per mm) at 10^{-6} lux face plate illumination. They are much smaller and largely overcome the loss of gain and noise contribution inherent in multiple photocathode and phosphor outputs (Wick 1987). Recently, GEN 3 type MCP image intensifiers, using a gallium arsenide (GaAs) photocathode, have

been designed to provide amplifications of up to 30,000 with a maximum red sensitivity. This higher red sensitivity is due to the lower band gap energy of GaAs compared to the silicon (Si) of the GEN 2.

In image cytometry, image intensifiers of single stage type are used (e.g. Jaggi et al. 1988) and the two stage image intensifiers are used in the Hammamatsu photon counting system (e.g. C1966-20, Hayakawa et al. 1985). These are only two examples of many quantum limited imaging systems using an image intensifier. Since, from a light sensitivity point of view all systems are essentially limited by the detector, many researchers and commercial image cytometry companies have replaced their microscope video cameras with a low light level camera for fluorescence work. For applications at higher face plate illumination (10^{-3} lux) cameras with higher spatial resolution (e.g. 36 lp/mm) are used such as the silicon intensified target (SIT) cameras or the intensified silicon-intensifier target (ISIT) cameras (e.g. Dage-MTI 66 series; Cohu Inc., 5000 series).

Continuous-Motion Scanning (CMS) provides a method for quantitative analysis where speed is optimized. Such systems are ideal for screening applications where a large number of stained, slide-mounted cells, are imaged for medical diagnostic purposes (Tucker et al., 1987; Bengsston et al., 1983). Continuous-motion imaging has also been used to scan large tissue culture flasks to detect and recognize live cells (Jaggi, Poon and Palcic 1986; Palcic, Jaggi and Nordin 1987; Palcic and Jaggi 1989). For the latter, a special device was designed and developed, the Dynamic Microscope Image Processing Scanner (DMIPS Cell Analyzer); the scanning method consists of using a linear scanner in one direction and moving a precision microscope stage in the other. Hence, large areas can be scanned in a continuous motion. The line

scanner is typically a linear charge-transfer device operated at a millisecond integration time or less. The basic operating cycle consists of integrating an image line, transferring the image line to a digital signal processor, processing the one-dimensional image, and then the cycle repeats. Such a cycle is completed within approximately a millisecond so that the motion of the system appears continuous. Continuous-motion scanning systems project the image onto the line array using a compound microscope. However, in the system developed by Palcic and Jaggi, the optics had been modified such that the object, i.e. the live cell, becomes a non-ideal lens and is part of the lens system. By doing so, this "lens effect" generates a characteristic signal or signature, to facilitate the recognition of live cells.

Continuous-motion scanning provides a large degree of scanning flexibility which is essential in scanning applications. Several different scanning techniques were studied: examples include continuous-motion scanning using time delay integration (TDI) to improve the SNR of the system and "selected area modes" using photodiode arrays or charge injection devices where only areas of interest within a 2-dimensional array are readout.

In the third method, called Video-Enhanced Microscopy (VEM), a conventional compound microscope is used to optimize contrast and the size of the smallest resolvable object (Allen 1981; Inoue 1987). Operating a microscope in the absorption mode, i.e. bright field transmittance microscopy, is not a very efficient way, since live cells are essentially transparent and do not absorb much light. Therefore, it is advantageous to modify the optics to optimize the signal of a live cell as has been done with the Cell Analyzer (Palcic et al. 1987) or alternatively to find a means by which to image the phase rather than

the magnitude of the optical signals. Video-enhanced microscopy using differential interference contrast (DIC) is using the latter approach. DIC optics offers both a continuous gray scale and a contrast-transfer function which accentuates high spatial frequencies. In DIC polarized light is produced. To achieve a fully illuminated aperture and supply enough light to nearly saturate the video tube, as is required by video-enhanced microscopy, critical illumination (Bradbury 1984) is used. The rationale for critical illumination is that the optics are inadequate to fill the front focal plane of the condenser with an in-focus image of an intense light source as it is required for Koehler illumination. The polarized light source optics is followed by a beam-splitter producing two beams of polarized light which are directed along different paths. The two paths are polarized along directions at right angles to one another, setting them out of phase. After one beam passes through the object and objective lens, a beam-combiner (Wollaston Prism) combines the two beams. This results in a signal indicating the phase shift between the two beams. The image produced by the analyzer from the DIC optics is projected onto a high resolution video tube camera where the gain is adjusted to optimize contrast. Although this method is not suitable for quantitative measurements, small single objects such as microtubules can be imaged even though the dimension of 25 nm diameter lies well below the resolving power of the optics (Schnapp 1986).

New and promising research has lead to the Near-Field Scanning Optical Microscope (NFSO) (Pohl 1988). The image is captured in the near-field resulting in far higher resolution compared to conventional visible light microscope. Three possible modes of operation have been demonstrated for near-field microscopy: the illumination, collection and reflection modes (Betzig et al. 1988). Conceptually, the illumination

mode is the easiest to understand. In this arrangement, an aperture with a sub-wavelength diameter is placed in the near-field with respect to the specimen. The specimen is illuminated on the opposite side with visible light. The aperture insures that the light transmitted is initially collimated such that it is independent of the wavelength. The illuminated aperture then acts as a light source (impulse of light) which dimensions, at least in the near-field, are not constrained by the limits of conventional far-field optics. To construct an image, the aperture of the illumination is scanned in a raster pattern while the objective and the detector acquires the image in the far-field. In this way, it is possible to achieve an image with the resolution determined by the illumination aperture size (Betzig et al. 1988). The key to this technique is to keep the sample within the near-field of the source of light, no further from the hole than about a half the diameter of the hole. The rationale is that once the light passes through the hole, it rapidly spreads out and no longer illuminates just one small part of the sample. However, very close to the hole, the spot of light will remain much less than one wavelength across. At the present time, spatial resolutions of 15 nm have been achieved and a theoretical limit of about 10 nm is predicted (Pool 1988).

Yet another approach is the Scanning Acoustic Microscope (SAM), (Briggs 1985) using GHz ultrasound waves. Such a microscope has recently been developed by Wild-Leitz, which together with several other commercial manufacturers make these devices commercially available. There are two advantages in using acoustic waves for producing microscopic images. The first is the ability of ultrasonic waves to penetrate materials that are opaque to visible light. The second represents the distinctive origin of the contrast due to mechanical

properties of the specimen. The acoustic microscope is a point by point scanner using a sapphire lens and a coupling fluid to focus the acoustic waves onto the sample. The reflected waves are then transduced and by scanning the object an image is acquired. The resolving power of the water-coupled instrument is somewhat lower than that of a high power light microscope, but it appears theoretically possible to produce ultrasound waves with the wavelengths comparable to, or even smaller than those of visible light. In that case, the resolution of the acoustic microscope with its excellent contrast will be as good or better than that of the conventional light microscope.

All optical microscopes employing visible light are limited by the wavelength of the visible light and by the optics. Therefore, with these microscopes a useful magnification factor of up to 1300X can be achieved. Larger magnification result in undesirable "empty magnification" (Spencer 1982). However, by changing the wavelength of the electromagnetic radiation, employing higher quantum energies, resolution power can be substantially improved. This, for example, is done in **X-Ray Microscopes** (**XRM**) (Trail and Byer 1988; Kirz and Rarback 1985) where an improvement over visible light microscopes of up to thirty times (maximum spatial resolution of 10 nm) can be achieved. However, x-rays are ionizing radiation with a wavelength of approximately 10 nm for "soft" and 0.1 nm for "hard" x-rays and generally harm the sample. At the present time no x-ray microscopes are commercially available.

Even higher energies particles can be used, i.e. electrons between 1-3 keV (100 to 300 KV tubes). The **Electron Microscope** (**EM**) (Chescoe and Goodhew 1984) achieves yet another thirty times higher resolution than x-ray microscopes (1000 times higher than visible light

microscopes). The electron microscope employs properties of the scattering of electrons as they pass through a particular type of a heavy metal stained specimen. There are two basic types of electron microscope. The conventional transmissions electron microscope measures only non-scattered electrons. Contrast is proportional to the ratio of unscattered electrons over scattered electrons. Operating at 0.04 Angstrom wavelength (λ [Angstrom] $\simeq$ 12/ {electron accelerating voltage[volts]}$^{1/2}$) magnification of up to 450,000X and resolving power of 3 Angstrom can be achieved. For lower spatial resolution images (50 to 100 Angstrom), a fine scanning electron beam is used where a product of electron scattering can be imaged in real-time. Electron microscopy is destructive to the samples and they must be placed in a vacuum in order to eliminate unwanted scattering of electrons by the atmosphere. The spatial resolution of the relatively new electron microscope technology in terms of wavelength approaches 100 * λ. In contrast, the best modern light microscopes, equipped with high power objectives, achieve a resolution of 0.5 * λ. The explanation for these differences lies in the optical imperfection of electron lenses and their low numerical aperture in comparison with glass lenses of the light microscopes. Nevertheless, electron microscopes are today's standard in high resolution microscopy and are widely used in engineering, science and medicine.

The Scanning Tunnelling Microscope (STM) and its cousin, the Atomic Force Microscope (AFM) are essentially mapping the topography of a surface with the highest resolution in both vertical and lateral directions (Binnig and Rohrer 1985). The principle of the scanning tunneling microscope is shown in figure 2. Typically, a very sharp tungsten tip which is biased with an appropriate tunnelling voltage

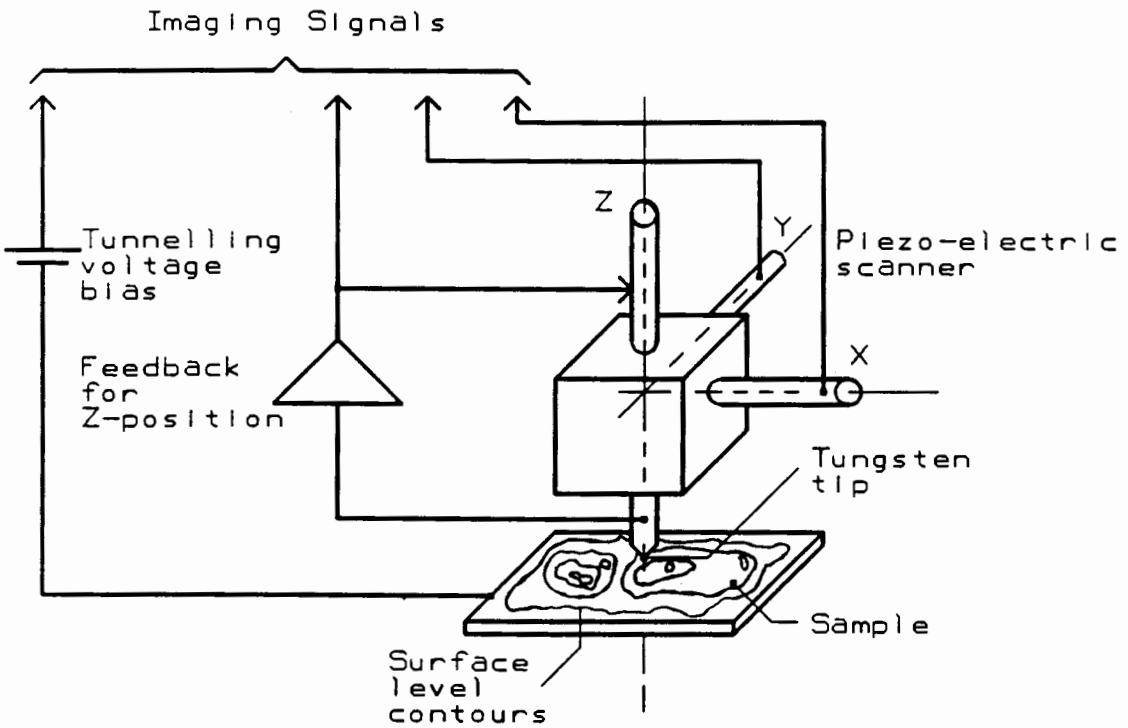

Figure 2: Principle of Scanning Tunneling Microscopy.

V producing a wavelength of 40 Angstrom) is mounted on a piezo electric x,y,z scanner. To induce quantum-mechanical tunnelling, the gap between the specimen and the tip is reduced to less than 10 Angstrom. The tunnelling current is exponentially proportional to the gap spacing and, therefore, very sensitive to changes in the gap spacing. Typically, variations of one Angstrom in the gap spacing can change the current by an order of magnitude. A feedback system detects the tunnelling current and drives the z (vertical) axis of the scanner so that the current and thus the gap spacing is maintained at a constant value. The mechanical scanning is performed on the x,y axis. At each x,y position, the computer records the displacement of the z-axis . This data represents the topography of the specimen surface and can be displayed as a two dimensional image. While the principle behind STM is simple, many critical points must be solved in order to achieve atomic resolution. The main considerations that must be taken into account in the construction of such a device are the manufacturing of sharp tunnelling tips, the suppression of vibration, the development of proper feedback control systems, the minimization of thermal drift, the machining of precision scanners and specimen positioners. With today's techniques, an axial depth resolution of about 0.01 nm has been achieved and the lateral resolution of about 0.25 nm (Park, Nogami and Quate 1988).

The AFM is very similar to the STM and, in fact, represents an evolution of the STM design. The only difference is that with the STM, the tunnelling occurs between the tip and the sample while with AFM, the tunnelling occurs between the back of the tip and the sensing electrode. The key to the operation of an AFM is the development of a system for sensing tracking forces that are small enough to avoid damaging the surface. The basic construction of the atomic force microscope consists

of a base plate which holds the piezo-electric x,y,z scanner and the sample. Above the specimen an enclosing compartment contains the tungsten tip which can be lowered toward the specimen. The interaction between the tip and the specimen is based on the interaction potential between atoms, as governed by the Van der Waals force. As a consequence of that force, the deflection of the tungsten tip changes. That change is measured and fed through the z position feedback loop. The AFM, unlike the STM, can resolve features of conducting and non-conducting surfaces down to the atomic level. Individual carbon atoms separated by 0.146 nm have been resolved on graphite using an experimental system (Marti et. al. 1988). Rows of molecules that are separated by 0.5 nm have also been resolved in an organic monolayer by the same group.

Applications: Depending on the objective of a particular research interest, the microscope requirements will differ emphasizing a particular microscope characteristics. For example, to answer some basic questions in biology related to "molecular motors" responsible for the movement in nerve cells of vessicle and other organelles along specialized tubular structures called microtubules, one would like to visualize, in real-time, individual and stained microtubules. For this Video-Enhanced Microscopy systems are most appropriate. If one is interested in rapidly scanning large areas at relatively low resolutions, Continuous-Motion Scanning systems are the best choice. In these two examples, the requirements on quantitative microscopy are entirely different from each other and if it was not for these specially developed microscopes, neither experimental system could be studied. Many other examples can be listed. These include those where cells are fixed on the microscope slide in a monolayer and then stained to study selected features of cellular components such as the mitochondria, the

DNA, the nuclear membrane, the proteins on the cellular membrane, nucleoli, etc. of a large number of cells. For these types of studies, the spatial requirements are greatly varied, ranging from 1 μm to the molecular sizes and hence, depending on the experimental objective, one must select the microscope most appropriate for the task ranging from ordinary visible light microscope to the atomic force microscope. One can find many other examples, however, the important point is, that the requirements vary widely and are dictated by the clinical and or biological question which one must answer.

1.4 Review of the State-of-the-Art Image Cytometry Systems

1.4.1 Cell Measurements

Image cytometry is concerned with studying images of cells and tissues, placed on a microscopy slide and stained with conventional or fluorescent stains. The images are acquired, digitized and processed. Image cytometry is used in the context of diagnostic and prognostic evaluation of cells as well as in basic cell biology research. It aims at quantitative characterization of cells. For most of the work since the introduction of image cytometry, fixed and stained cells have been used. More recently, image cytometry of live, unstained cells has been introduced (Palcic and Jaggi 1989) an approach which promises new insights in cell biology.

Cell measurements provide quantitative data of cell morphology such as size and shape, nuclear size and shape, amount and distribution of nuclear material in the nucleus, and features of nuclear and cytoplasmic contour. These are the parameters which have been used to classify cells in studies related to biology and medicine. To measure these features, cells must first be fixed and then stained. For

quantitative analysis, in analytical cytology, stoichiometric stains must be used where the amount of stain is proportional to the cellular material it is supposed to stain. Thus, the sample preparation and staining procedures are an important part of image cytometry since they determine the spatial, photometric and spectral properties of the input image. In this mode one measures the spatial distribution of absorption values as determined by individual pixels (picture elements) based on the Beer-Lambert absorption law:

$$I_{OUT} = I_{IN} * e^{-z * A} \qquad (1)$$

where I_{IN} and I_{OUT} are the light intensities projected onto and transmitted from the sample, * is used to represent multiplication, z represents the thickness of the absorbing material and A is a constant relating to the absorption (Mayall and Mendelsohn, 1979). The Beer-Lambert law states that a linear relationship exists between the optical density and the amount of chromophores in the field of view of the detector. The optical density is the logarithm of the flux of incident light over the flux of transmitted light. The chromophores, usually referred to as the stain, bind to DNA, protein, lipids or other macromolecules within a cell. The number of chromophores in stoichiometric stain is directly proportional to the amount of substance they bind to.

A second type of image cytometry measurements is the measurement of quantitative fluorescence (e.g. Taylor, Waggoner and Murphy 1986; Ploem and Tanke 1987). In some molecules light energy that has been absorbed excites the molecule to a higher electronic energy state and a higher vibrational state. Subsequent return to the ground state occurs with a loss of energy in the form of emitted light, that is

fluorescence. Compounds that exhibit this phenomenon are called fluorochromes. As a first approximation the fluorescence intensity, F, is equal to the quantum efficiency of the fluorochrome, Φ, and the difference between the absorption illumination light intensity, I_{IN}, and the transmittant light intensity, I_{OUT}:

$$F = \Phi * (I_{IN} - I_{OUT}) \qquad (2)$$

Using Beer-Lambert's Law, fluorescence intensity becomes:

$$F = \Phi * I_{IN} * (1 - e^{-z * A}) \qquad (3)$$

Assuming very small amounts of absorption, a reasonable assumption in the fluorescence context, and neglecting higher order terms of the series e^{-z*A}, fluorescence becomes directly proportional to the concentration of fluorochromes:

$$F = z * k * c * \Phi * I_{IN} \qquad (4)$$

since absorption A is equal to k*c where k is a constant and c is the concentration (Ploem and Tanke 1987). To obtain, for example, the total DNA content in a cell nucleus stained with DNA specific fluorochrome, the total fluorescence intensity must be measured. Using fluorescence, a single measurement of total signal over the cell nucleus is sufficient for the exact determination of DNA content. In absorption microscopy, fine scanning of the object is required to find optical density values of each pixel, which when added together, give the value of total amount of DNA. Without measuring local values, the "distributional error" will greatly distort the results in most cases (Vinter et al. 1985).

A particularly powerful method of using fluorescence is to couple chromophores to specific antibodies of different macromolecules,

receptors and other specific sites in cells. Using this technique cell surface, cell skeleton, intracellular pH, oxygen level, concentration of free Ca^{++} ions, and many other parameters have been measured (Taylor et al. 1985; Haugland 1989). Without doubt, fluorescent staining is the stain of the next decade and beyond for quantitative cell measurements.

Morphometric measurements of live, unstained cells are limited to size, shape and contour measurements. However, other features can be measured such as cell cycle time (the time between successive divisions), cell division time (process of the division itself), the amount of time which cells spend in a particular phase of the cell cycle, cell colony forming ability, cell movements and motility parameters, etc. This is possible because with live cells, repetitive measurements in time provide additional data, unavailable with fixed and stained cells. For example, cell colony forming ability, i.e. the ability of cells to divide indefinitely under optimal growth conditions, has most often been used to describe dose response curves of cells treated with a variety of physical and chemical agents. Cell behavioural properties such as cell motility parameters, cell to cell contact, cell shape and size changes as a function of time and/or treatment are other parameters which can be expressed in quantitative terms (Palcic and Jaggi 1989; Thurston, Jaggi and Palcic 1986; Spadinger, Poon and Palcic 1989). Depending on the nature of the study, one or more of the above endpoints can be measured.

It is theoretically possible to use live cells and stain their macromolecule without significantly perturbing their properties. For example, DNA of live cells can be stained with "viable" DNA stain such as Hoecht 33342 (Arndt and Jovin 1977). In this way, both nuclear features and cellular features of live cells can be measured at the same

time. If this technique is developed for image cytometry, it promises many new discoveries in cell biology.

1.4.2 Image Cytometry Systems

A typical quantitative image cytometry device is composed of a computer controlled microscope, an image transducer, signal conditioning device and a digitizer with a frame memory, an image processor and a host computer with peripheral/output devices, figure 3. The image acquisition of the microscopic objects is performed by the microscope with its transducer and has been discussed in section 1.3 in terms of their limitations and applications. All of those microscopes can be used as "magnifiers and transducers" for image cytometry systems. However, the conventional compound microscope remains the most widely used microscope and the one most often used in image cytometry systems because of its flexibility. Numerous image cytometry systems for image acquisition and processing have been designed, developed and built by research laboratory groups and are also now commercially available. Examples of such systems are the Magiscan (Joyce-Loebel), CAS-200 (Beckton-Dickinson), and the IBAS-2000 (Kontron/Zeiss). Typically, these systems are composed of a conventional compound microscope, a video-based detector, a 512 x 512 x 8 frame grabber, and one or more frame memories, dedicated image processors, input and output look-up tables, a corresponding gray level display, and a PC-based host computer. A summary of state-of-the-art image cytometry systems with their respective specifications is given in Table II. These systems have powerful interactive programmes and were developed to analyze images. All of the systems above are considered general purpose image processing systems where the microscope is optional; it is up to the

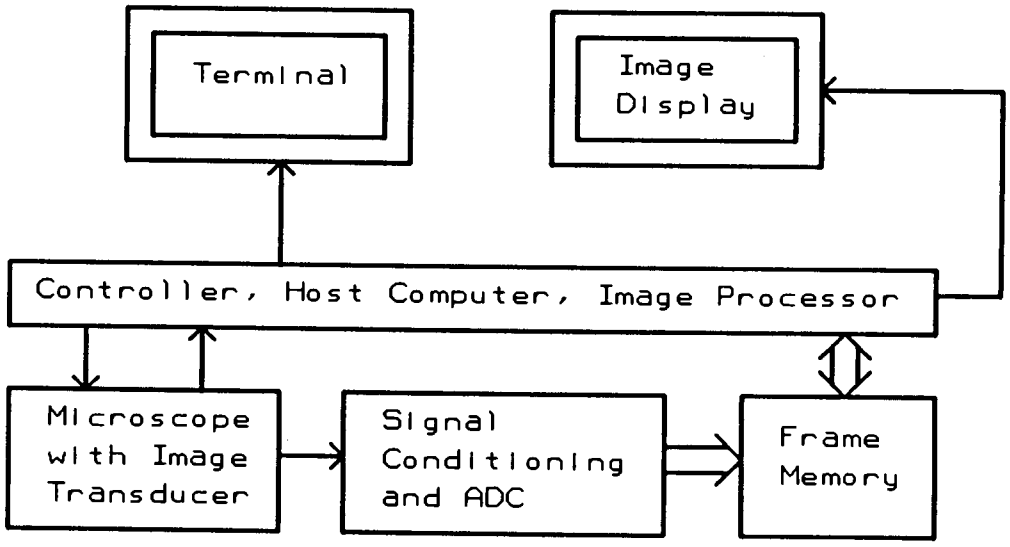

Figure 3: Conceptual Representation of an Image Cytometry System.

COMPANY *PRODUCT	DETECTOR	DIGITIZ-ATION	IMAGE MEMORY	HOST COMPUTER	PROCESSING HARDWARE	MECHANICAL SCANNING	MICROSCOPE	APPLICATION SOFTWARE	DESCRIPTION AND APPLICATIONS
Joyce-Loebl (Vickers) *Magiscan	1" chalnicon Options: RGB,SIT,ISIT MCP,CCD	6 bit	1024 X 1024 X 8 512 X 512 X 8 variable	IBM PC/AT	front end processor (opt.) 3 X 256 input LUTs 3 X 256 output LUTs variable overlays	X,Y autofocus	Microflex Microphot Optiphot (Nikon)	menu driven image analysis user programmable application specific	general imaging system cytogenetic analysis
Becton Dickinson Inc. *CAS 100/200	384 X 491 CCD camera fluorescent camera (opt.)	8 bit	384 x 485 x 8	IBM PC/AT	image processing board (256 X 256) 3 X 256 output LUTs	none	Diastar, Microstar IV (Reichart-Jung)	menu driven application specific	general purpose quantitative DNA analysis cell measurement automatic cell selection
Leitz (Bioquant) *BQ System IV	B/W or color video	8 bit	512 X 512 X 8	IBM PC/XT/AT	image processor (opt.) 8 color LUTs overlay (opt.)	X,Y	Ortholux, Orthoplan Diavert, Dialux (Leitz-Wild)	menu driven software modules application specific	automated image analysis particle counting bone morphometry
Kontron Bildanalyse (Zeiss) *IBAS-2000	CCIR,NTSC standard	8 bit	512 X 512 X 8 768 X 512 X 8 1024 X 1024 X 8 (opt.) expandable to 16MB	16/32 bit (opt.)	pipeline array processor real time arithmetic (opt.) 4 LUTs multiplier 1 bit overlay	X,Y autofocus	Axioplan, Axiophot, Universal (Zeiss)	menu driven routines	general purpose chromosome analysis autoradiography automated cell analysis
Cambridge Instruments *Quantimet 970	high precision video (tube opt.)	6 bit 8 bit (opt.)	1024 X 1024 X 1 512 X 512 X 4 256 X 256 X 8 4 Mbit expandable to 16Mbit	DEC LSI 11/73	chord parameter processor 16 bit ALU shading corrector LUT	X,Y autofocus	(Reichart-Jung)	softkey functions interactive programming system	general purpose
Hamamatsu *C1966-AVEC system	RS-170,NTSC video (tube opt.) intensifier (opt.)	8 bit	640 X 483 X 16 512 X 512 X 16 3 planes	(opt.) interfaces IEEE DEC	hardware processor	none	compound microscopes	keyboard instructions	photonic microscope system for enhancement of microscope images closed system
Milton Roy, Dynatech Artek, *Omnicom 3500	RS-170 standard	10 bit	512 X 512 X 1 512 X 512 X 8 (opt.) 3 planes	Data General Eclipse	grey level image processor (opt.) shading correction LUTs	X,Y autofocus	(Baucsh & Lomb or Nikon)	menu driven pseudolanguage user programmable	quantitative image processing system
Tracor Northern *TN-8502	512 X 480 TV camera	8 bit	512 X 512 X 16 1024 X 1024 X 16 (opt.) expandable to 8MB	68020 CPU	pipeline processor real time histogram barrel shifter LUT	X,Y autofocus	Optiphot, Microphot (Nikon)	menu driven user programmable	general purpose system automated analysis
Quantex Corp *QX-7	RS-170 standard	8 bit	640 X 480 X 12 expandable to 4 planes	IBM PC/AT or compatible	coprocessor pipeline processor 12 bit X 4K LUT float point processor (opt.) convolver (opt.)	none	compound microscopes	image processing libraries menu driven and function keys	general purpose

Table II: Overview of the State-of-the-Art Image Cytometry Systems, Summer, 1988. (From Palcic and Jaggi 1989, © Butterworth Publishers).

user to project the images, with whatever microscope, onto an RS170 video-based transducer, which is the input to all these systems. If these systems are used in conjunction with the conventional compound microscope, as is usually the case, neither the interface (Harms et al. 1986) nor the system components are optimal. The problems arise from the "mismatch" between microscope and video camera as well as from the "qualitative" nature of these components.

The need for rigorous quantitative data has dictated the search for optimization of spatial, photometric and spectral resolution. Spatial resolution is not only used to resolve fine structures, but it is critical for measurements of distances between these structures. Photometric resolution must respond linearly to illumination, provide good contrast and signal-to-noise ratio. At present, photometric resolution is often used to provide optimum conditions for the human observer employing a non-linear response. For quantitative microscopy, photometric and spatial resolutions combined must be optimized for measurements of texture features and to improve segmentation. A third variable, spectral resolution allows one to discriminate between wavelengths, to segment, and to measure both spatially and photometrically. Optimization of these parameters will result in minimized distortions, clearly separating qualitative and the quantitative systems.

1.5 Microscopy and Video Problems

The limitations of the conventional quantitative image cytometry devices are mainly due to the two key components of the image acquisition system: the microscope and the transducer. Both of these

image acquisition components are designed for human vision and not for computer vision.

Conventional Light Microscope: It has been pointed out by Young et al. (1982) that in the evolutionary process of the microscope, certain design constraints or constants became embodied in all visible light microscopes. These include tube lengths, binocular interpupillary distance, and definition of magnification. The constraints can and should be changed, together with reductions of aberrations and distortions, to find optimal solutions for quantitative microscopy. For example, the conventional light microscope is designed for human vision at 250 mm, the nearest distance for convenient human viewing. As such, it is also used to define the microscope magnification, M_{mic} (Pluta 1988):

$$M_{mic} = M_{obj} * M_{proj} = \frac{L_{OTL}}{F_{obj}} * \frac{250}{F_{proj}} \qquad (5)$$

where M_{obj} is the objective lens magnification, M_{proj} is the projection lens magnification, L_{OTL} is the optical tube length of the objective lens, F_{obj} is the focal distance of the objective and F_{proj} is the focal distance of the projection lens. These definitions impose many design constraints irrelevant for quantitative microscopy. Furthermore, the total magnification required for a particular detector is different from the human eye.

As a consequence of the above, some researchers have designed and developed their own optics to ensure accurate quantization and optimization. For example, Shoemaker et al. (1982) designed a new objective lens since they found that the objective lens is crucial to

the performance of the ultrafast laser scanning microscope as it determines in large part the parameters of other elements in the system. For their microscope, an ordinary microscope objective is not suitable and only imposes requirements, such as the definition of magnification, unnecessary for their design. Kirk (1987) studied aberration effects in optical measuring microscope. He determined their effects on image profile of narrow (approximately 2 μm) line objects by examining different microscope objectives. His results show that very few commercially available objective lenses are adequate for accurate measurements of dimensions near the limit of resolution of an optical microscope and that careful selection of the objective is required.

Video Transducer: The video transducer (Inoue 1986) is based on the TV broadcast standard which was also developed for human vision and is completely dominated by the TV industry. In practical terms, this means a 4:3 aspect ratio for conventional TV signals and unless this ratio is corrected by digitizing the video signal with a 1:1 aspect ratio, or unless the image is corrected for in software computations, the measurement of x,y distances become cumbersome and lengthy. Spectrally, the broadcast standard is a broadband three color (red, green, blue) system which is not appropriate for image cytometry since in fluorescence and stoichiometric stains, specific wavelength bands are of interest. Typically, the image is scanned in a 2:1 equalizing mode to make the imaging of movement more pleasant to the human eye, given the bandwidth limitation of the TV standard. This standard also restricts the integration time to one 1/30th of a second and imposes a frame scanning format which is not necessarily compatible with the detector. The detector in most cases is a vidicon-like tube or a CCD with interlace capability. The vidicon tube lacks spatial accuracy and

its gray scale resolution is limited to approximately 7 bits. This is sufficient for human vision since the gray level sensitivity is about 5 bits (Green 1983). The vidicon-based tube is also highly non-linear and has a non-unity gamma factor, i.e. a non-equal gain at different gray levels. Due to the phosphor response, blur and image lag are common and sensitivity at low light levels is poor. Even CCD technology is driven by the TV industry and is not compatible with the scientific (quantitative) requirements (Janesick et al. 1987; Hiraoka, Sedat and Agard 1987). Although CCDs improve the video response in terms of spatial accuracy and linearity, they are plagued by other problems. In particular the interlaced mode of CCDs requires that part of the sensing area is masked. These masked areas are used for the storage of previously collected charges waiting to be read-out while a new image is acquired. Hence these devices have a fill factor of less than 50% and much decreased sensitivity. Furthermore, even though the CCD is a discrete sampler, the signal is converted into a continuous analog signal as specified by the broadcast standard and at a later point the analog signal is resampled by the digitizer, resulting in an additional sampling error. Video systems are generally associated with complex high speed analog circuits to provide automatic gain control and superimposed synchronization signals. Inherent to such circuits is interference and noise causing yet more distortions. A very severe limitation is the video standard's inability to provide scanning flexibility, i.e. there are no alternative ways to scan the image or part of the image. This is one of the reasons why continuous-motion scanning, time delay integration and laser scanning was developed. Even though high definition television (HDTV) will provide higher image definition, it will not be an adequate standard for quantitative

microscopy since the aspect ratio will be maintained (4:3, 5:3, 16:9 depending on the HDTV standard), interlacing will continue to be a problem, since the standard will be optimized for human vision.

Some of the limitations of the video-based camera are fundamental such as its accuracy, non-discrete nature of tubes, and photometric resolution. However, many other problems associated with video detectors have been partially solved in the last two decades as scientists have become more and more aware of the needs in quantitative microscopy. For example, the automatic gain control has been disabled on video cameras, replacing it with a manual gain control. Cameras have been modified to allow for non-interlaced scanning and to provide somewhat faster or slower acquisition rates. However, these have been only partial solutions as they do not yet solve the basic problem, namely that the whole transducer system is based on a standard inappropriate for quantitative measurements.

1.6 Requirements in Image Cytometry

The general problems described in the image acquisition of microscope/transducer systems relate directly to specific issues in image cytometry. For example, in morphometric assessment of leukemic cells, white blood cells are often misclassified due to insufficient resolution (Harms 1982). The largest problem lies in differentiation of cells within a peripheral blood smear between lymphocytes, atypical monocytes, plasma cells and the mature plasma cells. None of the commercial interactive white blood cell systems analyze the blast cells directly even though they are most important in the leukemic assessment (Harms 1982). These problems have also been observed in automated blood cell analysis such as the ADC-500, Hematrak and diff 3/50 or diff 4,

which were routinely used for blood cell analysis (Green 1979, Preston 1979 and 1980). The proper classification of such cells necessitates texture analysis of subtle differences in nucleus and cytoplasm which cannot be achieved using conventional image cytometry devices (Harms et al. 1982; Aus et al. 1986)

In chromosome analysis, if karyotyping is performed, the visible light microscope must be pushed to the limit of spatial resolution as it is very difficult to analyze the chromosome bands within individual chromosomes. On the other hand, a large field of view is required as one wants to analyze all 46 human chromosomes together and correlate their various bands for proper chromosome identification. It has been shown that in proper karyotyping, classifying the individual chromosomes by comparing them among each other is a necessity (Lockwood et al. 1988).

A third area represents the classification of pre-malignant (dysplasia) and malignant cells (e.g. carcinoma *in situ*). Inherent in these classifications are diagnostic and prognostic determinants. Again, texture is a parameter of great interest. Texture features have many forms but virtually all depend on the image's high frequency components. A simple texture feature, for example, is the variance of intensity which is calculated from the differences of individual pixels to average value of optical density. Another example is entropy, describing the average information associated with a discrete random variable such as pixel intensity. Average information is defined as the negative logarithm of the probability which brings pixels to equal value of gray level. In all, over 50 independent nuclear texture features have been defined and used in analysis of cervical cells (Aus et al. 1986; Vidal, Schulter and Moore 1973; MacAulay et al. 1989). Yet,

despite the texture feature's great importance, conventional microscopy provides very poor detection to extract these features.

A different requirement relates to screening applications where a microscope slide must be scanned for the presence of odd, atypical (potentially pre-malignant and malignant) cells. Here, the requirements are a large field of view with the resolution close to the limit of the optical microscope. The sample preparation must be minimal and the digital image acquisition non-destructive. An example of such an application is screening of cervical smears and other exfoliated cells of human tissue suspect of containing premalignant and/or malignant foci. A large number of stoichiometrically stained cells must be scanned in a short time (several hundred to a few thousand cells in a few minutes).

The above issues summarize improvements needed in quantitative microscopy for image acquisition related to analytical cytology. These improvements must occur in the area of spatial and photometric resolution while at the same time providing large fields of view together with distortion free image data.

These requirements have been defined over the years by a number of scientists involved in analytic cytology, (Shoemaker et al. 1982; Young et al. 1982; Prewitt 1965; Mendelsohn 1966; Jaggi et al. 1988) and can be summarized as follows. The spatial resolution of the system must be 0.2 - 0.5 μm with a minimum amount of geometric distortion. The photometric resolution, i.e. the $\sqrt{SNR}$ of the system must be at least 500:1 with a photometric contrast of 8 bits. Thus, optical density measurements within the range of 0.0 - 2.7 optical density (OD) (Mayall and Mendelsohn 1966) are possible. The spectral response at the wavelength range of 400 nm to 700 nm with a narrow spectral band of

±10 nm and a chromatically corrected image must be achieved. A large field of view of no less than 500 μm x 500 μm at a sampling density of 0.5 μm must be provided together with real-time data access. Finally, a large dynamic range allowing the acquisition of images within 10^{-4} to 10^{2} lux must be possible.

CHAPTER 2: CONCEPT OF THE SOLID STATE MICROSCOPE

In order to appreciate the Solid State Microscope (SSM) design, one needs to understand the details of a compound microscope, the theoretical issues relating to the sampling theorem, diffraction of light, noise related issues, as well as the construction of the conventional visible light microscope. The theoretical aspects will be addressed in Chapter 3. The compound microscope, using both finite and infinity corrected objective lenses are described below. The description is based on geometrical optics and is essentially based on ray diagrams which are sufficient to explain the basic principles of microscopy. The rays in geometrical optics indicate the direction of the travelling wavefront deflected by the refractive indices of the lenses. Within the framework of geometrical optics, the lens systems can be reduced to one representative lens to discuss the function of the microscope. However, later on in Chapter 3 geometrical optics will not suffice to discuss issues of resolution and aberrations. For that diffraction theory and Fourier optics will be required.

2.1 The Compound Multiple Lens Microscope

A conventional quantitative visible-light microscope, as it is presently used in image cytometry, is shown in its simplest functional form in figure 4 (Spencer 1982; Bradbury, 1984; Pluta 1989). Such a microscope consists of a two lens systems and the transducer. The object, O, assumed as a luminous point source, is magnified, inverted and projected by the objective lens system onto the primary image plane (PIP; also referred to in the literature as intermediate image plane or in a single lens system simply as the focal plane), O'. The second lens

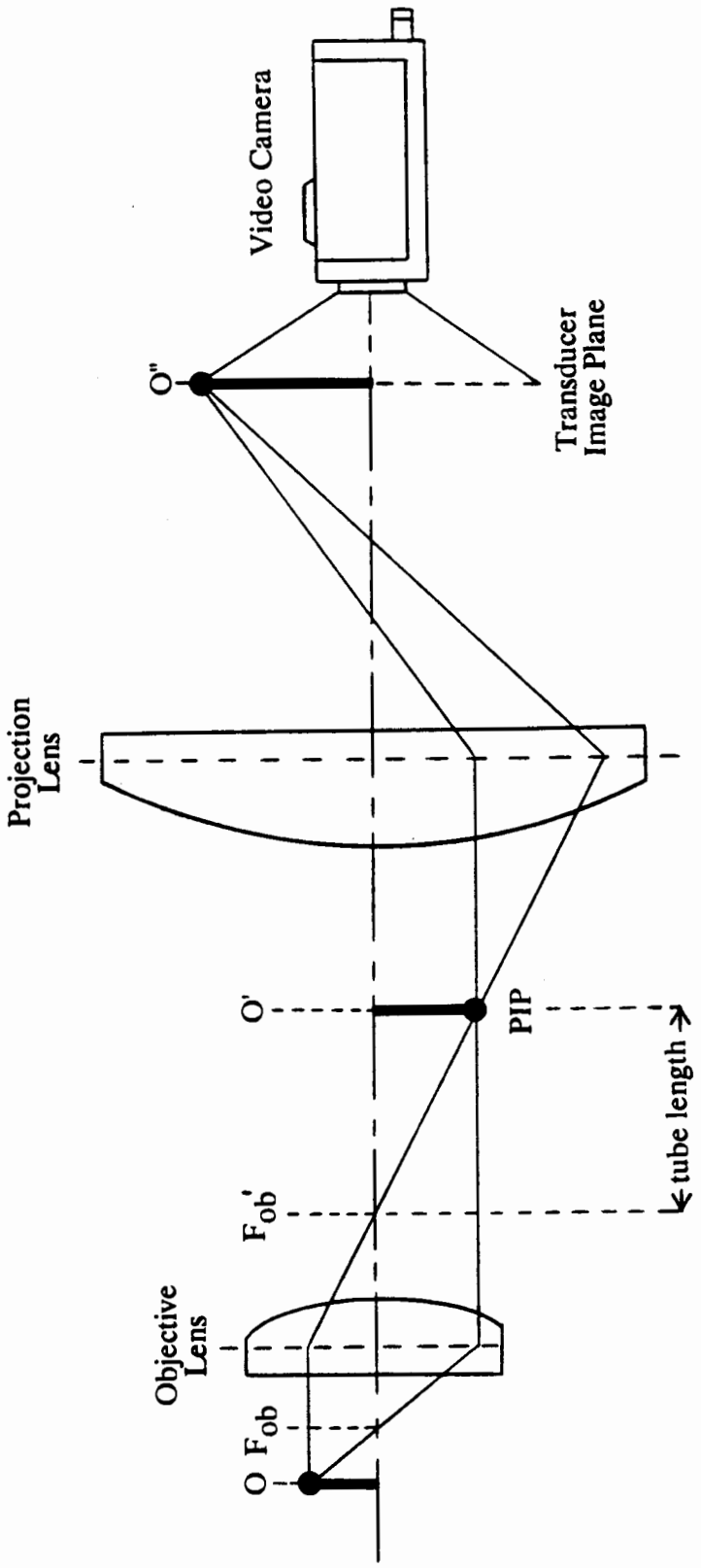

Figure 4: Principle of a Compound Microscope with an Objective Corrected for Finite Tube Length. (See Jaggi and Palcic 1989a, © SPIE).

system is the ocular for a human observer or the projection lens for a video camera. The projection lens system corrects for distortions and further magnifies the image O′ from the PIP onto the video detector, O" (Wakimoto 1979; Pluta 1988). Since the two magnifications, that of the objective lens and that of the projection lens, multiply to give the overall microscope magnification, the microscope is called a compound microscope. In describing the conventional microscope all mirrors were neglected as well as any other lenses and optical surfaces which are usually found in a conventional microscope, but whose function is only to make a microscope more convenient to use, bringing the images to appropriate imaging ports and proper heights for convenient human viewing. Figure 4 shows an objective corrected for a finite tube length. The tube length (optical tube length) is defined as the distance from the objective back focal plane, F_{ob}', to the PIP, O′. The tube length guarantees a parfocal system for different objectives with the same tube length, thus the focus need not be adjusted even if the objectives are changed. However, the tube length is mechanically restrictive and makes it difficult for microscope designers to keep the microscope flexible. Furthermore, if additional optics is introduced to achieve phase contrast, dark field, differential interference contrast, or epi-fluorescence the path of the image forming beams is modified changing the tube length. These issues were first addressed by Carl Zeiss Inc. in 1986 with microscopes using infinity corrected objectives. The principle of a simplified compound microscope with objectives corrected for infinite tube length is shown in figure 5. In this case, the image forming beams emerging from individual object points, O, exit the objective in parallel and only at some distance away from the objective an additional tube lens projects the image onto the PIP. This

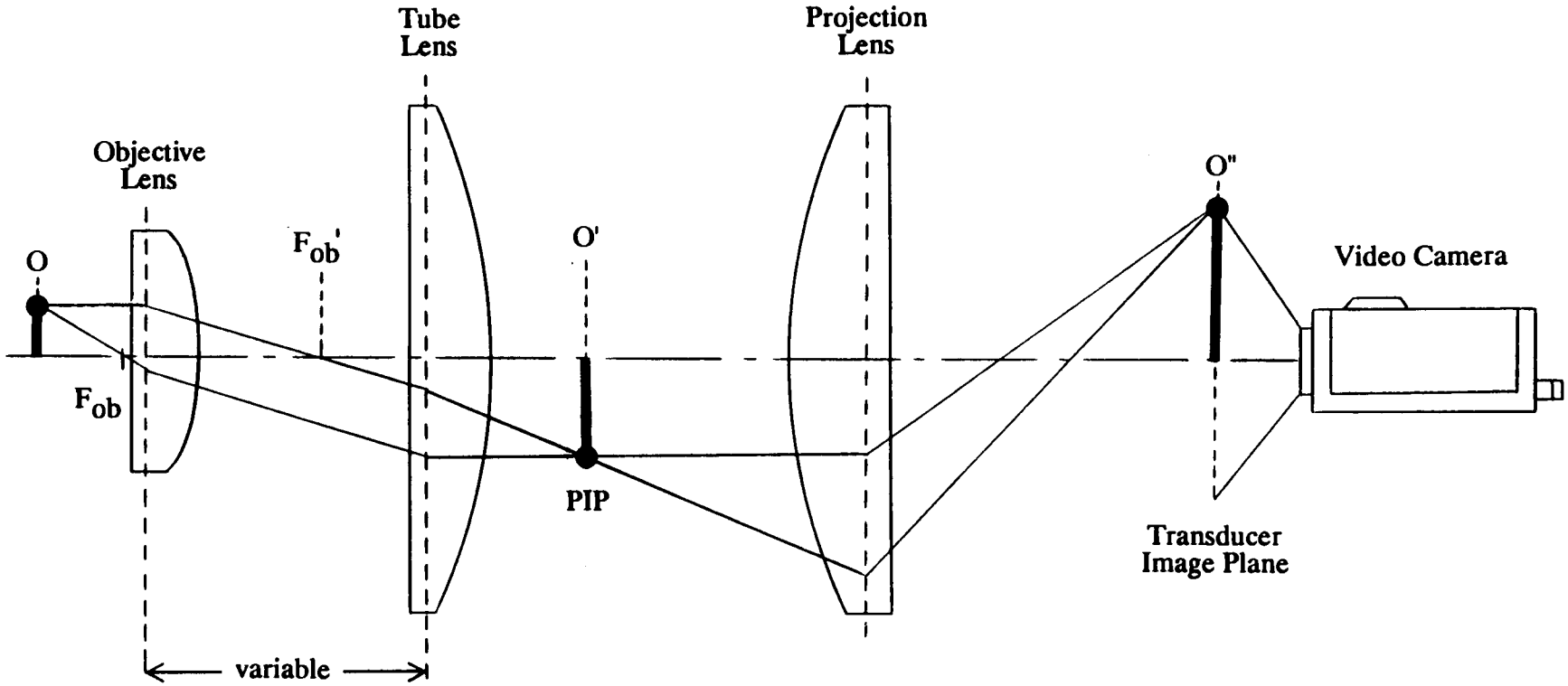

Figure 5: Principle of a Compound Microscope with an Infinity Corrected Objective.

means that different additional optical elements can be situated in the space between the infinity corrected objective and the tube lens, such as filters, polarizers (analyzers), compensator beam splitter, etc., without causing any disturbances in the path of the image forming beams. In short, infinity corrected objectives make it possible to design more versatile microscopes by using a simpler means compared to the case where objectives corrected for infinite tube lengths are employed. However, an additional tube lens must be inserted into the image forming path.

The function of the projection lens in the conventional microscope is not only to provide a further magnification, but also to correct distortions produced by the objective lens. In the past, it has been very difficult to manufacture objective lenses that provide a flat field, corrected for chromatic differences in magnifications and other distortions in the PIP. However, recently objective lenses and the projection lenses were made to match (Pluta 1988) using CAD optical design programs. Compensating projection lenses, as they are called, are computed to introduce an equal and opposite amount of chromatic difference of magnification so that the final image is virtually free from colour fringes. A number of objective lenses are now available which are classified in terms of magnification, numerical aperture, degree of projection, as well as the spectral response. These types are Achromat, providing a simple correction for chromatic aberrations; the Fluoride, minimizing autofluorescence and providing better corrections for chromatic aberrations with better transmission of UV light for fluorescence measurements; Apochromat, providing the best corrections for chromatic and spherical aberrations; and the Plan objectives, corrected to eliminate the curvature, therefore providing a flat field.

Finally, the latest state-of-the-art objectives allow for combinations of the above, an example of which is the Plan Apochromat (Planapo) objective.

2.2 Basic Idea of the Solid State Microscope

The Solid State Microscope (SSM) is a visible light, quantitative microscope. The essence of its design is to eliminate multiple lens systems used in compound microscopes as well as to use a scientific charge-coupled device (CCD), which together with the objective lens optimizes conditions for quantitative measurements in image cytometry. The basic idea of the SSM consists of placing the CCD into the primary image plane (PIP) of the objective lens. Therefore, the object, O, is magnified and projected by a single objective lens onto the CCD, O'. This design concept is illustrated in figure 6. The configuration eliminates the projection lens and other lenses and mirrors, common to conventional microscopes. Most importantly, it replaces the video detector with a scientific CCD as the light transducer. With this design, one minimizes optical distortions, substantially decreases light loss, and achieves a higher spatial and photometric resolution. However, various optical corrections performed by the projection lens in a compensation optics system, together with its magnification factor are lost. Because of that, and because the conventional video camera is replaced by an integrated circuit, the SSM design imposes a number of stringent requirements relating to the resolution, sampling density, dynamic range and signal-to-noise ratio. To determine the requirements of the objective lens as well as of the CCD, diffraction theory and Fourier optics are required (Chapter 3).

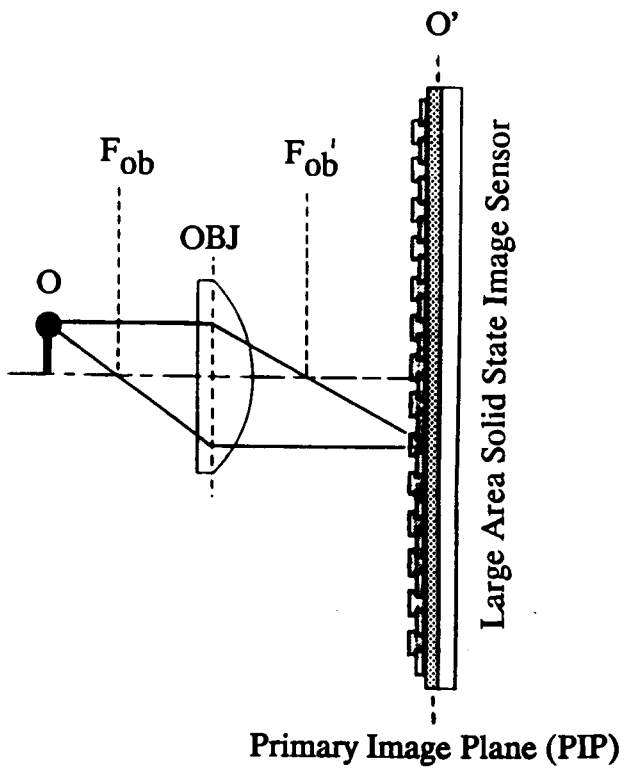

Figure 6: Principle of the Solid State Microscope (SSM) using a Diffraction Limited Objective Lens with a Large Area Solid State Image Sensor in the Primary Image Plane. (From Jaggi and Palcic 1989a, © SPIE).

Figure 7 shows an artist's rendition of the major components of the Solid State Microscope together with its processing circuits and display monitor. Using Koehler illumination the image of the microscope specimen is captured, magnified and projected onto a large area CCD positioned in the primary image plane. The pixel array is mapped into a frame memory that allows continuous display of the memory content. For image processing purposes the memory can be accessed by a workstation. Although the SSM is simple in concept, the design and its requirements are complex. Conventional microscope optics and transducers cannot be used if a gain in resolution, an increase in the size of the field of view and flexible scanning modes are to be achieved.

Microscopists have in the past tried to circumvent projection lens and other optical surfaces mainly to avoid light losses that are particularly significant in fluorescence microscopy applications (Inoue, 1986). To date, they have failed to achieve good results, precisely because the imaging field projected by the objective lens in the primary image plane is distorted and contains a large degree of shading, particularly in its periphery. Furthermore, the detectors used could not provide sufficient resolution, nor could the objectives provide sufficient magnification. However, in the past three years, advances in the manufacturing of objective lenses (Pluta 1989; Nikon Application Notes 1985), and more recently advances in VLSI (very large scale integration) CCD's (Stevens et al. 1987; Janesick 1984) provided an opportunity to conceptualize and develop an entirely different quantitative microscope, the SSM.

The proposed design relates to visible, incoherent, far field, light microscopy in the range of 450 nm to 700 nm. This wavelength range is essentially limited due to the use of the glass-based objective

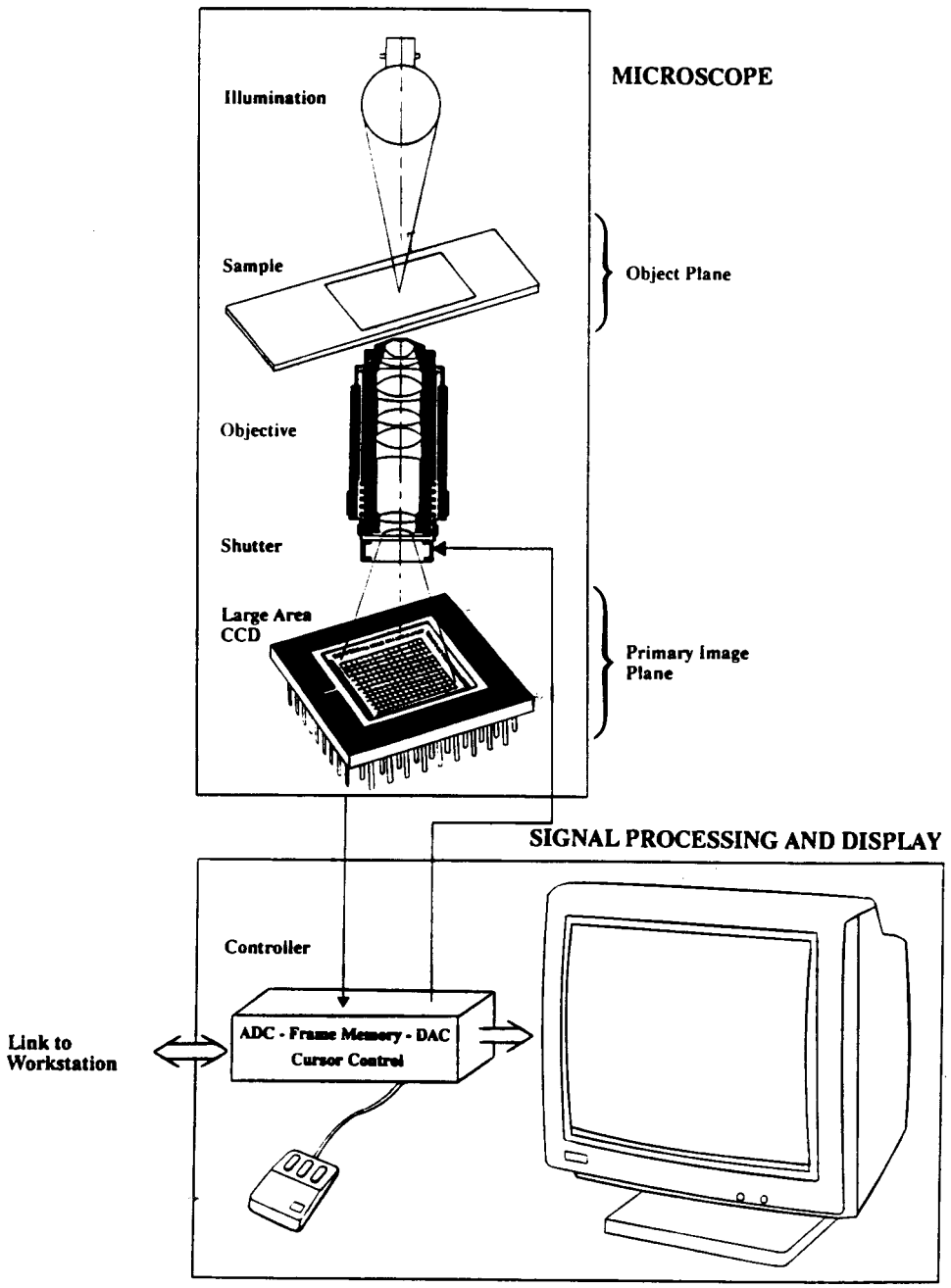

Figure 7: Artist's Rendition of the Solid State Microscope. (From Jaggi and Palcic 1989a (modified), © BIS CAP International, former Institute for Graphic Communication).

lenses and the silicon-based CCD. Although, the objective lens could be replaced by a quartz lens which has an adequate response in the UV (200 - 450 nm) region, the quantum efficiency of the CCD is near zero for that region. In the 450-700 nm region, the CCD response and the transmittance of the objective are optimized lens.

The SSM is a research tool and requires a great deal of flexibility in terms of optics, illumination, mechanics and scanning. The design allows one to easily insert optical elements, to provide different microscopy modes and spectral images. In principle, the design also includes confocal imaging since the CCD is already a "multiple pinhole detector" thus only the light source must be modified to a point source to yield confocal illumination. Laser scanning and broad band epi-fluorescence illumination is also possible. However, the device remains basically an area scanner and only for special circumstances could be converted into a line or flying spot scanner.

In summary, the SSM promises improved spatial and photometric resolution, a large field of view, as well as a minimum amount of distortion and light loss. Given the quantitative nature of this device, the digital representation of the image is seen on a large screen gray scale monitor. Hence, the microscopist would work and interact directly with a representation of the digital data.

CHAPTER 3: DESIGN RATIONALE

3.1 Summary of Design Calculations

In order to ensure an optimized design, to avoid aliasing, and to minimize geometrical distortions, the objective lens and the transducer must be considered together. The lens and transducer are the key components in the design of the solid state microscope. Since incoherent Koehler illumination is used which is a standard in quantitative microscopy (Pluta 1988) and since the CCD signals are directly digitized, the remainder of the system is digital and thus does not significantly affect resolution and related parameters. The main issues relating to the SSM design relating to the objective and the CCD parameters are the spatial resolution which determines the resolving power of the system, the field of view, the dynamic range which allows different microscopy modes, and the signal-to-noise ratio for photometric accuracy. Calculations of these and other parameters are summarized in Table III. In these calculations, two objective magnifications at a high numerical aperture have been assumed, namely 60/1.4 oil and 20/0.5 using incoherent Koehler illumination at $\lambda = 0.55$ μm.

The first three parameters of Table IIIa/b deal with spatial resolution. The calculations indicate that for the x,y primary image plane (PIP) a sampling density of at least 7 μm pixel spacing is required. This high sampling density is crucial to the design and affects all other parameters. For example, the sampling density and the signal-to-noise ratio (SNR) are not independent of each other: as the numerical aperture of the objective gets smaller, the spatial resolution decreases requiring a smaller sampling density. This causes the contrast

PARAMETER	REFERENCE	FORMULA	RESULT	CONCLUSION
Resolving Power, R_{opt}	-Rayleigh criterion -Abbe (Fourier) approach	$-R_{opt} \simeq \frac{1.22 \times \lambda}{NA_{cond} + NA_{obj}}$ $-R_{opt} \simeq \frac{\lambda}{NA_{cond} + NA_{obj}}$	$-R_{opt} \simeq 0.29\ \mu m$ @ 60X $-R_{opt} \simeq 0.68\ \mu m$ @ 20X	-pixel spacing < 7μm in x and y at a 100% fill factor
Sampling Resolution, f_s	-Nyquist -Inoue, Harms, measured	$-f_s$ theoretical: twice R_{opt} $-f_s$ practical: 2 to 5 times R_{opt}	$-f_s \simeq 10$ samples/μm at 60X $-f_s \simeq 3$ samples/μm at 20X	
Spatial Resolution, (point spread function) ^psf	-Section 3.3	$\hat{}psf_{sys} \simeq [\hat{}psf_{opt}^{\ 2} + \hat{}psf_{det}^{\ 2}]^{1/2}$	$-\hat{}psf_{sys} \simeq 0.36\ \mu m$ at 60X $-\hat{}psf_{sys} \simeq 0.96\ \mu m$ at 20X	
Depth of Field, -object plane, $2\Delta z$	-Francon, measured	$-2\Delta z \simeq \frac{\lambda}{4n * \sin^2(\alpha/2)}$	$-2\Delta z \simeq 0.29\ \mu m$ at 60X $-2\Delta z \simeq 2.2\ \mu m$ at 20X	-defines the requirement of flatness of the detector
-primary image plane, $2\Delta z'$	-Pluta, measured	$-2\Delta z' \simeq M_{obj}^{\ 2} * 2\Delta z$	$-2\Delta z' \simeq 1$ mm at 60X $-2\Delta z' \simeq .8$ mm @ 20X	

Legend: NA is numerical aperture; sys is system; opt is optics; det is detector; obj is objective; cond is condenser.

Table IIIa: Summary of the Design Calculations (continued).
(From Jaggi and Palcic 1989a (modified), © SPIE)

PARAMETER	REFERENCE	FORMULA	RESULT	CONCLUSION
Field of View, W	-Castleman, Nikon Canada Inc.	-Diameter of field $D \simeq 25/M_{obj}$ -field of view $W \simeq (\text{pel spa} * \text{array size})/M_{obj}$	-$W \simeq 150\ \mu m \times 115\ \mu m$ at 60x -$W \simeq 450\ \mu m \times 350\ \mu m$ at 20X	-pixel array $< 1000 \times 1000$ -ultra wide flat field objective required
Illumination, I Light Loss, L	-Bradbury -Melles Griot Canada	-$I \simeq (NA)^2/M^2$ -L ≃ 1% /optical surface		-increased sensitivity with no occular - minimize # of optical surfaces
Dynamic Range, DR	-Pontifex et al. -Chang et al.	-$DR \simeq \text{sat.}/\text{noise}_{rms}$	-$DR \simeq 10^6$	-thermoelectric cooling or MPP mode for increased DR
Signal-to-Noise-Ratio, SNR	-Analog Devices -Ott	-$\sqrt{SNR} \simeq \frac{\text{signal}}{\text{noise}_{rms}}$ $-SNR^{-1} \simeq SNR_{sample}^{-1} + SNR_{opt}^{-1} + SNR_{det}^{-1} + SNR_{qu}^{-1} + SNR_{elec}^{-1}$	-$\sqrt{SNR}_{sys} \simeq 500{:}1$ -$\sqrt{SNR}_{det} \simeq 1000{:}1$	-10 bit digitization -8 bit signal representation

Legend: pel spa is picture element spacing; M_{obj} is magnification factor of objective lens; NA is numerical aperture; M is total microscope magnification; Sat is saturation signal; qu is quantization; elec is electronics.

Table IIIb: Summary of the Design Calculations.
(From Jaggi and Palcic 1989a (modified), © SPIE)

and hence the SNR to increase. The SNR calculations for the system show an $\sqrt{SNR}_{sys}$ of approximately 500:1 which is sufficient for most medical and biological applications. Such signal-to-noise performance requires a detector with a $\sqrt{SNR}_{det}$ of 1000:1 or 60 dB. The depth of field calculation defines the z-tolerance in the PIP for the image projected by the objective as well as the flatness requirement of the CCD sensing area.

One of the important advantages of visible light microscopes using area detectors is the large field of view which is optimized in the SSM design for screening applications (e.g. screening of a microscope slide for abnormal cells). A large field of view is also necessary because the SSM provides no ocular, and the image can only be seen on a high resolution monitor. An ultra-wide flat field objective and a CCD array with more than a 1000 x 1000 picture elements could satisfy these requirements. Such a design provides a digital field of view that is typically six times larger than that of a conventional image cytometry system.

For low light level measurements (e.g. measurements of fluorescently labelled cells or phase contrast images) it is important to minimize the light loss due to the optical elements. The high numerical aperture, low magnification and a minimum number of optical surfaces provide significant advantages of the SSM over the conventional image cytometry systems. To capture high (typically 10^{2} lux for bright field microscopy) and low (typically 10^{-4} lux for fluorescence microscopy) light level images with the same detectors, the transducer must provide a large dynamic range. Therefore the CCD should provide variable integration time and be operated such that the dark current is minimized.

The above considerations show that for an objective lens, corrected for axial and lateral chromatic and spherical aberrations, a 25 mm diameter field of view and minimized light loss due to optical surfaces, a large area CCD with more than 1000 x 1000 picture elements at a high sampling density of pixel size 7 μm x 7 μm and the signal-to-noise ratio of 60 dB is required. The derivations of these requirements are discussed in the section below.

3.2 Design Parameter Calculations and Derivations

Resolving Power, R_{opt}, is a critical, but difficult parameter to measure. For a two point circular aperture, the resolving power can be estimated by the Rayleigh criterion (Bradbury 1984; Pluta 1988). Although commonly used in image cytometry, and as such, useful only for comparison of one system with another, it must be noted that this criterion is only an approximation. A complete treatment would require an analysis of the noise characteristics, which are the ultimate resolution limiting factors (Reynolds 1989). The Rayleigh criterion states that the minimum distance, R_{opt}, between two point objects is proportional to the wavelength, λ, and inversely proportional to the numerical aperture, NA:

$$R_{opt} = \frac{1.22 * \lambda}{NA_{obj} + NA_{cond}} \quad \text{where } NA = n * \sin \alpha \qquad (6)$$

and where λ = wavelength is in micrometers, NA_{obj} = numerical aperture of the objective, NA_{cond} = numerical aperture of the condenser, n is the index of refraction of the medium between the lens and the object and α is half the angle of the cone of light that is captured by the objective. For example, at a wavelength of 0.55 μm, NA_{obj} of 1.4, and

NA_{cond} of 0.95, two points can be distinguished as long as the distance between them is greater than 0.29 μm.

The Rayleigh criterion is based on the idea of a minimum distance, R_{opt}, between two overlapping Airy disks such that they can still be resolved. The Airy disks are generated by two point sources located at infinity which are imaged by an objective lens with a circular aperture onto the PIP. The two resulting diffraction patterns seen in the PIP can be described in terms of two overlapping Bessel functions of the first order, $J_1(X)$ (Pluta 1988; Young 1982). The one-dimensional expression for intensity of a single point source is:

$$I_{PIP} = \left[\frac{2 * J_1(X)}{X} \right]^2 \qquad \text{where } X = \frac{2\pi * NA}{\lambda} * x \qquad (7)$$

and where x is the distance from the center of the symmetric diffraction pattern I_{PIP}. The assumption in the calculation of R_{opt} is that if the central maximum of one Airy pattern coincides with the first minimum of the other, the two points can just be resolved. Hence,

$$R_{opt} = \frac{(X \text{ at first zero crossing}) * \lambda}{2\pi * NA} = \frac{0.61 * \lambda}{NA} \qquad (8)$$

In this case, NA refers to the average system aperture of both objective and condenser, and thus both apertures must be taken into account as is the case in equation (6). The Rayleigh criterion for the two point resolution is graphically demonstrated in figure 8.

An alternative approach in computing the resolving power is to use Fourier analysis, a method first proposed by Abbe (Spencer 1982; Pluta 1988, Reynolds et al. 1989). The method is based on the laws of interference which states that smaller spacing of a sinusoidal grating

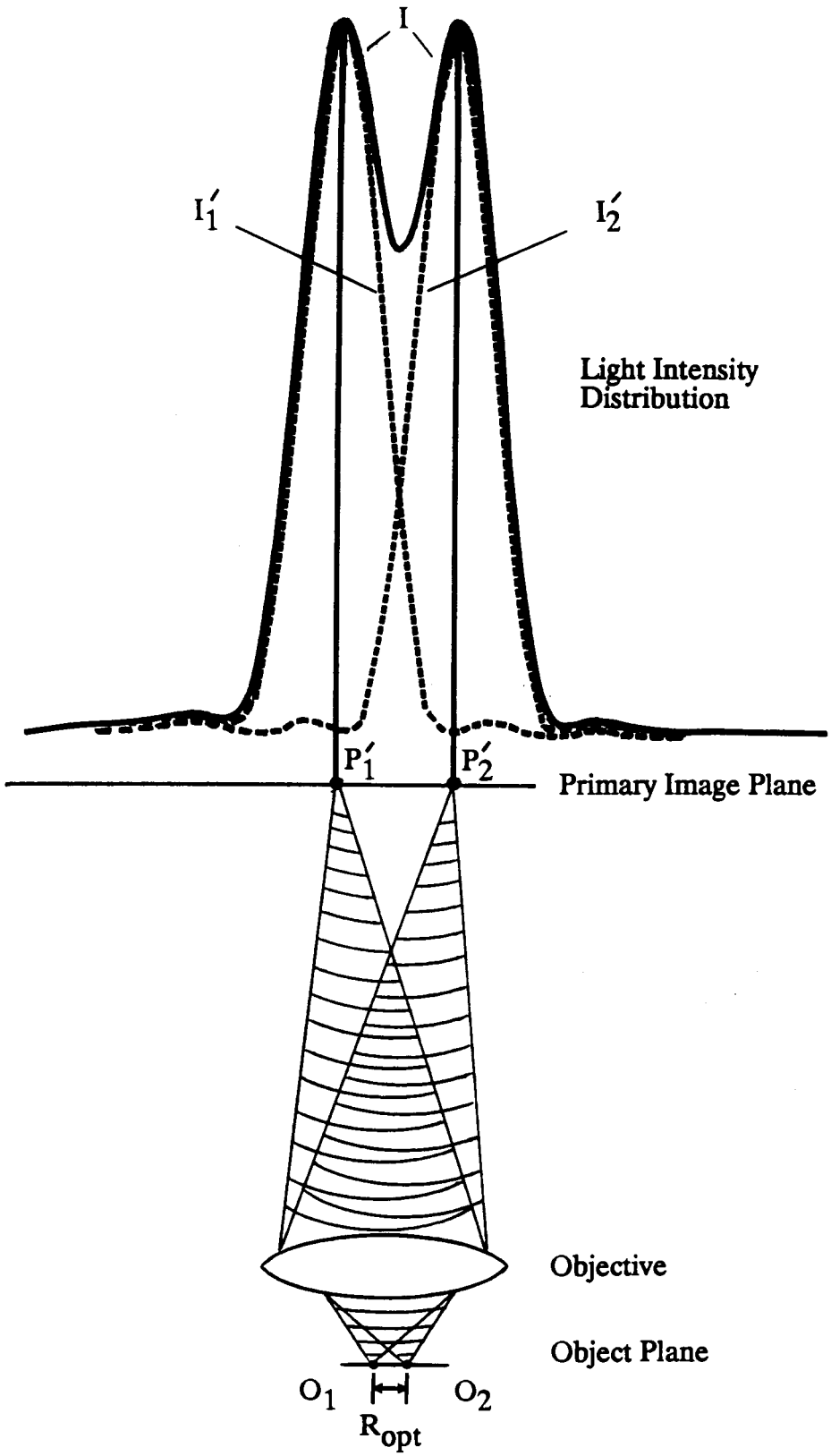

Figure 8: Rayleigh Criterion for Two Point Resolution using One-Dimensional Optics.

will give larger values of the diffraction angle. Therefore, beyond a certain diffraction angle, the objective lens, with its finite numerical aperture, cannot collect sufficient information to reconstruct the high spatial frequency sine-wave. Based on Fourier theory, the image can be reconstructed by using a number of sinusoidal gratings and the objective lens acts as a low pass filter. With respect to the resolving power, the assumption is that one must collect the zero order and first order spectra from the objects for them to be resolved. This approach results in an expression similar to the Rayleigh criterion and also implies that a high numerical aperture objective lenses with matching apertures of the light source must be used.

While the Rayleigh and Abbe criterion deal with the objective, the Sampling Density (sampling resolution), f_s, relates to the transducer. It can be estimated from theoretical considerations (Section 3.3) based on sampling and Fourier theory derivations (Castleman 1979) or from experimental measurements (Section 3.4; Jaggi and Palcic 1989; Inoue 1986; Harms and Aus 1983). The Nyquist criterion states that the sampling frequency must be at least twice that of the highest frequency component of the objects. However, for various practical reasons, this sampling should even be higher. For example, let us consider the case where a sine-wave with a frequency f_o is sampled at the zero crossing. The Nyquist sampling frequency in this case is $2*f_o$, however the sine-wave could not be reconstructed on the basis of these sampling points. Because the field of view decreases as the sampling density increases and because of noise considerations, it is advantageous to optimize the sampling density. By measuring resolving power versus sampling density, one can determine that the minimum resolving distance which must be sampled is three to four times (Jaggi and Palcic 1989; section 3.4).

For magnifications of 20, 40, and 60X with respective matched numerical apertures of 0.5, 0.95, and 1.4, a pixel spacing of approximately 7 μm will be optimal. This results in sampling densities of 3, 6, and 10 samples/μm, respectively. In this way, one achieves the resolution limit of the visible light microscope and avoids aliasing. Higher magnification than 60X or sampling density higher than 10 samples/μm will not provide more information. In fact, the image content will slightly decrease due to Fourier considerations and the lower numerical apertures of the 100X objectives.

Depth of Field (depth of focus), $2\Delta z$, defines the z-tolerance and the degree of flatness which must be achieved by the objective projection and the detector. Based on the Rayleigh quarter-wave criterion, the depth of field in the object plane is proportional to the wavelength and approximately inversely proportional to the square of the numerical aperture of the objective lens (Inoue 1986; Pluta 1988):

$$2\Delta z = \frac{\lambda}{4n * \sin^2(\alpha/2)} \qquad (9)$$

where $2\Delta z$ is the depth of field in the object plane and $n*\sin(\alpha)$ the numerical aperture. Therefore, the higher the numerical aperture, the more critical is the depth of field in the objective plane. The depth of field is approximately 0.3 μm for a 60/1.4 objective and 2.2 μm for a 20/0.5 objective. However, in the primary image plane of the objective lens, the projected image stays in focus within $2\Delta z'$ (depth of image), which is in the order of millimeters since:

$$2\Delta z' = (M_{obj})^2 * 2\Delta z \qquad (10)$$

where M_{obj} is the lateral magnification of the objective. This equation is derived from the quadratic relationship between the lateral magnification, M_{obj}, and the longitudinal magnification, $M_{obj\text{-}long}$, derived from the lens equation (Pluta 1988).

Equation (9) shows that the microscope does not need to be adjusted even if objective lenses with slightly different mechanical tube lengths are used. Thus, this design is parfocal as are the conventional microscope objectives which greatly facilitates the construction of the microscope. Another matter related to the depth of field is flatness which is a critical parameter and requires special purpose objective lenses. In addition, if one uses ultrawide field objectives, only the central portion of the field must be used to eliminate higher aberrations in the periphery of the field. These are important considerations in the SSM design since no additional lenses are used to correct the distortions of the objective lens as is common practice in conventional microscopes (Pluta 1988).

Field of view, W, is determined by the field projected onto the monitor and is a function of the field of view of the objective lens and the CCD array size. There are several reasons why a large field of view is desirable in image cytometry and one often finds that the current standard 512 x 480 pixel image size employed in conventional image cytometry systems is not sufficient. Let us consider, for example, a typical epithelial cervical cell which has a diameter of 60 μm. If one wants to study the cell at the resolution limit requiring a sampling density of 10 samples/μm, the field of view must be greater than 600 x 600 pixels. Furthermore, a practical point of view, since no binoculars are used, a large field facilitates the location of a particular area within the slide. A large field is particularly relevant for screening

applications where large areas on microscope slides are scanned to locate regions of interest. For screening of exfoliated cells such as cervical, lung, and other cells, it was found that the CCD detector should ideally have at least 1,000 x 1,000 pixels which calls for a large field objective lens.

The actual diameter, D_{act} of the microscope field of view at the intermediate focal plane is equal to (Bradbury 1984)

$$D_{act} = D_{obj}/M_{obj} \tag{11}$$

where M_{obj} is the magnification of the objective as in equation (10). D_{obj} is the diameter of the field of view in the PIP which for standard objectives is 18 mm and for ultra-wide field objective from 25-32 mm. In order to achieve minimum distortion only the central region of the projected image by the objective must be used (not more than 20% of the total area) requiring the use of an ultra-wide field objective.

Dynamic range, DR, is another critical parameter for a quantitative microscope. DR is defined as the ratio of CCD-well saturation over the electron noise floor for a constant integration time. In the context of this work, DR requires variable integration times to be useful. A low electron noise floor permits long integration times and hence acquisition of low light level images while for high light intensity images short integration times prevent saturation of the CCD-wells. For image cytometry, DR must span over several decades if one is to use the same detector in various microscope configurations, ranging from bright field (average illumination level: $\simeq 10^{2}$ lux) to fluorescence microscopy (illumination level: $\simeq 10^{-4}$ lux). Using the same detector for these measurements will minimize the registration error and allow measurements without delay. There are many examples in medicine

and biology where such measurements are required (Taylor et al. 1986). For example, in the platelet suspension immunofluorescence test (PSIFT) (von dem Bornet et al 1978) platelets are visually recognized using bright field microscopy and immediately thereafter the percent of fluorescing platelets is established in order to determine platelet compatibility.

The simple optical path, high sampling density requiring low magnification objectives, full frame imaging, and fewer optical surfaces result in a minimum light loss for the SSM. Nevertheless, some loss remains and to estimate it, one must consider the actual loss due to the reflections in the optical surfaces, the reduction in quantum efficiency due to the ratio of the sensing area divided by the total detector area, and the decrease in illumination due to the magnification and pixel size. The number of optical surfaces in a conventional microscope compared to the SSM is approximately twice as large resulting in a loss of 5 to 10%. A full frame CCD imager acquires at least two times (typically 4 times) more photons than an interlaced imager (Martin, Womack and Fischer 1988). This is due to the additional storage area (non-sensing area) used in the interlaced imager. The decrease in illumination is inversely proportional to the square of the magnification (Bradbury 1984). Since the SSM has an approximately 3 times lower magnification, the loss in illumination is lower by a factor of 9 when compared to the conventional microscope with a video camera. However, since the SSM uses a pixel size of approximately 7 μm x 7 μm and video cameras use a typical pixel size of 20 μm x 20 μm the number of photons projected onto the video camera is about 9 times greater than that of the SSM transducer. Therefore, both factors of 9 cancel out and nothing is gained in that respect. Illumination is also directly

proportional to the square of the numerical aperture, NA. The implication is that it is worthwhile to maximize NA not only from a resolving power point of view, but also to minimize illumination loss.

Signal-to-Noise Ratio, SNR_{sys}, of the complete system is a function of SNR_{sample}, SNR_{optics}, $SNR_{detector}$, $SNR_{electronics}$ and $SNR_{quantization}$. The $\sqrt{SNR}$ is defined as the ratio of the maximum signal amplitude at low spatial frequencies over the root-mean-square (rms) noise. This definition is consistent with the general definition of SNR as the ratio of signal power over noise powers, however, in image cytometry one tends to work with $\sqrt{SNR}$ (e.g. Young 1982). Assuming that the noise in the various system components is uncorrelated and has a Gaussian distribution (white noise), the SNR of each component can be added by taking the sum of squares. $\sqrt{SNR}_{sample}$ is limited by the stain used to specifically and stoichiometrically stain selected macromolecules of the cell. Most stained cell specimens fall within a range of 1000:1, that is three optical density units (Castleman 1987). $\sqrt{SNR}_{optics}$ is dependent on the unwanted interference of optical surfaces within the objective lens and its limit is also in the order of 1000:1 (Castleman 1987). While $\sqrt{SNR}_{sample}$ and $\sqrt{SNR}_{optics}$ are more or less given, $\sqrt{SNR}_{detector}$ and $\sqrt{SNR}_{electronics}$ leave some flexibility since they range from 100:1 to 10,000:1 depending on the detector and the electronic circuits. The $\sqrt{SNR}_{quantization}$ of a digitizer after quantization is given by (Castleman 1987; Young 1983):

$$\sqrt{SNR}_{quantization} = 20 \log 2^B + 11 \quad [dB] \simeq 59dB \simeq 900:1 \qquad (12)$$

where the $\sqrt{SNR}_{quantization}$ is measured in decibels and B is the number of bits used. The example in equation (12) assumes 8 bits of gray levels. To optimize the signal-to-noise ratio of all of these

components they must be matched. Therefore, the $\sqrt{SNR}$ of the CCD and the electronic circuits (CCD output stage amplifier) must be of 1000:1 each. The signal-to-noise ratio of the complete system can now be calculated:

$$\sqrt{SNR}_{sys} = [SNR^{-1}_{sample} + SNR^{-1}_{optics} + SNR^{-1}_{detector} + SNR^{-1}_{electronics} + SNR^{-1}_{quantization}]^{-1/2} \quad (13)$$

$$\simeq [5(1/1000)^2]^{-1/2} \simeq 500:1$$

A $\sqrt{SNR}_{sys}$ of about 500:1 is well within general quantitative microscopy requirements and a digital representation of the signal by 8 bits will be sufficient (Young 1982).

Spectral Response: Spectral information is another important matter in image cytometry. Although the entire visible spectrum between 450 to 700 nm is generally used, the 450 to 500 nm region (violet-blue) is of particular interest since most quantitative DNA stains absorb light in the blue and green wavelength regions. Thus, it is important that the detector's quantum efficiency in the blue approaches that of the longer wavelengths. That will allow one to acquire structures within the nucleus with good photometric resolution. A number of fluorescent dyes also emit in the blue spectrum. In addition, a shorter wavelength results in greater resolving power, as is shown by the Rayleigh criterion, equation (6). Therefore, wherever the spatial resolution is of key importance, it is advantageous to employ a light source with an enhanced violet-blue spectral output. Generally, in terms of quantum efficiency, solid-state detectors perform well in the red region, whereas performance in the blue spectrum decreases rapidly due to the absorption of the light by the polysilicon electrodes in front of the silicon oxide and depletion region. Because of the above considerations, it is important to select detectors with enhanced blue

response, such as back illuminated, thinned, or virtual phase CCDs. Alternatively, organic phosphor (e.g. Meta Chrome-2 from Thomson-CSF) coatings applied to the CCD sensing area can also improve the blue response.

3.3 Systems Analysis Approach

3.3.1 Assumptions

The Solid State Microscope can be modeled using Fourier theory to describe the illumination system, optics, specimen, detector, associated circuits and analog-to-digital converter. This system analysis approach allows one to compute the overall response as well as to estimate the effect of several of the component parameters on the performance of the complete system (Castleman 1979; Hansen 1986; Harms and Aus 1984;). For example, the contribution of the sampling density of the detector in the PIP and detector window size can be investigated together with the effects of additional lenses and display systems. The rationale that the same mathematical tool can be used is that there is a direct correspondence between electrical and optical systems. The impulse response of an electrical system is the point spread function (psf) of an optical system, the shift time invariant system is an isoplanatic system, the frequency response is the optical transfer function (OTF) and the magnitude of the frequency response is the modulation transfer function (MTF). However, in order to properly apply Fourier theory a number of assumptions must be made. These are discussed below for both the optical and electrical system.

Shift Invariance: For the optical system, the assumption is that the system is shift invariant. In optics, shift invariant or stationarity means that the shape of a spot image essentially undergoes

no change regardless of where it is located in the field. This is a reasonable assumption (Reynolds et al. 1989; Castleman 1979) particularly for the SSM as its optics is aberration free and a large part of the peripheral field of view is not used (i.e. only ≈20% of the field of view provided by the ultra-wide field objective). Mathematically, shift invariance means that if $f_{(x,y)}$ is an input image of a system that produces an output image $g_{(x'y')}$ then a displaced image $f_{(x-d,y-e)}$ produces $g_{(x'-d',y'-e')}$ where d and e are the displacement distance in the x,y object plane. x', y', d' and e' are location and displacement distances respectively in the magnified PIP plane. Electrically the assumption of shift invariance is also reasonable since in the CCD all picture elements can be assumed to be of equal size and spatial distortions are negligible. The pixel content of all pixels is processed by the same floating diffusion diode, the same output stage amplifiers and the same analog-to-digital converter (ADC) (Chapter 4), which means that the signals are treated the same way if one assumes ideal charge transfer efficiencies and no time variance. Sub-pixel size effects (tessellation error) can be neglected because the optics band limits the spatial frequencies and the image is oversampled.

Linearity: The optical system must also be assumed to be approximately linear, i.e. superposition applies. Mathematically superposition means that if $f_{(x,y)}$ produces $g_{(x',y')}$ and d(x,y) produces $e_{(x',y')}$ then $[f_{(x,y)} + d_{(x,y)}]$ produce $[g_{(x',y')} + e_{(x',y')}]$. Generally, linearity is a reasonable assumption for lenses if one employs incoherent light (Reynolds et al. 1989; Castleman 1979). The critical question relates to the incoherence of light. Under monochromatic illumination, an object can be represented by point sources. The condition of incoherent illumination means that all point

sources have a random phase relationship. A coherent field interferes or diffracts, which renders the image non-linear, whereas an incoherent field does not. In visible light microscopy, incoherent illumination can be achieved by setting the condenser numerical aperture equal to the objective lens numerical aperture. While $NA_{cond} < 0.26\ NA_{objective}$ results in coherent, $NA_{cond} \geq NA_{objective}$ results in incoherent illumination (Pluta 1988; Reynolds et al. 1989). The assumption of linearity for the transducer, amplifier and ADC is also reasonable. First, CCDs are known to be highly linear in terms of illumination vs signal output for a given spatial frequency, although there are small variations among pixels. Second, the amplifier was chosen such that it provides a constant gain over a large range of frequency (0 to 70MHz) with a high slew rate (300V/μs). And third, the ADC is typically linear within $\pm 1/2$ of its least significant bit (LSB) (Section 4.5). Furthermore, the signal amplitude of a CCD with its associated circuits decreases exponentially with increased spatial frequency, whereas the phase shift is approximately constant and there is no frequency transformation due to the system. Hence, for image transducers, it is common practice to consider the MTF_{camera} only (Hanson 1986) and assume linearity.

One of the basic assumptions in this modeling is that an absorbing object illuminated from behind (trans-illuminated) can be thought of as a two-dimensional distribution of point sources of light. The distribution of light in the PIP image resulting from a specimen in the object plane can be calculated from the knowledge of the distribution in the image of individual points. The image of such an object is the summation of spatially distributed point spread functions. This means

that the image can be described as a multiplication or convolution of the objects with a point spread function of the optical system.

Below, an SSM model is described that allows one to compute the microscope's response to an input object. The analysis is carried out on one-dimensional images for simplicity. This can be done without loss of generality since the objective, the CCD and associated circuits respond approximately equal to the horizontal and vertical scanning as one has isoplanatic optics and square pixel elements. Furthermore, one-dimensional Fourier Theory can be easily extended to two-dimensional Fourier Theory (Gonzalez and Wintz 1987; Reynolds et al. 1989).

3.3.2 Derivation of the First Approximation Model of the Solid State Microscope

A first approximation model of the solid state microscope can be achieved by characterizing the optics including the light source with a single point spread function, $psf_{opt}(x)$, and by characterizing the detector including its circuits with another single point spread function, $psf_{det}(x)$. The system response, $psf_{sys}(x)$, can then be calculated as the square root of the sum of the square of $\hat{}psf_{opt}$ and $\hat{}psf_{det}$, respectively (Castleman 1987):

$$\hat{}psf_{sys} \approx [\hat{}psf_{opt}^{\,2} + \hat{}psf_{det}^{\,2}]^{1/2} \qquad (14)$$

where $\hat{}$ is used to represent the approximate full-width half-maximum of the main lobe of the particular point spread function. However, equation (14) in the digital system is only valid if the Nyquist criterion is adhered to:

$$f_s > 2 * \text{highest frequency component of } \{\mathfrak{F}[psf_{opt}(x)]\} \qquad (15)$$

where $\mathfrak{F}$ is the Fourier transform and f_s is the effective sampling frequency of the detector in the PIP. Equation (14) and its condition, equation (15), are important results in terms of the spatial and photometric resolution of the solid state microscope. They are derived below together with a discussion of the underlying assumptions.

Equation (14) is based on the convolution of the two point spread functions, $psf_{opt}(x)$, and $psf_{det}(x)$, which results in the overall $psf_{sys}(x)$:

$$psf_{sys}(x) = psf_{opt}(x) ** psf_{det}(x) \qquad (16)$$

where ** is the convolution operator and x is the spatial dimension. To determine ^psf one can use the definition of rms[1] (IEEE 1984):

$$\hat{psf}^2 = \frac{1}{\int_{-\infty}^{+\infty} psf(x)\,dx} * \int_{-\infty}^{+\infty} \left[x - \frac{\int_{-\infty}^{+\infty} x * psf(x)\,dx}{\int_{-\infty}^{+\infty} psf(x)\,dx}\right]^2 psf(x)\,dx \qquad (17)$$

assuming zero centroid, i.e.symetric about x=0 and psf(x)<0 for all x:

$$\hat{psf}^2 = \frac{\int_{-\infty}^{+\infty} x^2 * psf(x)\,dx}{\int_{-\infty}^{+\infty} psf(x)\,dx} \qquad (18)$$

the psf(x) can be normalized i.e. the denominator is equal to one. Therefore equation (14) can be proven by combining equation (16), (18).

---

[1]This was pointed out to the author by Dr. Jim Cavers, School of Engineering Science at Simon Fraser University.

$$\hat{}psf_{sys}^{\,2} = \int_{-\infty}^{+\infty} x^2 * psf_{sys}(x)\, dx = \int_{-\infty}^{+\infty} x^2 [psf_{opt}(x) ** psf_{det}(x)]\, dx \quad (19)$$

by changing the order of integration and changing variables appropriately, one obtains:

$$\hat{}psf_{sys}^{\,2} = \int_{-\infty}^{+\infty} x^2 * psf_{opt}(x)\, dx + \int_{-\infty}^{+\infty} x^2 * psf_{det}(x)\, dx \quad (20)$$

$$\hat{}psf_{sys}^{\,2} = \hat{}psf_{opt}^{\,2} + \hat{}psf_{det}^{\,2} \qquad \text{q.e.d.} \quad (21)$$

What are the point spread functions of the optics, $psf_{opt}(x)$, and of the detector, $psf_{det}(x)$? It will be shown that it is reasonable to assume that these functions can be approximated by Gaussian functions. The Gaussian approximation of the point spread functions for the optics and the detector are shown in figure 9 together with $psf_{sys}(x)$. Both functions, $psf_{opt}(x)$ and $psf_{det}(x)$, satisfy the conditions assumed in equations (18) and (19).

The diffraction pattern, $psf_{opt}(x)$, is described by a Bessel intensity function shown in Section 3.2, in equation (7). A good estimate of the width of the $psf_{opt}(x)$, is the Airy disk using the Rayleigh criterion for resolution as shown in figure 8, i.e. width of $psf_{opt}(x) = \hat{}psf_{opt} = R_{opt}$. Shown in figure 10a is the Bessel intensity function for an $R_{opt} = 0.29\ \mu m$, using a 60X objective lens, Koehler optics and incoherent light. This is compared with the square of a Gaussian function where $\sigma_{opt} = {}^{1}/_{2} * R_{opt}$. The Bessel intensity function is scaled by a factor of $\{1/(\sqrt{2\pi} * \sigma_{opt})\}^2$ such that the two functions coincide at their maxima. The two functions are very similar for higher intensity values and therefore the Gaussian $psf_{opt}(x)$ is a good approximation.

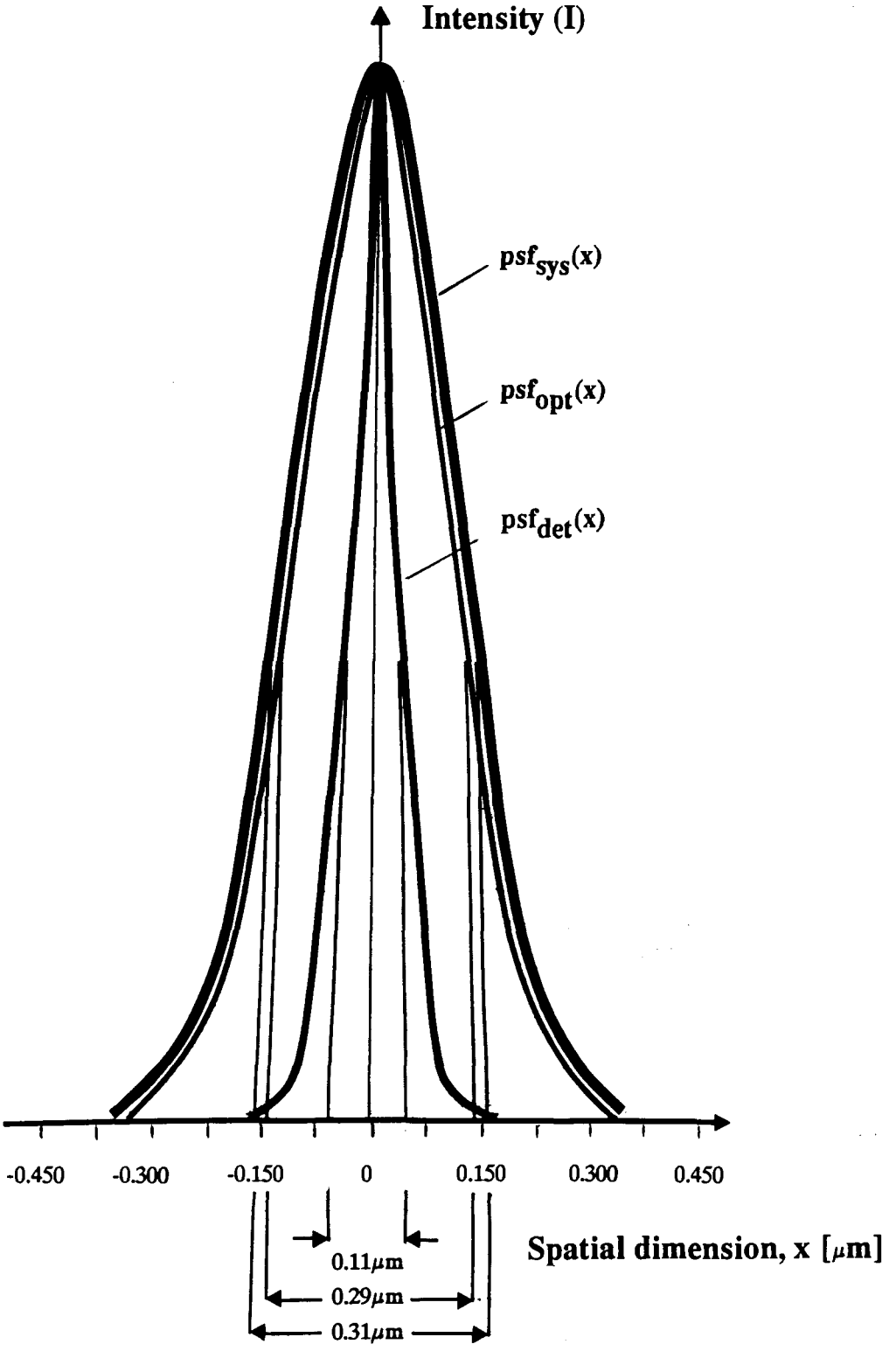

Figure 9: Point-spread Functions of Optics, Detector and System for the SSM.

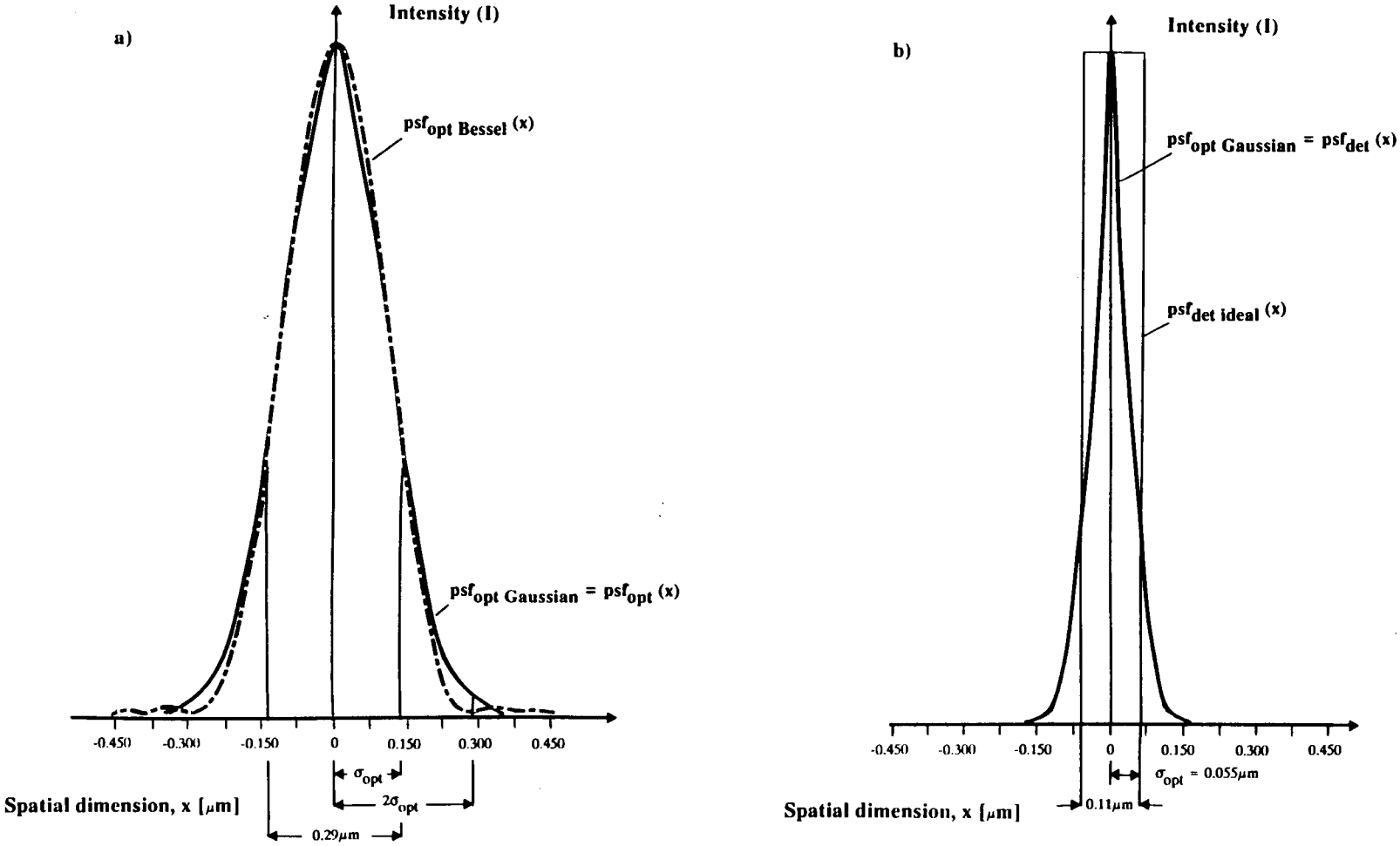

Figure 10: Gaussian Approximation of Bessel-based $psf_{opt}(x)$ (a) and Gaussian Approximation of $psf_{det}(x)$ (b) based on CCD Data.

The impulse response of an ideal detector, $psf_{det\ ideal}(x)$, is a rect(x/Δx) function with a width of Δx = (pixel size/magnification) (Dyck 1982; Martin et al. 1988). The justification for this width is that the effective pixel size which is equal to the pixel spacing and the sensitivity distribution are the single most important parameters in the determination of $psf_{det}(x)$. Furthermore, the width of Δx is consistent with the Nyquist criterion for the following reasons. In the spatial frequency domain, the rect(x/Δx) response is a sinc(Δx*f) function with its first zero crossing at ±(1/Δx). If one neglects the side lobes of the sinc(Δx*f) function, the ideal detectors bandwidth corresponds to (1/Δx) implying a sampling frequency 2/Δx. Intuitively, one would expect such a sampling frequency since 2/Δx corresponds to 2 pixels per cycle of the maximum spatial frequency. Therefore, the $\hat{}psf_{det\ ideal}$ = (Δx), is a reasonable first approximation. However, a more realistic assumption is that the point spread function of a CCD, $psf_{det}(x)$, is approximately Gaussian (Seib 1974; Barbe 1975; Hansen 1986). To establish the width of this Gaussian function, $\hat{}psf_{det}$, technical MTF data of the CCD was employed (Martin et al. 1988). The data was approximated by a Gaussian function and transformed into the spatial domain. This resulted in another Gaussian function, $psf_{det}(x)$, with a standard deviation of approximately $\sigma_{det} = {}^{1}/_{2} * \Delta x$. The result of these approximations is graphically shown in figure 10b, where the two point spread functions, $psf_{det\ ideal}$ and the Gaussian psf_{det} are compared.

Since the Fourier transform of a Gaussian function is also Gaussian, $psf_{opt}(x)$ has an infinite bandwidth and therefore, condition (15) can never be satisfied. However, it is reasonable to assume that

the frequency components above 2 standard deviations ($2*\sigma_{opt}$) of the frequency spectrum of the optical system can be neglected. Therefore, equation (15) becomes

$$f_s = (\text{magnification/pixel size}) > 1/\sigma_{opt} = (2/\hat{}psf_{opt}) \qquad (22)$$

A numerical example of the model, given by equation (14), follows. At 60X magnification, numerical aperture of objective 1.4 (oil), numerical aperture of the condenser 0.95 (dry) and 7 μm pixel size results in $\hat{}psf_{opt} = 0.29$ μm and $\hat{}psf_{det} = 0.11$ μm. Hence, using (14), a minimum resolvable distance of

$$\hat{}psf_{sys} = [0.29^2 + 0.11^2]^{1/2} = 0.31 \ \mu m \qquad (23)$$

can be achieved. This is the theoretical limit of SSM employing visible light. The Nyquist condition given by equation (22) where the effective sampling density in the PIP is $\Delta x = 0.11$ μm and

$$f_s = 1/0.11 = 8.6 > 2/0.29 = 6.9 \ [\text{samples}/\mu m] \qquad (24)$$

is satisfied and therefore equation (14) and (23) are valid for the 60X objective.

The above model of the SSM allows one to plot 2 sets of curves relating resolving power to the detector sampling density. They are shown in figure 11. The three upper curves are relating to equation (14) and the two lower ones are the result of the Nyquist condition given by equation (22). The curve with square data points shows the maximum achievable resolving power of the optics assuming diffraction limited objectives. It is calculated by the Rayleigh criterion,

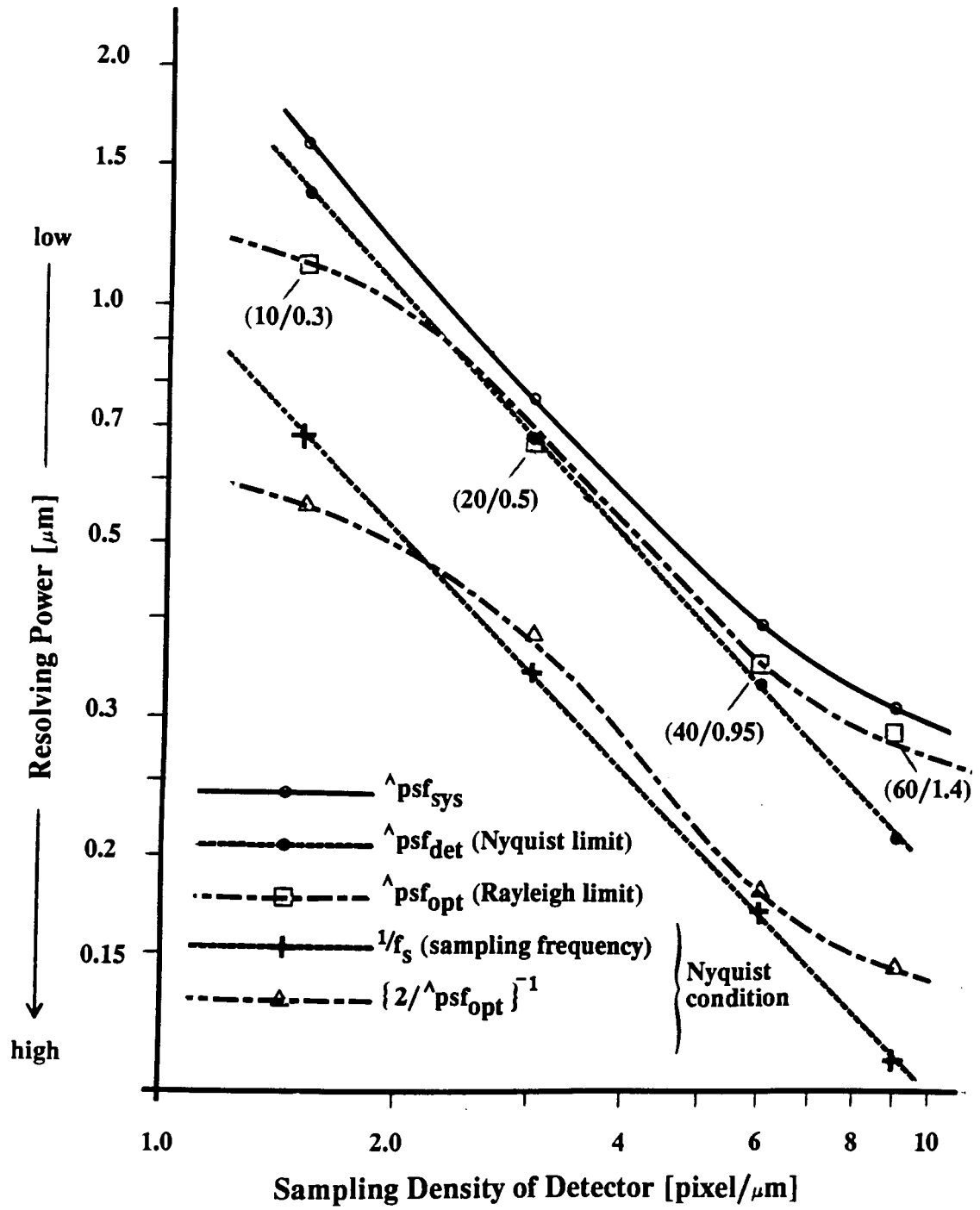

Figure 11: Theoretical Resolving Power of SSM for Matched Objectives and 7 μm x 7 μm Pixel Size Detector.

equation (8), at a wavelength of 0.55 μm. The Rayleigh curve strongly depends on the choice of the numerical aperture of the objective lens. At each square the objective magnification and the associated numerical aperture value are indicated. The objectives used are matched by adjusting the NA of the objective such that the Rayleigh curve lies above the Nyquist curve (dot data points). The rationale for this relationship is that the objective acts as an anti-aliasing filter. The curve with dot data points shows the theoretical limit for the detector, based on the Nyquist criterion. This curve is valid for $\hat{}psf_{det}$, if one assumes that two impulses can be distinguished if the distance between the two impulses is at least $2*\sigma_{det}$. The sampling density values of the SSM microscope are derived for magnifications of 10, 20, 40, and 60X, respectively, employing a detector with 7 μm x 7 μm sensing elements. The third curve with circles shows the system response based on equation (14). As for the lower two curves, they graphically illustrate the Nyquist condition as defined by equation (22). The left hand side of equation (22), is plotted (crosses) as: resolving power (f_s) = $1/f_s$. To satisfy the Nyquist criteria, it must be lower than the right hand side of equation (22) which is plotted (triangles) as: resolving power (fs) = $(2/\hat{}psf_{opt})^{-1}$. The Nyquist condition is fulfilled for the 20, 40 and 60X objective, but not for the 10X objective.

3.3.3 Refined Model of Solid State Microscope

The above model can be refined and further analyzed. The optics of the SSM can be represented by the illumination system, I(f), the microscopic object (specimen) M(f), and the objective lens, O(f). The detector consists of the transducer aperture (size of the array), T(f), the sampling aperture (size of pixel), W(f), the sampling function,

S(f), other CCD parameters, C(f), the output stage, A(f), and digitizer, D(f). The CCD frequency response, C(f), can be further refined by two MTFs: the $MTF_{CCD\ trans}$ due to the charge transfer efficiency and the $MTF_{CCD\ diff}$ due to the diffusion of charge between photon absorption and photoelectron collection (Barbe 1975). This refined mathematical model of the system response is shown in figure 12. Convolution and multiplication of the individual responses allows one to compute the overall response if the individual MTF are known. The order of multiplication and convolution in this diagram is based on "physical reasoning", that is, filters multiply in the frequency domain and apertures multiply in the spatial domain.

In the first approximation model of the SSM (Section 3.3.2), the illumination, the microscope sample and the objective are represented by $psf_{opt}(x)$. For the $psf_{det}(x)$ the transducer aperture, the window of the transducer, the sampling function of the transducer, the CCD function, the amplifier and digitizer function are combined. These two point spread functions are also shown in figure 12 together with the elements included in the approximation (double boxes). The single boxes $M_{(f)}$, $T_{(f)}$, $S_{(f)}$, and $D_{(f)}$ were neglected in the first approximation model.

The impulse response of the SSM is graphically shown in the spatial and frequency domain in figure 13a-h. In the spatial domain the amplitude of the signal is plotted on the ordinate while on the abscissa the spatial dimension x is shown. In the frequency domain the magnitude of the spatial frequency, MTF, is plotted on the ordinate while on the abscissa the spatial frequency f is shown. The point spread function modulation transfer functions are normalized to 1 at $x = 0$ and $f = 0$ respectively. Since an image can be represented by the superposition of the impulse responses, the input image for simplicity is an impulse,

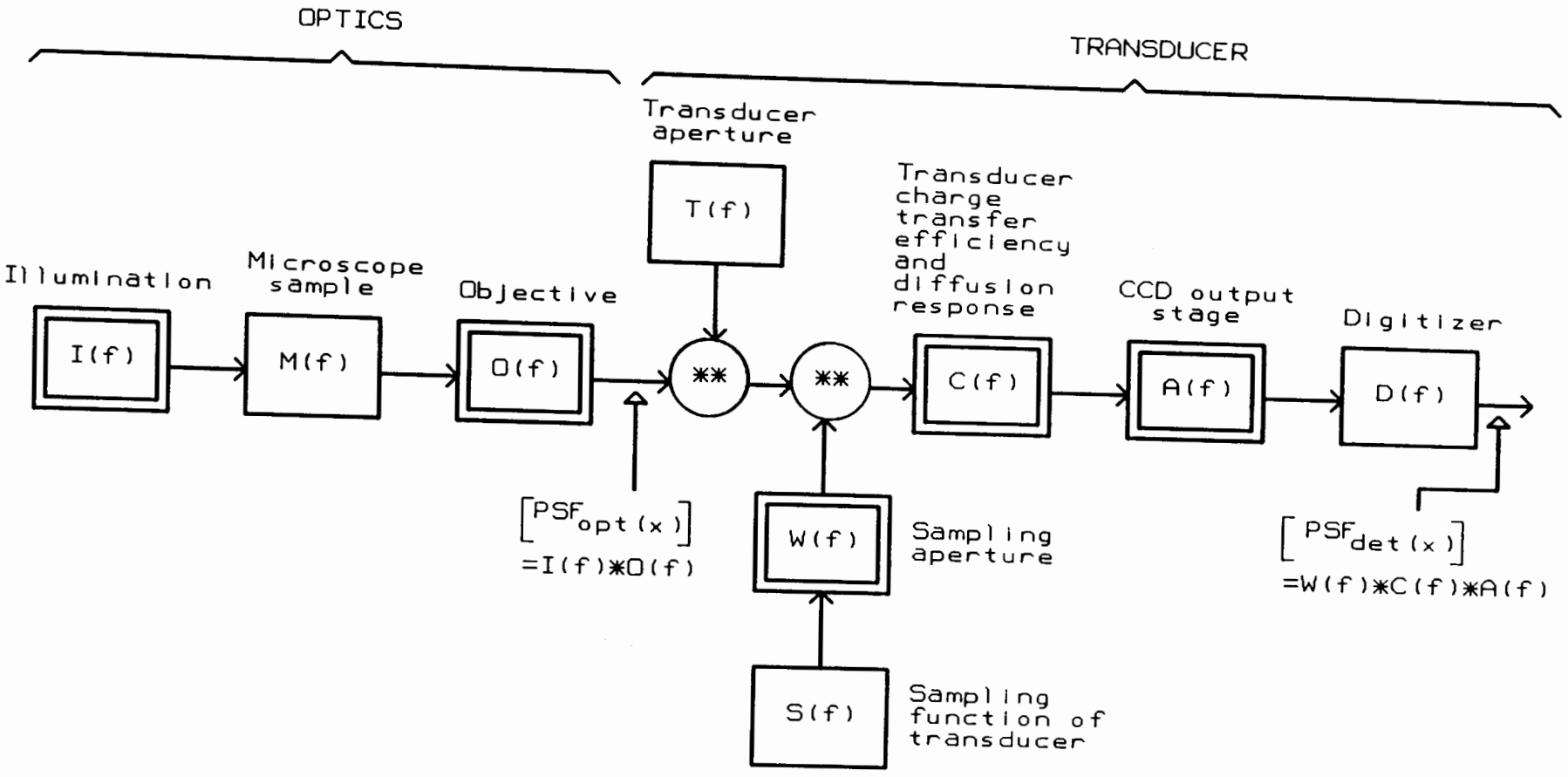

Figure 12: Block Diagram of the Refined Mathematical SSM Model.

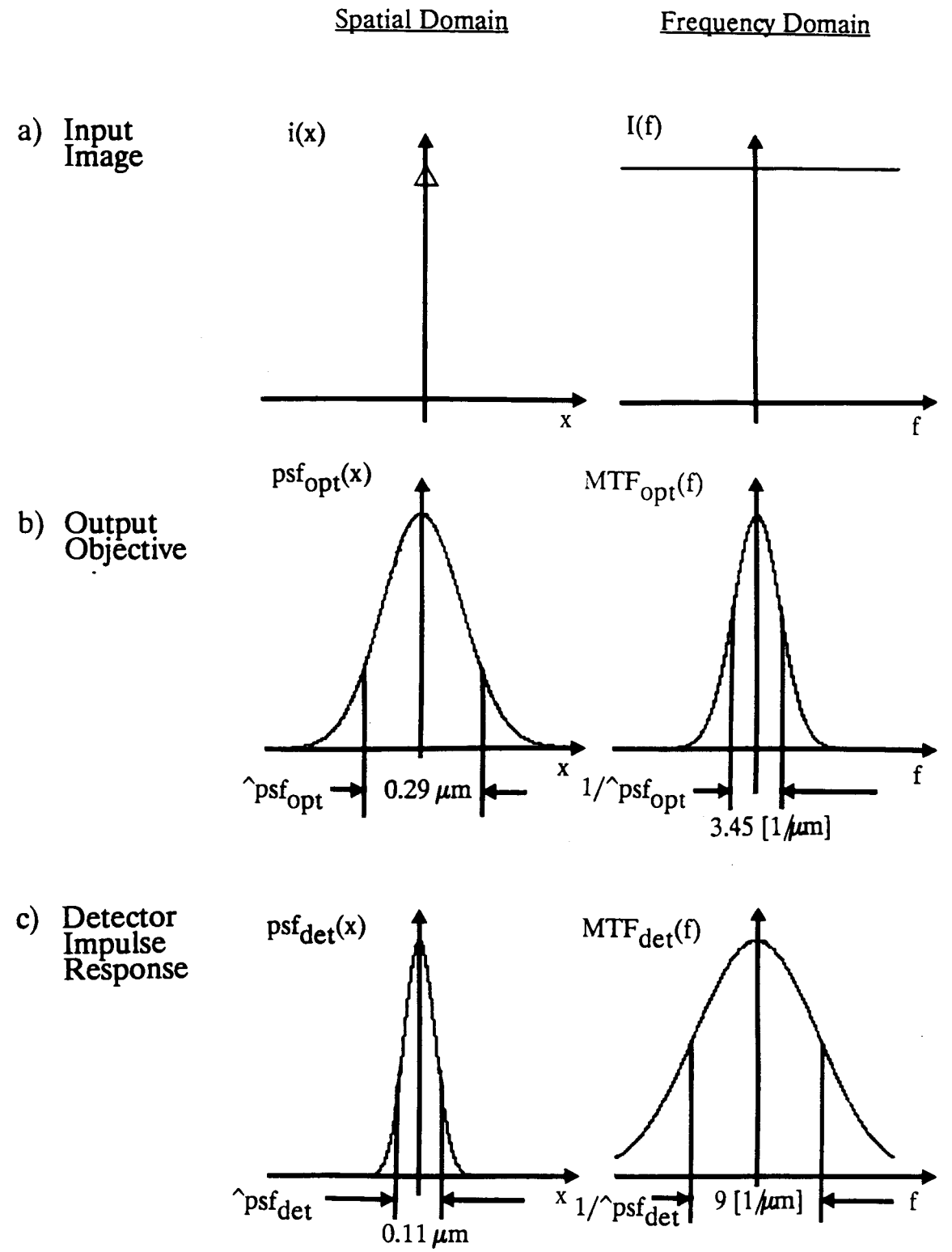

Figure 13a-c: Graphic Representation in the Spatial and Frequency Domain for SSM Components (Continued).

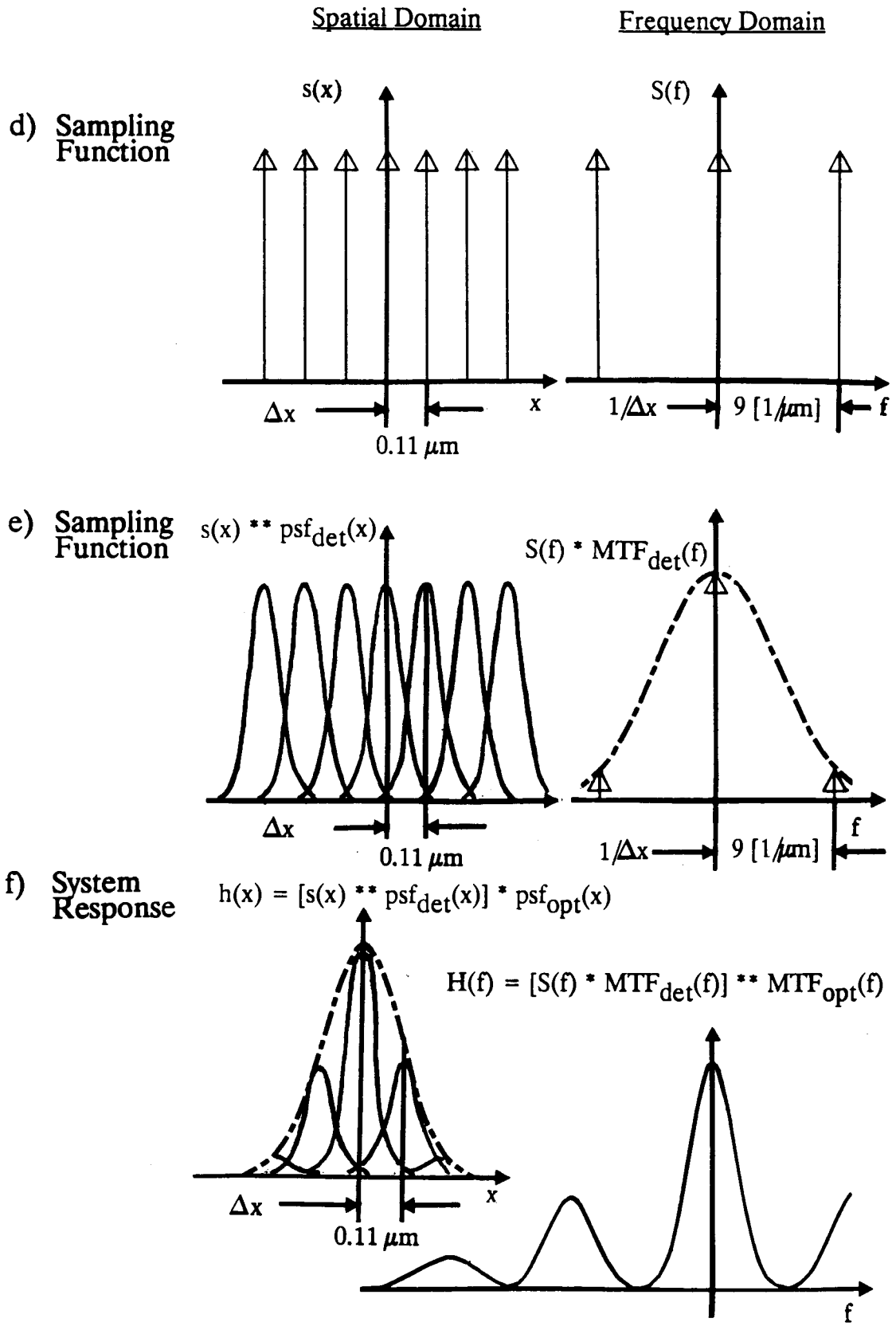

Figure 13d-f: Graphic Representation in the Spatial and Frequency Domain for SSM Components (Continued).

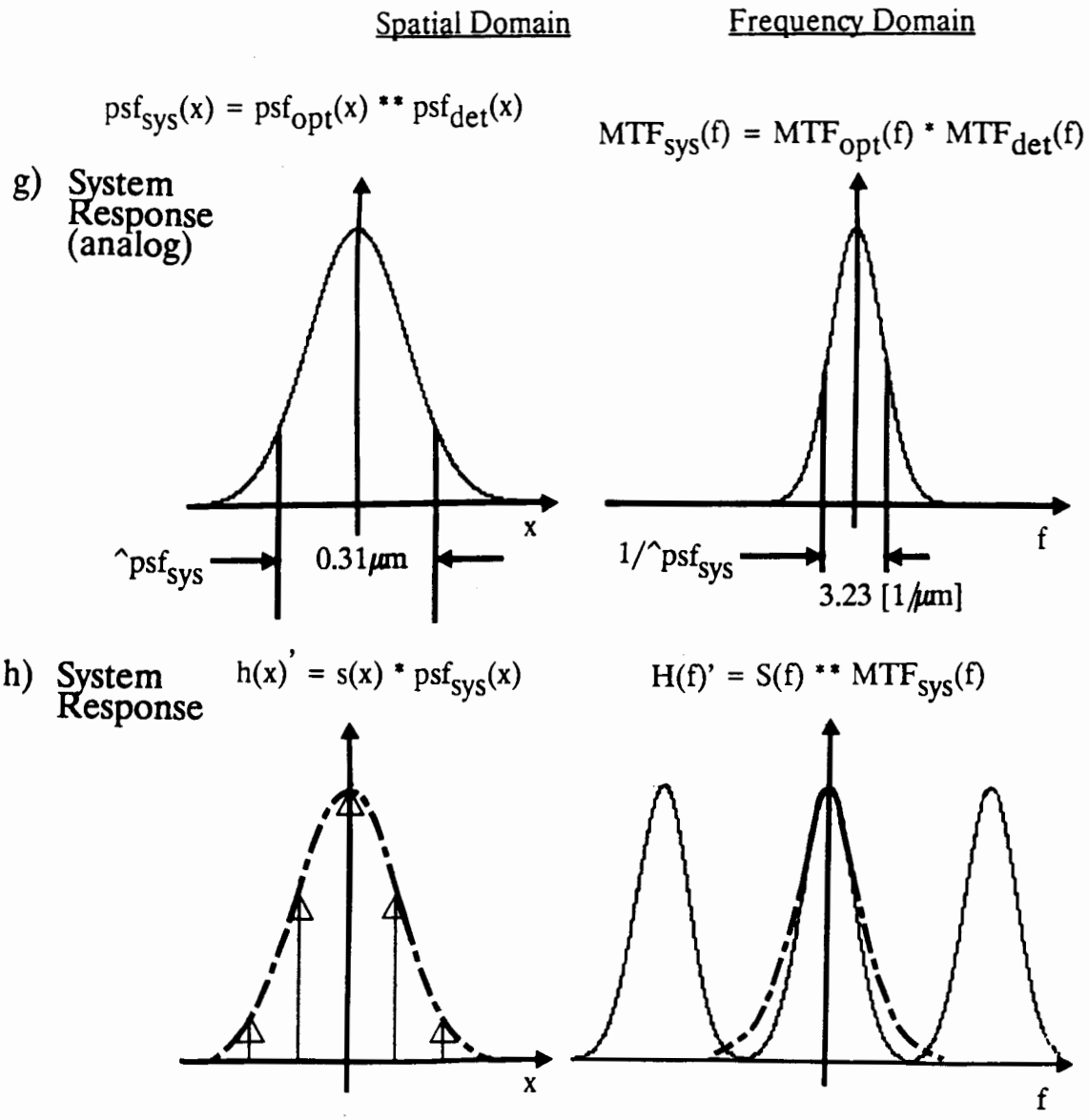

Figure 13g-h: Graphic Representation in the Spatial and Frequency Domain for SSM Components.

$i_{(x)}$, in the spatial domain and a dc-level, $I_{(f)}$, in the frequency domain (figure 13a). The optical system modifies the impulse and generates an output, $psf_{opt}(x)$, that is described by equation (17) and its MTF (figure 13b). The impulse response of the CCD, $psf_{det}(x)$, is assumed to be Gaussian as well and is described in section 3.3.2 (figure 13c). The sampling sequence, s(x), of the detector can be described as a comb(Δx) function (figure 13d) and is convolved with $psf_{det}(x)$ which results in figure 13e. The final system response is shown in figure 13f and given by:

$$h_{(x)} = [s_{(x)} \;**\; psf_{det}(x)] * psf_{opt}(x) \qquad (25)$$

where $h_{(x)}$ is the system response which includes the sampling sequence. From a theoretical system analysis point of view this equation is correct since one expects a convolution for $s_{(x)}$ and $psf_{det}(x)$, and a multiplication with the image $psf_{opt}(x)$. The equation is also consistent with figure 12.

An alternative approach suggested by Harms (1985) is described in figure 13g-h. Harms states that for a real imaging sampler:

$$h_{(x)}' = [psf_{det}(x) \;**\; psf_{opt}(x)] * s_{(x)} \qquad (26)$$

is a better model since it modifies the frequency spectrum, $H_{(f)}'$, in both the baseband and sideband. The result of $psf_{opt}(x)$ convoluted with $psf_{det}(x)$ is shown in figure 13g. This $psf_{sys}(x)$ was the one used in the first approximation model (section 3.3.2) of the SSM neglecting the $s_{(x)}$ term. In figure 13h, the sampling sequence, s(x), is multiplied with $psf_{sys}(x)$ which results in a repeated equal spatial frequency spectrum. Each of those spectrum corresponds to the Fourier transform

of $psf_{sys}(x)$. Comparing 13f and 13h one indeed finds that the theoretically correct model (figure 13f) shows a baseband approximately equal to $\mathfrak{F}\{psf_{opt}(x)\}$ while the empirical model (figure 13h) shows a more realistic baseband $\mathfrak{F}\{psf_{sys}(x)\}$.

Since the sampling criterion of equation (22) is satisfied, no overlapping in the frequency representation occurs with the repeating spectrum, thus no aliasing. Aliasing (an artifact) means that lower spatial frequency components (lower compared to the sampling frequency) within the image are changed due to the overlapping of the repeating spatial frequency spectrum where the repetition is caused by the sampling process (Hanson 1986). If, however, as is the case at 10/0.3 objective power (figure 10), where $w_s = 1/0.68 = 1.47 < 2/1.12 = 1.79$ [samples/μm], (equation (22) is not satisfied) than the spectra overlap and $psf_{sys}(x)$ gets distorted.

3.4 Measurements of Sampling Density and Resolving Power

Of particular importance is the determination of the required sampling density given by the chosen objectives. Although this has been theoretically addressed in Section 3.3 and the analysis resulted in the determination of the requirements of the objective NA for a given aperture and the pixel size, these important parameters must also be measured. The issue of sampling density is often not addressed in image cytometry devices where high numerical aperture objectives together with low sampling density of the video camera result in undersampling of the images which causes aliasing.

3.4.1 Method

All measurements were made on the Cell Analyzer Imaging System described by Jaggi et al. (1988). The image of a transmittance compound microscope (Optiphot, Nikon) was sampled by a 3-chip 510 x 492 CCD RGB camera (DXC-3000A, Sony), and digitized by a 512 x 480 x 8 square pixel framegrabber and image processing board (MVP-AT, Matrox). The digital data were averaged in real-time 256 times and stored for processing and display in a 1 Mbyte memory with an overlay buffer (MVP-AT, Matrox). The sampling densities were varied by using different objective lenses (4/0.2, 10/0.45, 20/0.75, 40/0.95, 60/1.4 oil and 100/1.25 oil Plan Apochromat objectives) and projection lenses (relative magnification factors: 1x, 2.5x, 3.3x, 4x, and 5x). The highest existing numerical aperture lenses were selected and the variable numerical aperture condenser were matched to the numerical aperture of the objective. The pixel size of the CCD camera is approximately 17 μm x 13 μm, however, due to the square sampling of the framegrabber, the effective pixel size was measured at 13 μm x 13 μm. The lowest sampling density was 0.32 pixels per micrometer and the highest sampling density was 31 pixels per micrometer, covering the full range of suggested sampling densities. The sampling density for a particular experimental condition was calculated from images of a Zeiss micrometer slide where a known distance of 10 μm was measured in terms of number of pixels.

The resolving power of the system was determined by imaging test slides. At low magnification, Nikon and Zeiss test slides were used on which black lines were engraved at regular intervals (figure 14). These intervals were 10 μm, 3.3 μm, and 1.67 μm respectively. For each slide, the lowest and highest magnifications that either allowed or failed to

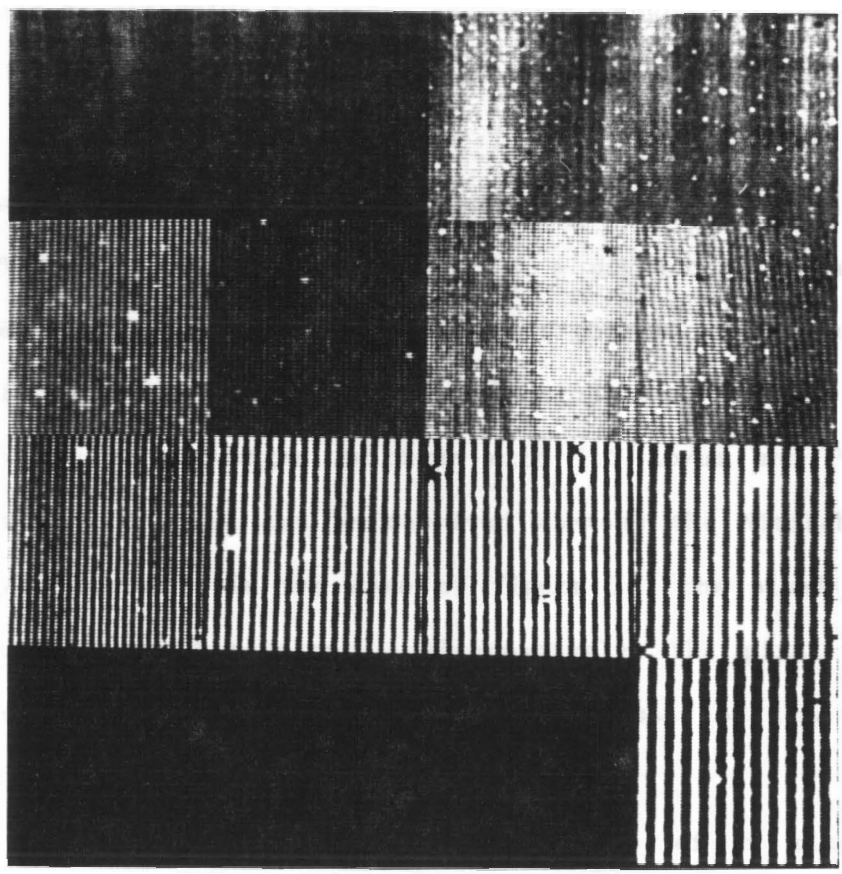

Figure 14: Test Slides to Determine the Boundary Between Resolvable Images and Non-resolvable Images at Different Sampling Densities using 600 line pair/mm Engraving Shown at Various Sampling Densities.

resolve the image were determined. The midpoint was assumed to be the optimal sampling density for that particular resolving power. For higher resolving powers, requiring higher magnifications, the test slides were diatoms (Vinyard 1979; Register and West 1984). The cell wall of a diatom called frustule has a fine structure whose regular patterns have been measured accurately using electron microscopy (figure 15). Eight different diatoms have been used with frustule spacings ranging from 0.25 μm to 1.25 μm (B 25D, Carolina Biological Supply Company). Different diatoms were selected for a particular magnification to determine the upper and lower boundary of the resolving power. All images were digitally stored for analysis and three methods were used to determine if a particular image could still be resolved. The first method was purely visual by looking at an analog RGB 600 line monitor (PVM-1271Q, Sony) to determine if a particular pattern could still be resolved. This method is shown in figure 16 where the frustule spacings of the diatoms Stauroneis Phoenocentron with 14 line pairs in 10 μm (1.4 lp/μm), Gyrosigma Balticum with 1.5 lp/μm and Plurosigma Angulatum with 1.9 lp/μm can be resolved whereas the Nitzschia Sigma with 23 lp/μm cannot. In the case of figure 16, the pixel size and magnification was held constant. Alternatively, the pixel size was varied by changing magnification for the same number of line pairs as shown in figure 14.

The second method involved the analysis of a single line perpendicular to the pattern of the acquired image. The lines could be resolved if one could fit a sinusoidal function through the measured points whose amplitude was above the noise level of the signal. The third method was employing calculations of mathematical features. Texture features such as entropy, variance of intensity, energy,

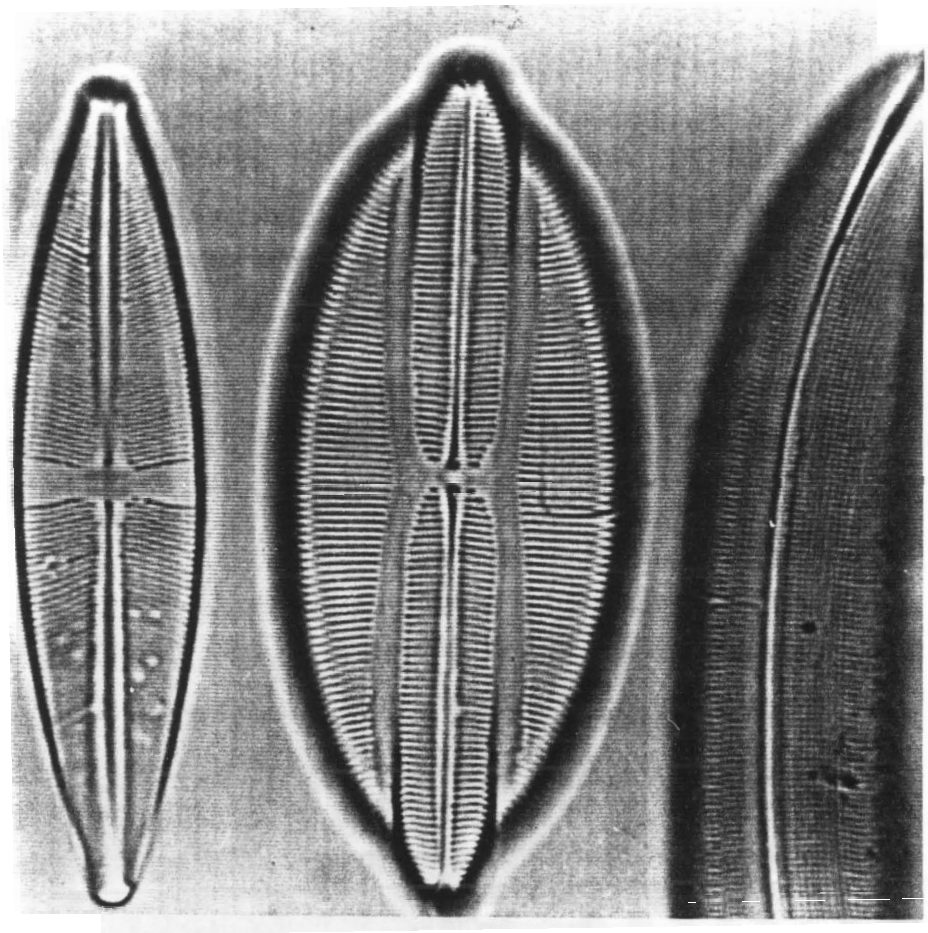

Figure 15: Diatoms Stauroneis Phoenocenteron, Navicula Lyra and Gyrosigma Balticum.

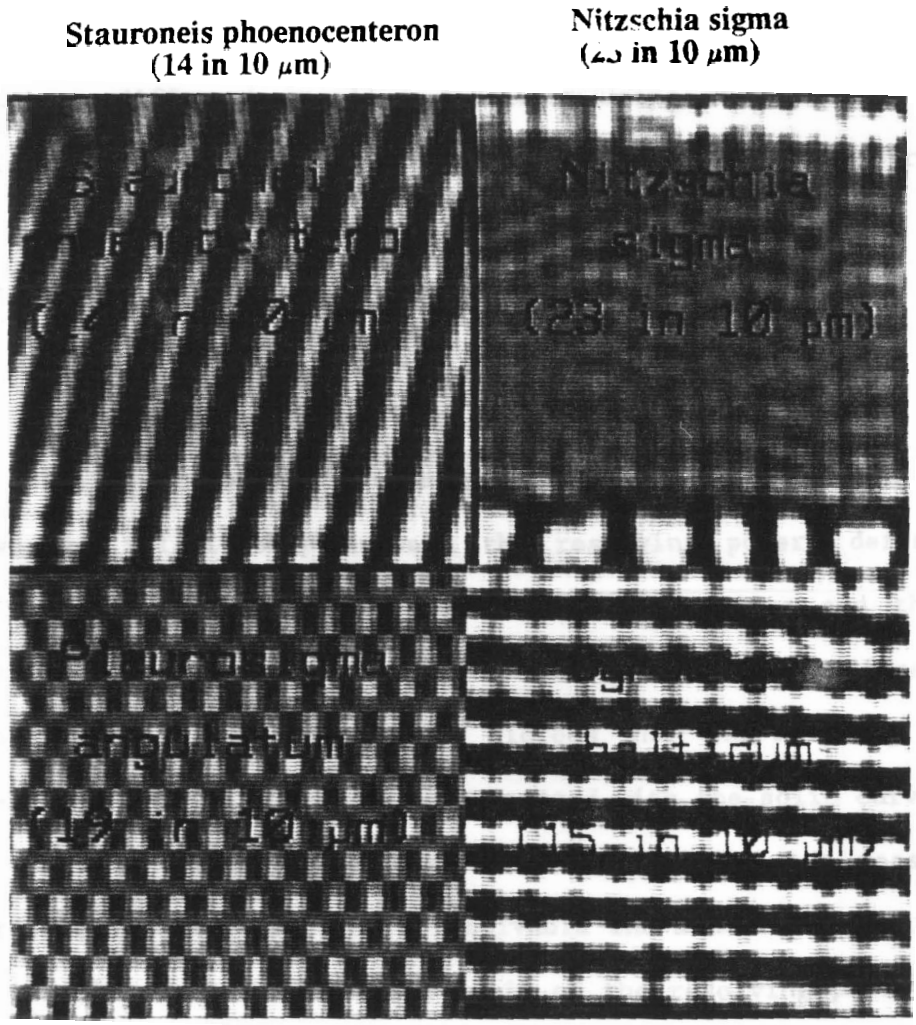

Figure 16: Visual Method using Diatoms to Determine the Boundary Between Resolvable and Non-resolvable Images

homogeneity, and others were calculated for each image (Unser 1986; MacAulay et al. 1989). When the most appropriate features are plotted as a function of pixel density, a sharp transition was observed where the resolving power is lost. The resolving power could be determined at the transition point of these plots. Figure 17 shows an example of the point of transition for the 1.67 μm line spacing (600 line pair/mm test slide) at different sampling densities using the texture features of variance of intensity and energy (Unser 1988). The error bars represent the range obtained by repeating the measurement three times. All three methods gave consistent results as shown below.

3.4.2 Results

The experimental results are plotted in figure 18. The figure shows the relationship between the resolving power, defined as the minimum resolvable distance, R, between two points and the sampling density, S, as determined by the detector and the magnification. The resolving power is measured in microns and the sampling density in pixels per micron. The squares connected with the solid curve represent the measured data. The bars associated with each measured point represent the range between a resolvable and a non-resolvable image and the midpoint is plotted as the limit of the resolving power. From the known values of the resolving power and the associated sampling density, the oversampling constant was computed. The oversampling constants represent the number of sampling points that are taken within the distance, R, and are given in parenthesis at each point. For the purpose of comparison, the width of the system point spread function, $\hat{}psf_{sys}$, in figure 11 is also plotted in figure 18 (circular datapoints).

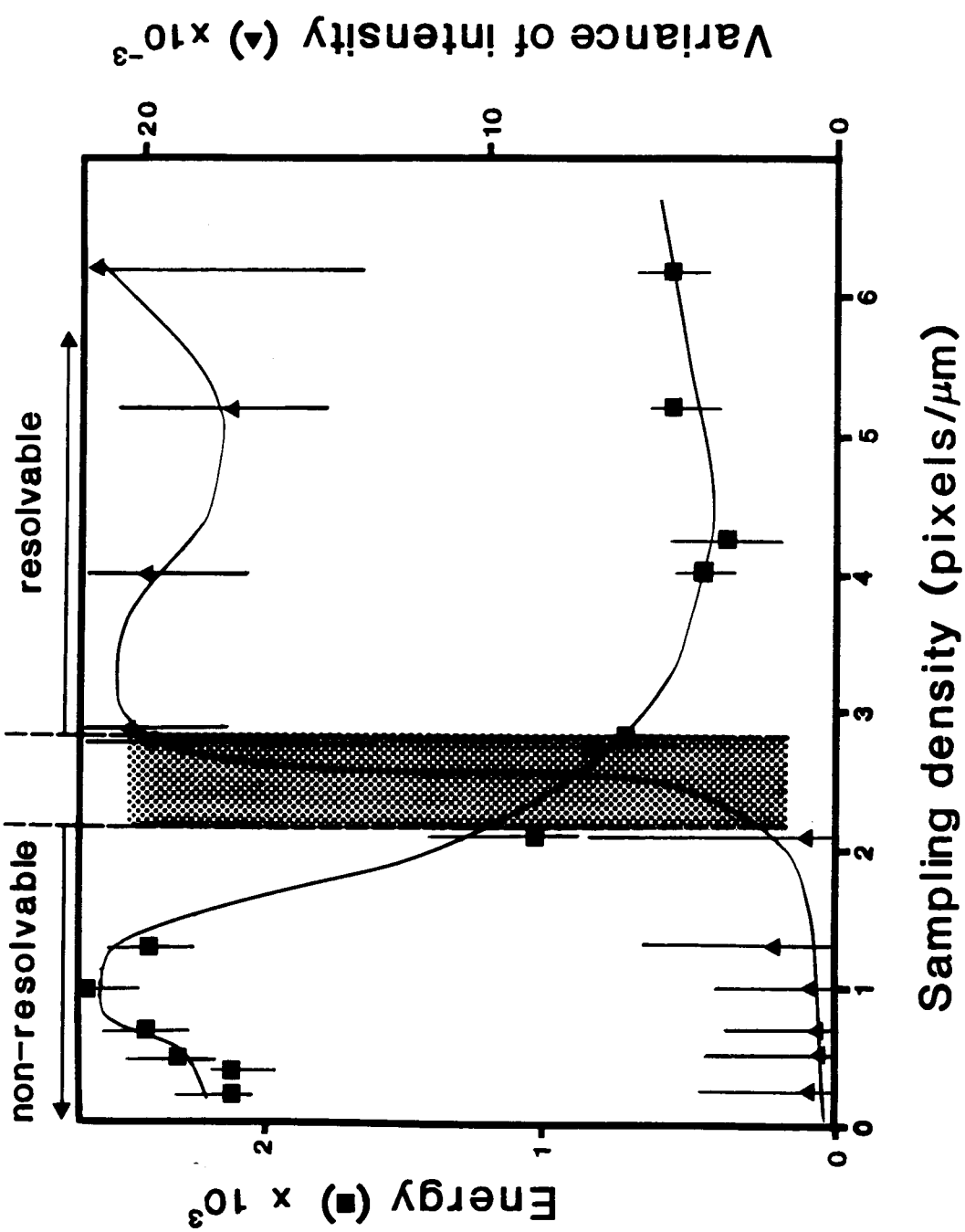

Figure 17: Determination of Boundaries between Resolvable and Non-resolvable Images Using Texture Features (From Jaggi and Palcic 1989, © SPIE).

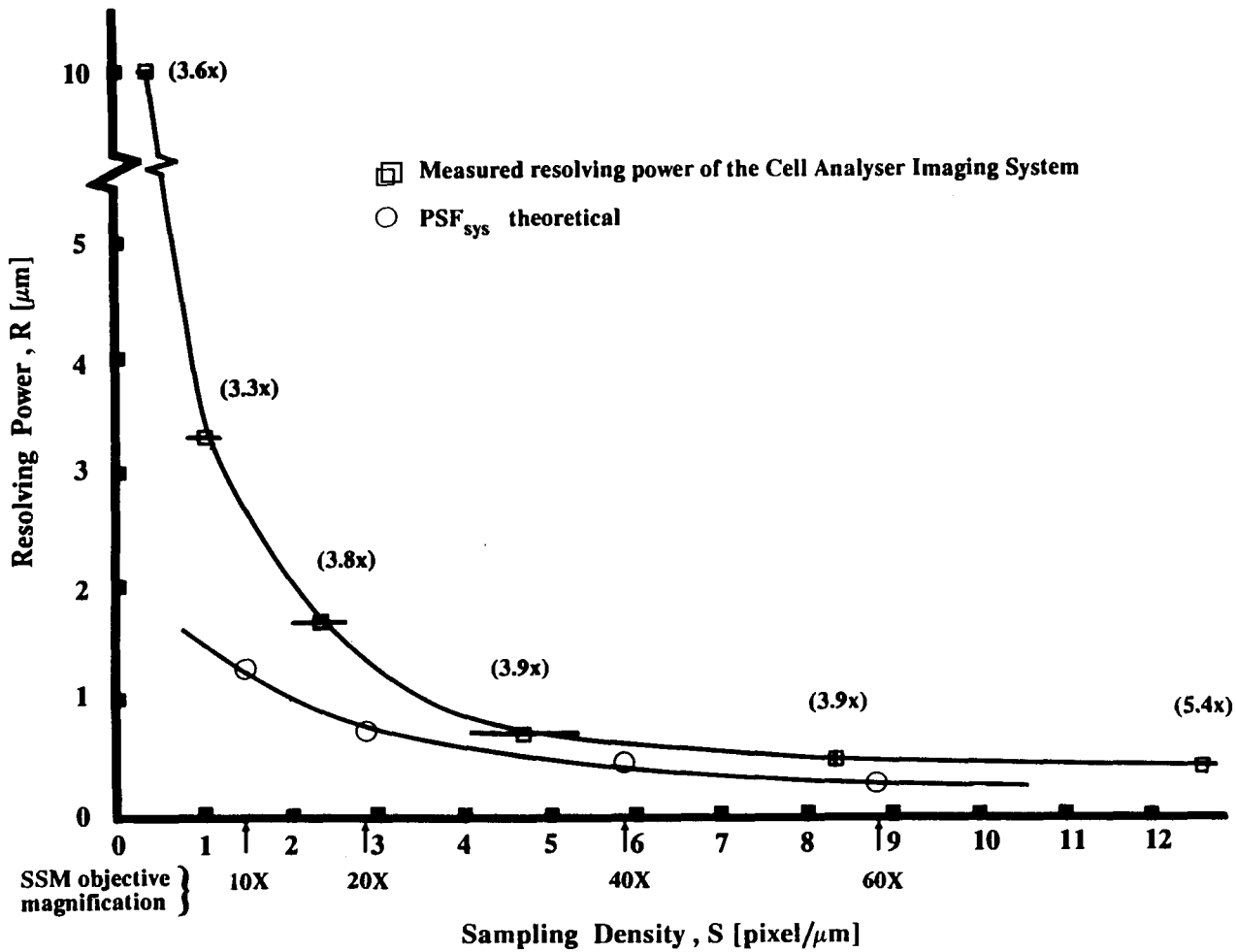

Figure 18: Measured Values of the Resolving Power, R, as a Function of Sampling Density, S, for the Cell Analyzer Imaging System (DMIPS) Compared with Theoretical Predictions for SSM (From Jaggi and Palcic 1989, © SPIE).

3.5 Discussion and Conclusion for Section 3.3 and 3.4

A proper selection of the sampling density is one of the most critical issues in the design of the solid state microscope. The sampling density influences other parameters of the system such as the size of the field of view, contrast, signal-to-noise ratio, and others. For example, while a higher sampling density will yield a better spatial resolution resulting in a more accurate geometry of the image, it will at the same time lower the contrast. Therefore, one must find the best balance between these factors while preserving spatial resolution close to its maximal value. The theoretical model in Section 3.3 and the measured data in Section 3.4 combined allow one to determine the optimal sampling requirement. The theoretical or expected data (circles in figure 18) for the SSM compared with the measured data of the Cell Analyzer image cytometry system (squares in figure 18) show a small but significant and important difference with the SSM being constantly better by approximately 0.2 μm.

The measurements in figure 18 and calculated data of figure 11 suggest that for the specified the SSM design, an oversampling between three to four times is close to optimal and that for the highest numerical aperture objectives at magnifications of 20, 40, and 60X, no aliasing will occur. Further magnification, using a projection lens or a higher magnification objective (e.g. 100X), will not provide any more information. The data also show that for magnifications below 20X, aliasing is expected unless the NA is significantly reduced.

The high sampling density of the CCD which is required in the SSM because of the elimination of the projection lens and the resolution requirements, call for small pixel size. This in turn affects the yield of the electrons generated by photons as the smaller size detector will

collect less of these than a larger one. However, the simple optical path of the SSM will significantly improve the illuminance. Also, illuminance is decreasing with the square of the magnification. For a given resolution, the SSM requires a lower magnification than a conventional quantitative microscope and thus one gains in illuminance. These two factors could greatly compensate for the smaller detector size.

The measurements in figure 18 show that for sampling densities larger than 4 pixel/μm, little is gained in resolving power. The results also indicate that the resolving power is close to the theoretical limit of the first approximation model. Below 4 pixels/μm sampling density, the resolving power decreases exponentially and deviates considerably from the theoretical limit. The measurements of the experimental points in figure 18 were performed by a compound microscope and an RGB camera. Using an SSM, the measured curve should be even closer to the theoretical curves due to higher sampling densities.

CHAPTER 4: PROTOTYPE IMPLEMENTATION

4.1 Overview of Prototype

A prototype was developed to investigate the design and to perform a feasibility study of the solid state microscope. A block diagram of the prototype is shown in figure 19 together with the expected design specifications in Table IV. The prototype consists of three modules: i) the microscope with its associated electronic circuits and stabilized light source, ii) the frame memory with digital interface and gray scale display, and iii) the workstation. The microscope illuminates the sample, acquires and transforms the image into discrete form using a large area, scientific grade CCD. The discrete image is digitized directly and 1:1 mapped via the digital interface into the frame memory for continuous display. The workstation allows one to initialize the system and it provides access to the frame memory to store, process and analyze data. This prototype is an open, modular design in optical, electrical and mechanical terms. There are two basic operating modes: In one mode, the digital image is continuously acquired at rates of 0.7 to 15 frames/s and displayed at a rate of 60 frames/s. In the other mode, the acquired digital image can be frozen and transferred to the main memory of the workstation via its bus. Extensive image processing functions and analysis of the images can then be carried out. For these purposes, an interactive menu-driven image processing program has been developed. The results of these image transformations can be presented on the workstation display monitor by loading the results into the graphics controller. The details of this SSM prototype will be described and discussed in Sections 4.2 to 4.7.

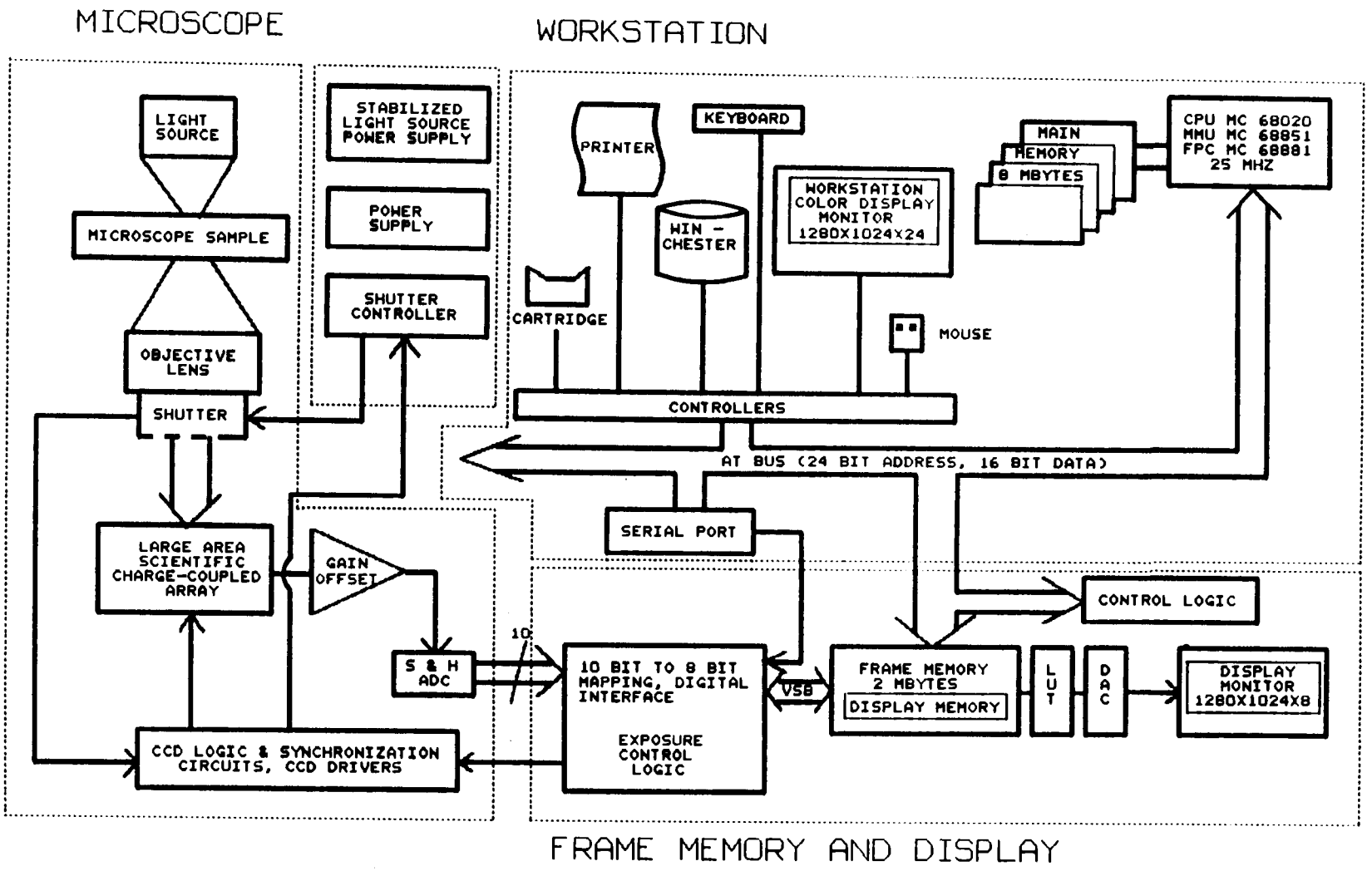

Figure 19: Block Diagram of Solid State Microscope Prototype.

- spatial resolution:	0.34 μm at 60/1.4 objective with negligible distortion
- sampling resolution:	10 samples/μm at 60x magnification
- signal-to-noise ratio:	500:1, 10 bit digitization 8 bit pixel digitization
- spectral resolution:	450 nm to 700 nm with a 30 nm bandwidth
- sensitivity range:	10^{-4} lux for fluorescence to 10^{+2} lux for bright field microscopy
- field of view:	1320 by 1035 pixels or 450 μm x 350 μm at 20x magnification
- image acquisition:	up to 10 Mpel/sec with 10 bits/pel
- image gray scale display:	80 Mpel/sec (60 frames/sec, non-interlaced)

Table IV: Summary Expected Performance Specifications for the SSM. (From Jaggi, B. and Palcic, J. 1989b (modified), © BIS CAP International, former Institute for Graphic Communication)

The approach in the construction of the prototype was to build the image acquisition module, labelled "microscope" in figure 19, starting at the component level. This was necessary because of the uniqueness of the proposed microscope. A conventional microscope system could not have been adequately modified nor is there an appropriate device under development in a scientific laboratory or commercial outlet. Conversely, in the area of large frame memory and high resolution displays, no circuit development was necessary since a number of adequate computer boards are emerging (Wilson 1987). Hence, the optical assembly and all circuits related to the CCD were developed at the B.C. Cancer Research Centre, while the large frame memory and display with high resolution and the workstation were obtained from commercial sources. The latter were evaluated, purchased and system-integrated. System integration required a construction of the digital interface circuit to transfer the digital data from the microscope to the VSB port of the frame memory.

4.2 Optical Path of Image Forming and Illuminating Rays

The light source of the SSM uses Koehler, rather than critical (Nelsonian) illumination. For advanced microscopy systems, the use of Koehler illumination is advantageous (Pluta 1988; Spencer 1982; Bradbury 1984). Koehler illumination, shown in figure 20a, images the light source (lamp filament) at the focal point of the condenser and consequently gives parallel (unfocused) light through the object plane. The light source is a stabilized, dc-driven, 50 or 100 Watt incandescent halogen lamp. To produce an enlarged image of the lamp filament in the condenser focal plane, a collector-lens (sometimes called a Koehler lens) is mounted in front of the light source. The collector lens with

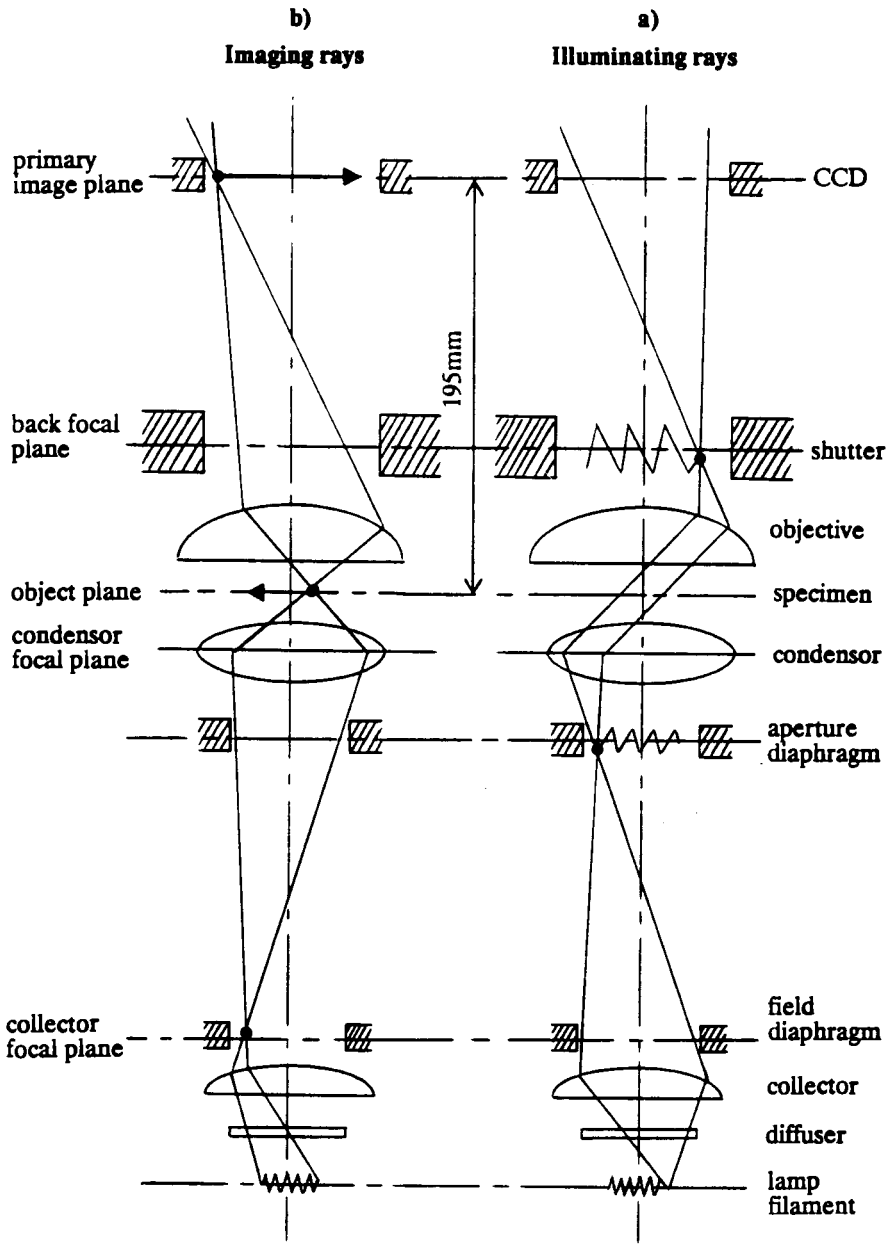

Figure 20: Image Forming and Illuminating Ray Diagram of SSM.

the field diaphragm (iris) serves as a secondary light source by projecting its illumination into the object plane of the microscope. The secondary light source is projected through the object plane by the condenser lens at the focal point wherein the aperture diaphragm is located. Each point of the lamp filament is magnified and produces a column of parallel light at a certain angle to the object plane. The numerical aperture of the condenser can therefore be adjusted with the aperture diaphragm (iris). The field diaphragm (iris) is used to adjust the illumination of the field of view in the object plane. By forming a further magnified image of the lamp filament in the back focal plane of the objective lens, it is possible to provide a wide cone of illumination for optimum resolution and to reduce the effect of dust and imperfections found between the condenser and the objective. The back focal plane projection of the filament in the primary image plane (PIP) means that the illuminating ray will be diffused over the entire field and provide even illumination.

The path of the image-forming rays (figure 20b) shows a real image in the PIP that can be back-projected through the optical system, i.e. the objective, the condenser lens and the collector lens to the filament. By projecting from the object plane back to the field diaphragm, one sees how the field diaphragm determines the width of the microscope field of view. This width is adjusted such that the optical field of view in the PIP is equal to the size of the CCD array. This minimizes glare and other forms of reflections.

An electromechanical shutter is located between the objective lens and the primary image plane. Its function is to block the image projection onto the CCD during the read-out time. This is necessary because the CCD is a full-frame imager, i.e. the same pixel locations

are used for integrating the photon charge as well as the read-out of the image. This results in a large fill-factor (nearly 100%) meaning that the entire CCD area is sensitive to light. The shutter can be opened and closed up to 20 times per second, or even 40 times per second if an appropriate heatsink is installed. A typical opening time is 1.5 ms and a typical closing time is 3 ms. As a consequence, for integration times of the order of a few milliseconds, the center pixels may have a significantly larger integration time than the peripheral pixels. The shutter efficiency, ϵ, i.e. the % difference in exposure time, is given by $\epsilon = 100(1-2t/T)$ where t is the average open/closure time and T is the integration time (Martin et al. 1988). For a typical integration time of 100ms, the shutter efficiency is about 5% which is reasonable since the charge-transfer inefficiency also results in 5% variation. However, at integration times below 20 ms the shutter efficiency becomes too low and the variation in illumination becomes a problem.

The shutter is activated by a TTL pulse, "expose enable/disable", and provides a feedback signal by means of an opto-electric sensing device within the shutter mechanism. This device senses the exact moment of the opening and closing of the shutter. The estimated lifetime of this shutter is approximately 20 million openings and closures. The shutter is the UNIBLITZ 214L19 and is controlled by a shutter driver/timer, Model SD1000 (Vincent and Associates, Rochester, N.Y.). The driver/timer generates the proper solenoid signal for the opening and closure of the shutter when instructed by a TTL pulse. It also generates a standard TTL signal indicating the actual (opened or closed) status of the shutter.

4.3 The Objective Lens

The objective lens is of critical importance. The design considerations and calculations call for a Plan Apochromat ultrawide, flat field objective lens where chromatic aberrations are minimized. Magnification and numerical aperture available are 60/1.4 (oil), 40/0.95, 20/0.75 and 10/0.45. Theoretical consideration based on the point spread functions discussed in Chapter 3 and summarized in figure 11 suggest that a numeral aperture of 0.5 for the 20X and 0.3 for the 10X objective will achieve better results. They are both available as Plan Achomat. All these objectives are from Nikon of the CF type (chromatic-aberration-free optics) and have been developed by Z. Wahimoto (Pluta 1988; Nikon 1985). The new 40, 20, and 10X objectives have an improved resolving power due to an increased numerical aperture. These increases are from 0.85 to 0.95, from 0.65 to 0.75, and from 0.3 to 0.45, resulting in increases of the resolving power from 0.5 to 0.45μm, 0.6 to 0.55μm and from 0.9 to 0.7μm, respectively. These objectives have approximately 20% larger numerical aperture compared with currently available standard objectives and are corrected for several aberrations including lateral chromatic aberration (chromatic difference in magnification) and axial chromatic aberration. The new CF objectives are also corrected for the image curvature and project a flat, ultrawide field (28 mm vs. the conventional 18 mm) into the primary image plane.

The light loss of these objective lenses is decreased resulting in an even brighter field. This is due to a multi-layer coating used to eliminate reflections, thereby reducing glare, flare, and "ghosts" in the optical path. The result of such coatings is an excellent contrast. The objectives have a parfocal length of 45 mm, a mechanical tube length

of 160 mm and the object plane to primary image plane distance of approximately 195 mm (see figure 20). They are available in both the Plan Apochromat for high resolution applications as well as the Plan Achromat for medium resolution applications. Similar objectives have also been developed by Zeiss Jena for use with their quantitative microscopes (Pluta 1988).

4.4 Sensors

The most important element in the SSM is the light transducer. A large-area, scientific CCD is the best choice for the image transducer, taking into consideration optical calculations and other aspects discussed in Chapter 3. Owing to the mass market orientation, the emphasis of the CCD technology is on the TV broadcast standard for which 500 x 500 pixels and 50 to 60 dB SNR with interlaced frame rates of 1/30 of a second (1/60 for a single field) is sufficient. High definition television (HDTV) standards have not yet been defined and although HDTV-CCD are based on increased resolution, they too are being optimized for broadcast requirements. It has been argued, however, that the full potential of CCDs lies far beyond what has been realized by video technology (Janesick 1984). This can be achieved by using scientific CCDs that have been developed with unique requirements, specifically in terms of array size and geometry, SNR at low light intensities, and scanning modes. At present only six of approximately two dozen CCD manufacturers produce large area CCDs adequate for scientific use. Over the past five years, some properties of these have been studied (Janesick 1984; Janesick 1987).

Two recently available CCDs may satisfy the target specifications of large area, small pixel size and high SNR requirements of the SSM.

These are the Kodak KAF-1400 (Stevens et al. 1987) 1,320 x 1,035 pixel and the Texas Instruments (TI) TC215 1,024 x 1,024 pixel arrays. Other CCD manufacturers, such as Thomson-CSF, Ford Aerospace and Tektronix have also announced 1 Mpixel chips, but are not able (or willing) to supply high grade samples with no faulty pixels. Furthermore, the pixel size of the latter are too large. Specifically, the Thomson-CSF THS31156 has the pixel area of 19 μm x 19 μm and Grade A (no faults) is not available. The Ford Aerospace VS1024 has the pixel area of 12 μm x 12 μm, is an experimental transducer and commercially not available while the Tektronix and Reticon both use larger pixel areas of 27 μm x 27 μm.

The present versions of Kodak and TI CCDs are equally suitable for the SSM. The main differences are in the sampling resolution and spectral response due to different manufacturing technologies. The Kodak CCD has a pixel area of 6.8 μm x 6.8 μm while the TI CCD pixel area is 12 μm x 12 μm. Although the TI chip has a larger pixel area, both CCDs have the same 60 dB signal-to-noise ratio. For the development of the SSM, the Kodak chip will be used because of its higher sampling density at similar SNR and because the Kodak chip is based on a relatively mature CCD technology. The Kodak (Martin, Womack and Fischer 1988) and TI (Model MX-1000 W FF) large area CCDs are now also available in the camera form, but the cameras do not satisfy the SSM image acquisition and scanning requirements. In particular, further development is required pertaining to the scanning modes, signal-to-noise ratio, readout rates, and digitization accuracy.

The Kodak charge-coupled device (KAF-1400) is a 1,320 (horizontal) x 1,035 (vertical) element full-frame CCD imager. This chip is manufactured by the Microelectronic Division of Eastman Kodak

(Rochester) for research purposes, and for some particular high resolution scientific monochrome imaging (Stevens et al. 1987; Chang et al 1988). The output buffer bandwidth, f_{-3dB}, is 45 MHz, making it possible to clock the device at 20 MHz and thereby generate 15 frames/s. The saturation charge per well or pixel is approximately 70,000 electrons and the noise level is 15 rms (root mean square) electrons at 27^{o}C. However, the noise level including the read-out noise is 50 rms electrons bringing the actual dynamic range to about 60 dB (KAF-1400 data sheet, 1988).

A functional block diagram of the KAF-1400 chip is shown in figure 21. The various input and output signals together with the reference voltage levels are also shown as implemented in the SSM prototype. Figure 22 shows the implemented timing signals used to operate the device. An image is obtained as a result of each CCD pixel collecting electrons by means of the photo electric effect (Streetman 1980). Spatial information is given by the pixel location and intensity information is given by the amount of electron charge collected in the pixel well (depletion region). During the integration time, the electrons are collected under the ϕV_1 = high. The amount of the charge stored is a linear function of the light intensity and integration time, and a non-linear function of the wavelength. To transfer the charge vertically, the two-phase complementary clock, consisting of ϕV_1 and ϕV_2, shifts to ϕV_2 = high causing the charge to move towards ϕV_2. Coupled with ϕV_2 is the transfer gate (TG) which allows transfer of the first row into the horizontal shift register. ϕV_1 and ϕV_2 are altered again such that all charges have now moved by a complete pixel width. The charges transferred to the horizontal shift registered are clocked out via the horizontal two-phase complimentary clock ϕH_1 and ϕH_2. The

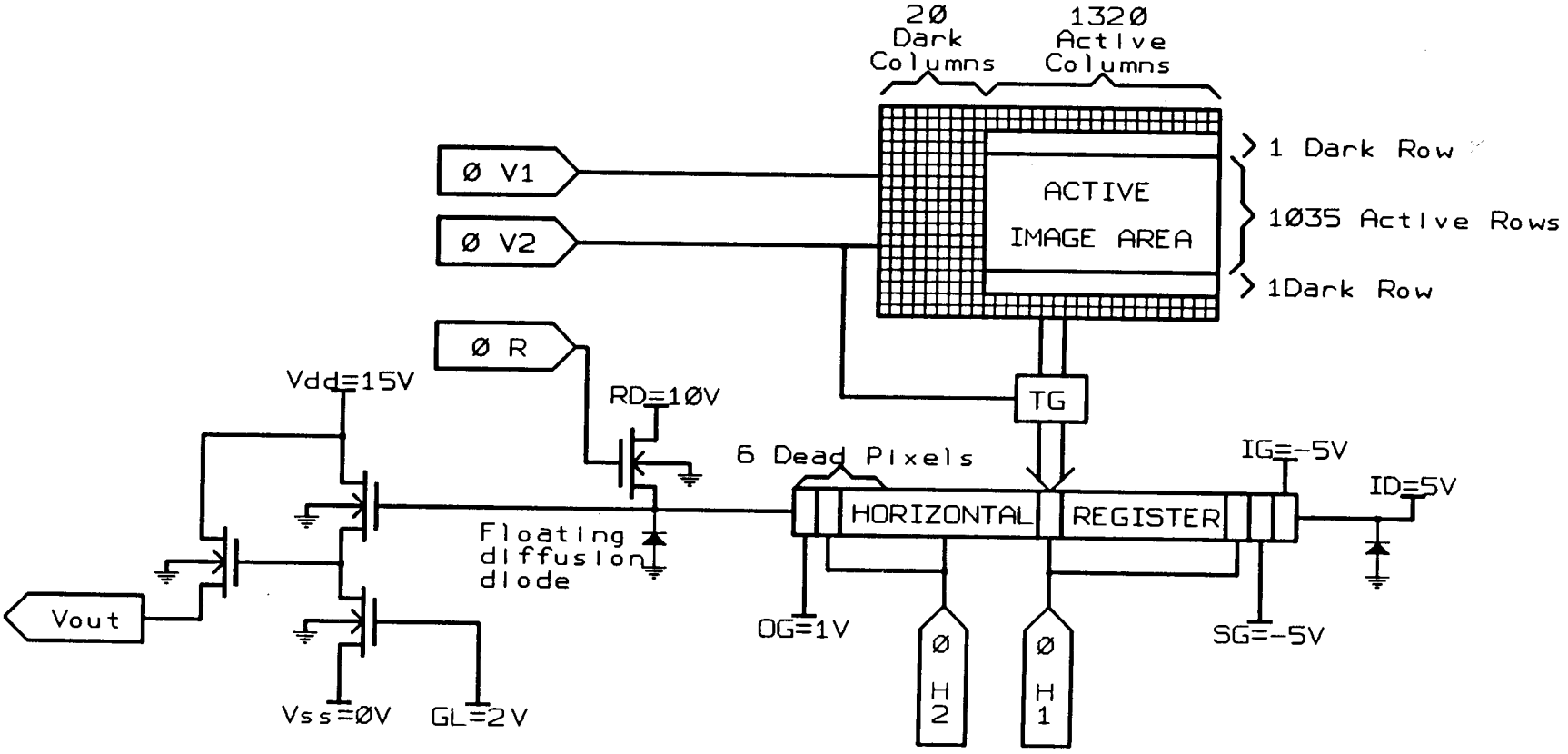

Figure 21: Functional Block Diagram of the CCD Array based on the KAF-1400 data sheet 1988.

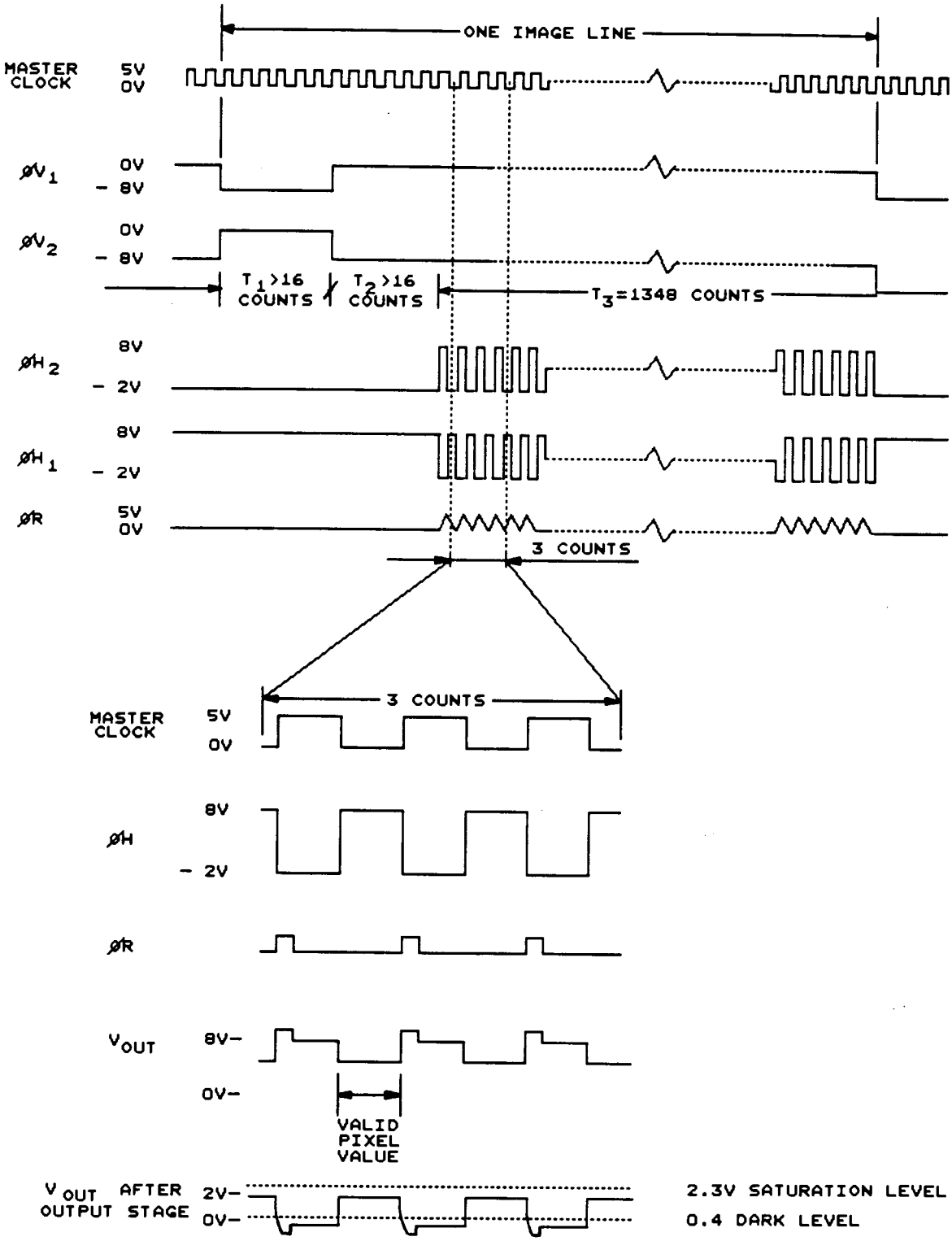

Figure 22: Timing Diagram for the CCD Array.

electron charges of each pixel are clocked out and sensed by a floating diffusion diode. The voltage potential of the electron charges, ΔV_{FD}, depends on the amount of charge contained in each pixel. $\Delta V_{FD} = \Delta Q/C_{FD}$ where ΔQ is the electron charge from the pixel and C_{FD} is the capacitance of the floating diffusion diode. This voltage level is buffered by a NMOSFET, two-stage source follower configuration that has a gain of A_v. Thus, the output voltage is equal to $A_v \Delta Q/C_{FD}$. A reset pulse, ϕR, connected to a switching NMOSFET resets the floating diffusion potential. The inputs IG, ID, and SG are for diagnostic purposes of the horizontal shift register. The remaining inputs V_{DD}, V_{GL}, V_{SS}, and V_{SUB} supply the CCD with appropriate voltage references. The basic cycle to shift a vertical line into the horizontal shift register and clock that horizontal shift register out, through the floating diffusion arrangement and the two source follower, is repeated 1,037 times of which the first and last line are dark lines and not part of the image. The horizontal shift register contains 1,348 sites of which 1,340 are functional and 1,320 are imaging pixels.

To take full advantage of the detector capabilities, its integration time should be variable and thermally generated charge (dark current) must be minimized. Variable integration time is easy to accomplish with full frame CCDs and dark current can be minimized by cooling the CCD or using it in the multi-pinned phase (MPP) mode which is also referred to as the accumulation mode. By cooling the CCD devices, a dynamic range of up to 10^6 can be achieved (Jaggi and Deen 1988; Pontifex et al. 1988). In the case of the MPP mode, ϕV_1 and ϕV_2 are both low 95% of the integration time. This is different from the standard signals shown in figure 22. In the MPP mode the number of thermally generated electrons in the interface region, which is the main

source of dark current, is minimized (Burkey and Chang 1989). Bredthaurerer from Ford Aerospace, Atkins from Photometrics, and Chang from Eastman Kodak have reported (Electronic Imaging West '89, 1989) a 25 to 100 fold reduction of dark current using this technique. However, the use of MPP technique also slightly decreases the full well capacity of the CCD.

4.5 CCD Logic, Drivers, Synchronization, Output Stage and Analog-to-Digital Converter

Electronic circuits associated with the CCD are part of the microscope as shown in figure 19, and provide high speed 10 bit digital data representation of the microscope images. An exposure pulse, initiated by the workstation, is generated by the digital interface to synchronize these circuits and the shutter. A functional schematic diagram of these circuits is shown in figures 23, 24, and 25.

The goal of the CCD logic and driver circuits, figure 23, is to generate ϕV_1, ϕV_2, ϕH_1, ϕH_2 and ϕR as they have been specified in figure 22. The timing sequence generated by the CCD logic circuit is based on three cascaded DM74AS161N synchronous, presettable binary counters which count 1,348 pulses. The output of the counters is connected to two 8-bit SN74LS688N comparators preset at 16 and 32 counts and two 74AS74N D Flip-Flops. These circuits enable and disable the master clock driving the ϕH_1 and ϕH_2 signals since they have to be enabled for 1,348 clock pulses and disabled during the horizontal retrace and integration time. The comparators also generate a signal, synchronized with ϕH, to drive ϕV_1 and ϕV_2 during the horizontal retrace time by 16 and 32 counts. The ϕR signal resets the floating diffusion gate and is synchronized with ϕH. ϕR uses a timing delay circuit to generate a pulse width that is a

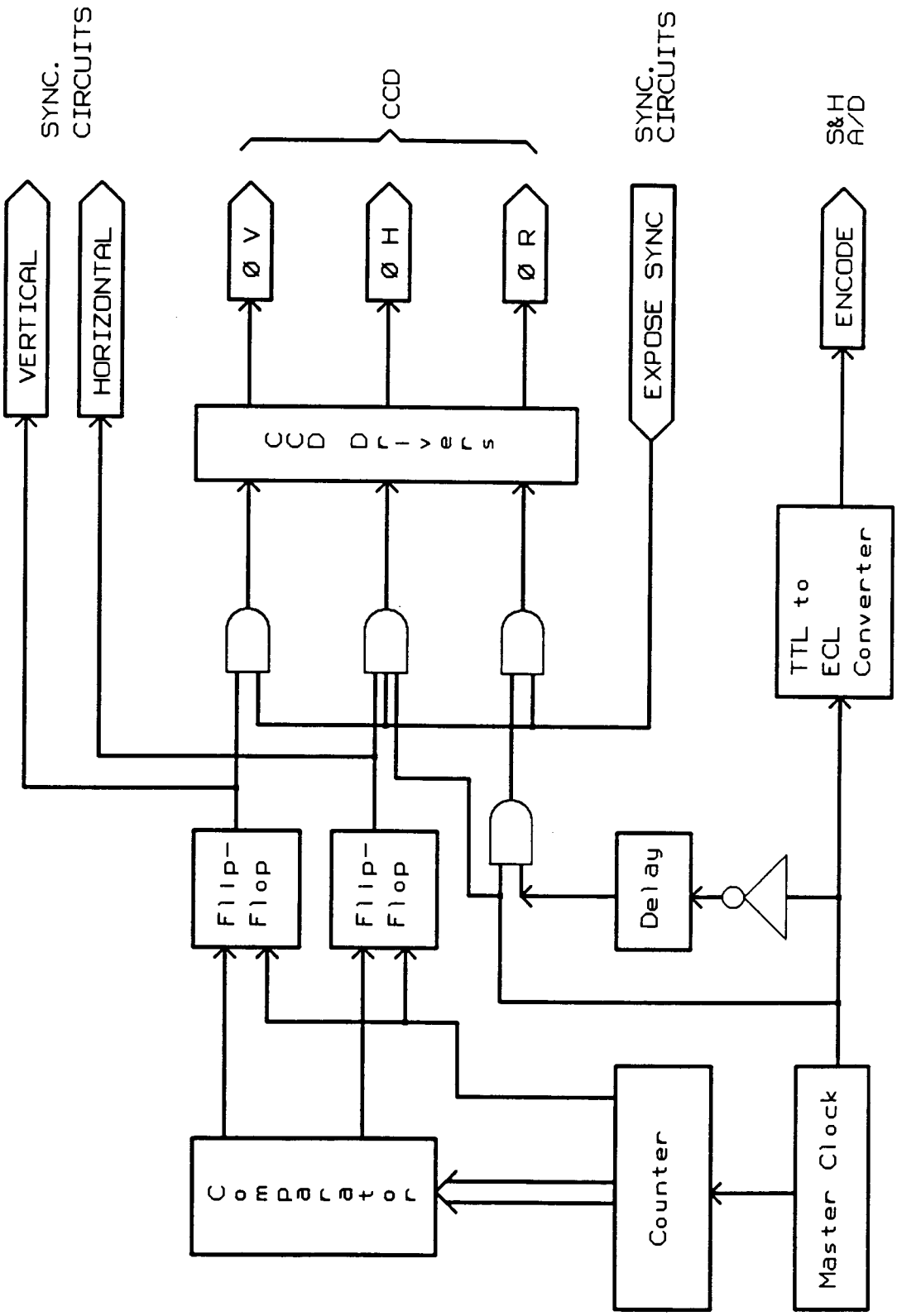

Figure 23: Functional Schematic of the CCD Logic and Driver Circuits.

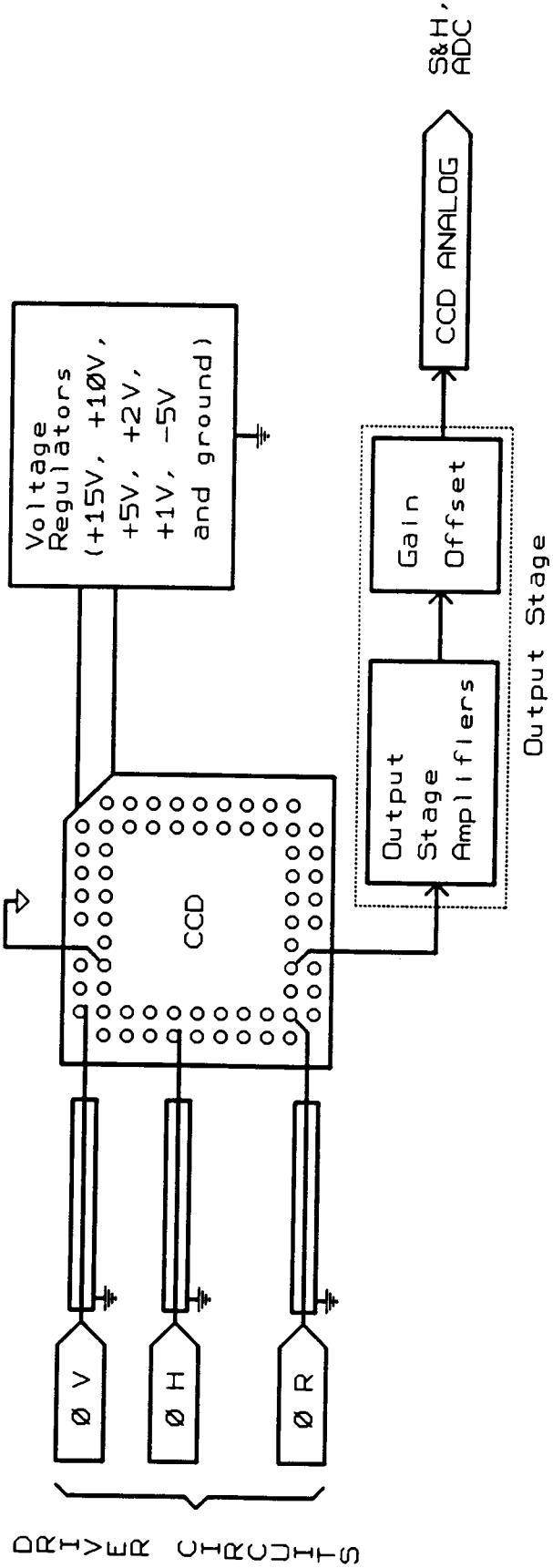

Figure 24: Functional Schematic of the CCD and Output Stage.

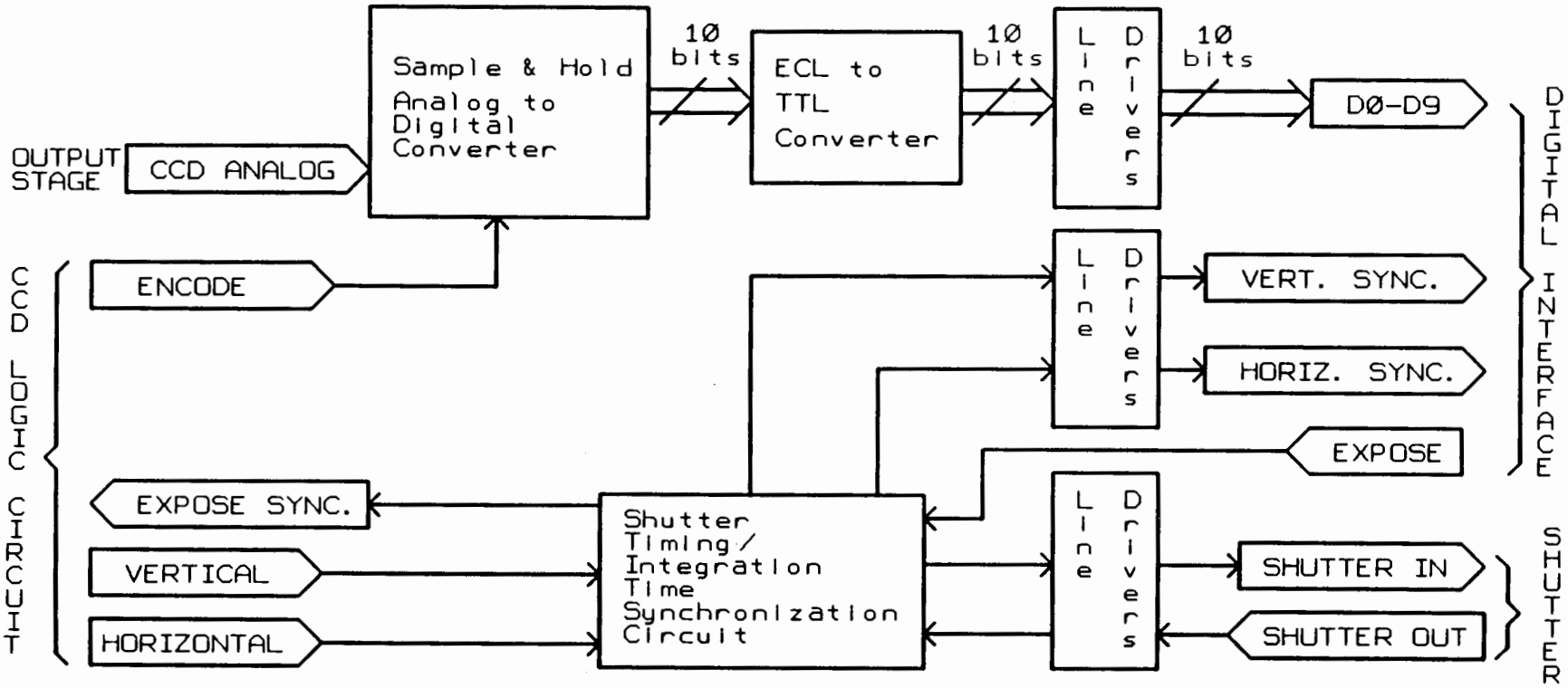

Figure 25: Functional Schematic Diagram of the CCD Synchronization and Digitization Circuits.

fraction of the master clock. Using a number of AND and OR gates, the ϕV, ϕH, and ϕR signals are enabled by the "expose sync" pulse which disables the signals when the CCD is integrating. Large voltage differentials are required by the CCD in order to shift the charge efficiently, i.e. to maximize the charge transfer efficiency. The voltage levels shown in figure 21 and 22 are those currently used. The signals are generated with MOS-based DSO026 or CMOS-based TSC0026, 5-10 MHz drivers. They convert the TTL signal sequences generated by the CCD logic circuits into large amplitude pulses. The TTL ϕH signal is also connected to a TTL-to-ECL MC10H124 convertor to generate the "encode" signals for the analog-to-digital converter. The master clock for the digital board currently uses a Wavetek 50 MHz pulse/function generator (Model 166) which will be later replaced with a thick film hybrid technology 1 to 10 MHz TTL clock oscillator.

The CCD is positioned in a 68 pin grid array (PGA). It is located together with the voltage regulators and output stage amplifier on the analog speedwire board (initially bread board) (figure 24). The voltage regulator is based on the linear LM10CN operational and reference amplifier. The output stage is using an emitter-follower that is biased with a J511 current regulator diode. This amplifier is followed by a high slew rate operational amplifier (HA2542) to set gain and offset such that the output signal ranges from 0 to 2V. This amplifier has a gain-bandwidth product of 70MHz and hence provides for low gains a constant gain from dc to 20MHz resulting in good linearity. The output voltage of the amplifier corresponds to the input range of the analog-to-digital converter (ADC). Located on a separate board with its sample and hold circuit (S&H), the ADC is based on ECL logic (figure 25) and was purchased from Analog Solutions (ZAD1025). The CCD analog signal is

sampled at the time determined by the "encode" command generated by the CCD logic circuit. The analog input signal is digitized to 4-bits using an high-speed (approximately 60 MHz) flash converter. Its output is applied to a 4-bit, video speed, digital-to-analog converter (DAC). The output signal of the DAC is subtracted from the delayed input signal. The result of the subtractions is then digitized by a 7-bit flash converter. The 4-bit approximation and 7-bit conversion are combined to provide a 10-bit output. This architecture is called Digitally Corrected Sub-Ranging (DCSR) and is designed for a high speed, high precision digitization. The 10-bit digital data is converted from ECL-to-TTL using MC10H125s.

The synchronization circuit on the digital board generates an "expose sync" signal (figure 25) which drives the CCD. This circuit also drives the shutter. "Expose sync" is driven by "expose" from the digital interface and takes into account the shutter feedback as well as dV and dH.

In the design of all these circuits a number of critical aspects had to be addressed: i) variable CCD driver voltage levels and timing delays, ii) high frequency, iii) minimization of noise levels, iv) large voltage differentials and v) accurate timing. The voltage levels and timing of the signals had to be optimized through various circuit adjustments in order to increase charge collection efficiency, to reduce crosstalk (overflow of charge into the neighbouring pixels) and noise. Due to the high clocking frequency of 1 to 20 MHz (initially 1MHz followed by 10MHz and eventually 20MHz) the following considerations were taken into account: high speed logic, impedance matching circuitry, short connection lengths, metal film resistors, tantalum and ceramic decoupling capacitors and minimization of the number of

integrated circuit components. The CCD logic, driver and synchronization circuits are housed on the digital speedwire board (initially breadboard) having a large ground plane and were, therefore, separate from the analog and the ADC boards. The above rules followed in the design of these boards are based on "Noise Reduction Techniques in Electronic Systems" by Ott (1987).

4.6 High Speed Digital Interface, Frame Memory and Display.

The high-speed digital interface between "microscope" and "frame memory" was designed and developed to input digital data asynchronously at a rate of 1 to 10 Mbytes/s. This interface also contains a circuit which determines the integration time and generates the "expose sync" pulse. It is housed on a speedwire board in a workstation (Section 4.7) together with the frame memory board. Due to the physical separation of "microscope" and "digital interface", two differential line drivers/receivers (AM26LS31 or AM26LS32) are required between those two units.

The frame memory and display controller is an AT-bus based board (UDC-2600, Univision Technologies). This board has a 2 Mbyte display memory of which 1,280 x 1,024 x 8 bits can be displayed together with two overlay bits. The display is an RS343 video output and provides a 60 Hz non-interlaced frame rate. The memory is accessible via an external digital port or alternatively interacts with the host computer through the AT-bus. The access to the digital port of the frame memory is provided by the high-speed video standard bus (VSB) protocol. The VSB host can transfer data to the UDC-2600 at rates of 10 Mbytes/sec. The board is controlled by an INTEL 82786 graphics controller and is also equipped with an output look-up table (LUT), for gray scale

conversion, a DAC, and video drivers for image display. An appropriate large screen high resolution fine pitch gray scale monitor (Philips 2064M) is used to display the image. It is based on the RGB RS343 video standard and has a bandwidth of 110 MHz. This monitor provides a standard display format of 1280 x 1024 x 8 with two bits of overlay. The last 40 columns and the last 12 rows (56,800 pixels) of the CCD will therefore not be displayed, although they are digitized and can be stored in the frame memory. At a later time, the display driver and monitor adjustment will be made to fit the whole screen by slightly increasing the display driver clock.

The data flow is controlled by limiting the access to the VSB bus and ignoring irrelevant data. Hence, once the circuits and workstation is turned on, the data is transferred to the interface board, but ignored until a scan is initiated. The interface circuit can be best understood through a flowchart describing the acquisition of a digital frame which is shown in figure 26. A frame scan is initiated through the Apollo serial port and synchronized with the expose counter and at the start of a frame. This enables the VSB communication protocol logic to send a starting address and the pixel data to the UDC-2600. The pixel data is continuously buffered in FIFO registers. Only valid data is put onto the VSB bus, however. Dark and dead pixels and pixels that fall outside the 1280 x 1024 array are ignored. Data is acquired pixel by pixel and sent in blocks of 4 pixels to the UDC-2600. The end of the line is detected with a horizontal counter that generates the X-address and the end of the frame is detected with the vertical counter that generates the Y-address. A functional schematic diagram of this digital interface circuit is shown in figure 27. All inputs from the CCD logic and ADC circuits are buffered using AM26LS32 line receivers. For data

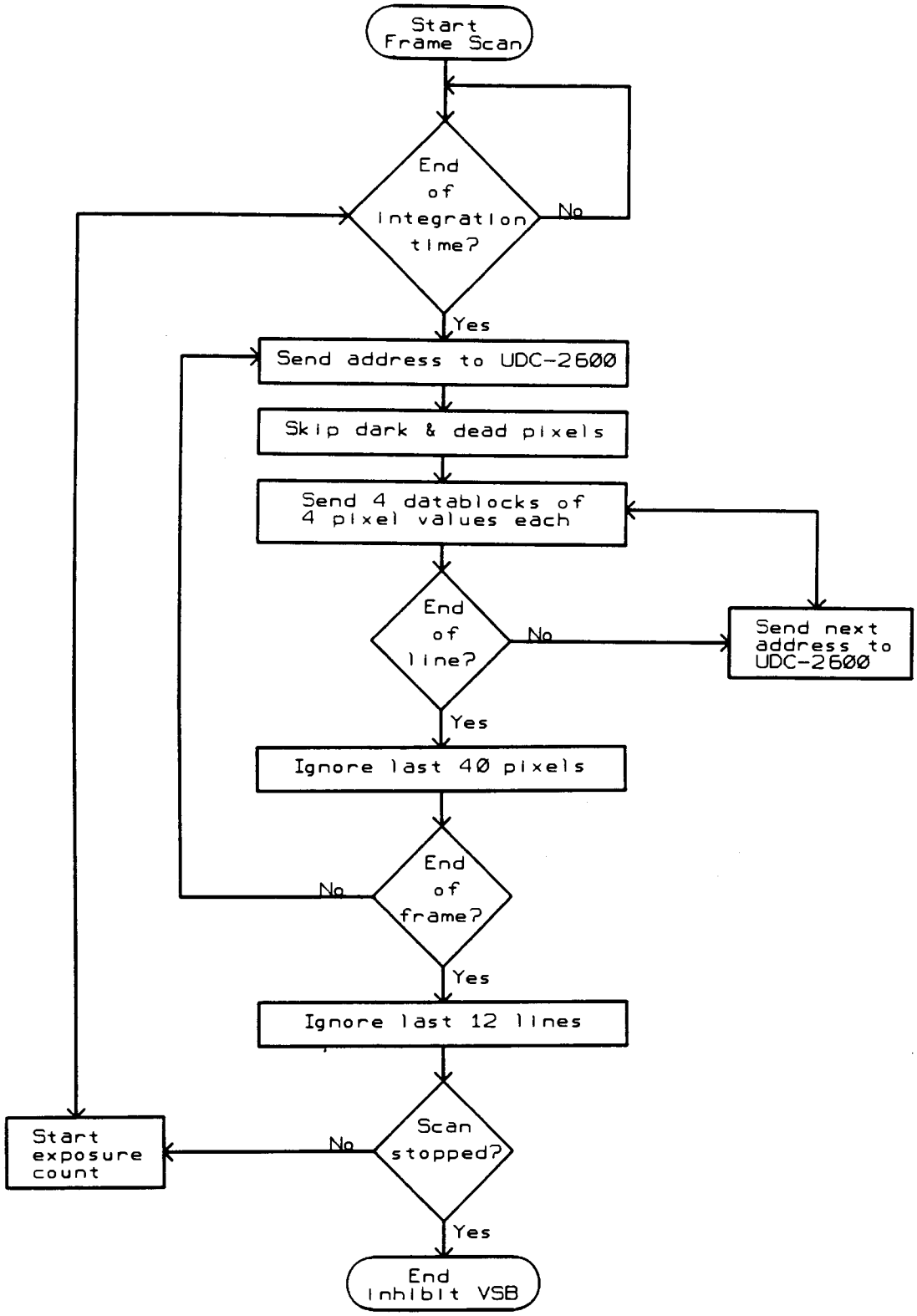

Figure 26: Flowchart of Dataflow for Image Transfer from the Microscope A/D Output Port to the Video Standard Bus.

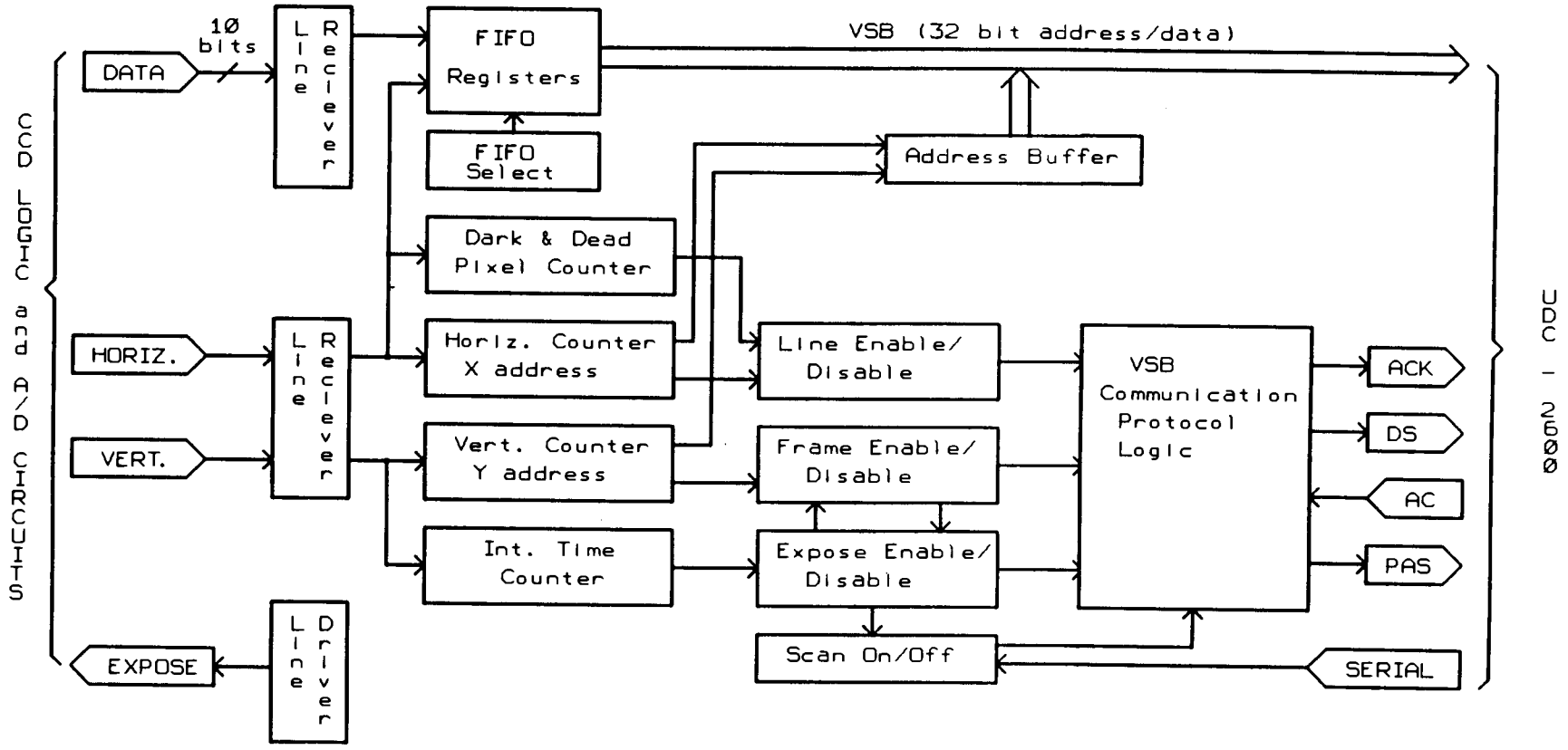

Figure 27: Functional Schematic Diagram of the Digital Interface Circuit.
(from B. Pontifex, B.C. Cancer Research Centre).

buffering, four IDT7201 512 x 9 FIFOs (first-in-first-out) registers are used. Their output is tri-stated to the VSB and so are the SN74LS373 address buffers. The FIFOs are selected using the SN74LS139 2 to 4 decoder. All counters are based on the SN74LS161 to count the number of dead and dark pixels, the horizontal pulses, vertical pulses and the integration time count. To enable and disable a line and/or a frame, comparators are used which are set at 1,280 divided by 4 for the line enable and 1,024 for the frame disable. The VSB communication protocol circuit is based on a number of AND and OR gates as well as SN74LS74 Flip-Flops.

4.7 The Workstation

For control, development, image processing and display purposes, an Apollo DN4000 workstation was chosen as the host computer. This workstation is based on a PC/AT compatible interface bus which is required by the UDC-2600. On the bus, a graphics controller is connected to display a 1,280 x 1,024 x 24 bit (color) image. For back-up and archiving purposes, a number of storage devices, such as a 60 Mbyte cartridge tape and a Winchester hard-disk drive of 155 Mbytes are connected through appropriate tape and disk-controller. Also, serial ports are linked to the bus. One of these is used to indicate to the digital interface that the microscope image acquisition is to be initiated. The actual CPU is composed of a Motorola 68020 CPU, a 68881 FPU and a 68851 MMU, all running at 25 MHz. Currently, the main memory contains 8 Mbytes and can be expanded up to 32 Mbytes. A processing power of 4 Mips has been measured on this workstation and 1320 x 1035 x 8 images can be transferred to main memory from the frame memory in 2 s.

The transfer time to the graphics controller from the main memory is 4 s.

The Apollo DN4000 runs under Domain/IX Unix System compatible with AT&T's system and for programming, Domain C version 4.89 (Apollo) is used. An interactive program (IMGPRO) has been developed by S.S.S. Poon of the B.C. Cancer Research Centre, to access the frame memory (UDC-2600), to process and analyze the images, and to display the images on the workstation monitor. For this purpose, software drivers had to be developed to communicate with the UDC-2600. The functions involved in setting-up and running the UDC 2600 are i) to link UDC 2600 control, data and status registers with Apollo virtual memory, ii) to reset and program the Intel 82786 graphics chip and iii) to set the output look-up table (LUT). IMGPRO was developed with these routines and windowing functions based on the paper by Jaggi et al. (1988). The main purpose of this program is to facilitate image evaluation using gray level and gradient histograms to determine noise level distributions, bit plane color to visualize noise levels, and various mathematical transformation to enhance faulty pixels and non-linear effects.

4.8 Mechanical Structure and Layout

In the prototype SSM, three physical modules are envisioned. The first represents the microscope with its optics, transducer and electronic circuits. The second is composed of a 19" control rack housing the stabilized light source power supply, the shutter controller and the power supplies for the circuits. The third module is the workstation, housing the digital interface and the frame memory with the two monitors. The mechanical structure of the microscope is based on an optical bench (Spindler & Hoyer). This design provides high stability,

large degree of flexibility and optical accuracy. The stability and accuracy is a result of the rigid structure inherent to optical benches and the horizontal layout. The large degree of flexibility is provided by the open structure of optical benches and will be important for further work in fluorescence, and inverted and reflectance SSM modes.

CHAPTER 5: DISCUSSION

One of the manifestations of the research and development in visible light microscopy has been the emergence of quantitative, digital microscopes which form the basis of modern image cytometry. The development of the Solid State Microscope was prompted by the realization that existing image cytometry devices do not provide data of the quality required in analytical cytology and other biological and medical applications. Hence, in this design, recent advances in the optics of objective lenses, VLSI large-area CCD arrays, high-speed image processors with associated large image frame memories, and high resolution display systems were exploited to overcome some of the previously discussed deficiencies.

The SSM design encompasses all the advantages of visible light microsopy, but emphasizes the quantitative rather than the qualitative aspects. In the design a system analysis approach based on Fourier theory and experimental verification allowed determination of the optimal requirements for the two key components, the objective lens and the charge-coupled device. In this respect, the crucial parameters are the sampling density and resolving power which directly relate to resolution and accuracy. Significant advantages of the SSM are the resolution near the diffraction limit with a high SNR, the large field of view and the dynamic range which makes it possible to capture fluorescence and bright field images.

5.1 Limitations of the SSM Design

The key issues in quantitative microscopy are the spatial resolution, signal-to-noise ratio (photometric contrast), field of view,

as well as spectral resolution and dynamic range. Spatial resolution of the SSM is limited by the optical properties of the objective to 0.29 μm. The limitation on the SNR is given equally by all system components achieving an SNR_{sys} of approximately 500:1. This determines the useable gray level resolution, that is the number of bits per pixel. For the SSM, this is 8 bits even though 10 bit data is available. The field of view is limited by the CCD array size requiring an integrated circuit with more than a million elements. Hence, the array size is restricted by the manufacturing technology of VLSI-CCD arrays. The spectral resolution is limited by the spectral response of the CCD since this transducer is generally significantly less sensitive in the blue than in the red. The dynamic range of the SSM is determined by the electron noise floor and the full well capacity of the CCD as well as by the available light. The minimum number of optical surfaces and the single lens magnification result in relatively small attenuation of light intensities. In bright field microscopy, the amount of light is limited only by the power output of the light source. However, light exposure, particularly at shorter wavelengths, could damage live cells. The sensitivity of a cooled CCD or one that is driven by an MPP circuit can be greatly increased by larger integration times. There are several limitations in the use of long integration time in measurements of cellular properties. In live cells, cell movement limits the duration of the integration time to seconds. In measurements of fluorescently labeled cells, the integration time is often limited to a fraction of a second due to photobleaching. Autofluorescence too, makes larger integration times impractical. Despite the above, the dynamic range of up to 10^6 can be achieved and used practically in most applications.

5.2 Status of the SSM Prototype

The SSM prototype, as described in Chapter 4, is fully operational. However, rather than an optical bench, a "stripped down, upside down" microscope is used to provide Koehler illumination and a microscope x,y,z stage. This experimental configuration also provides a structure for an objective lens to project an aberration free image in the primary image plane. Quantitative microscope images can be acquired near the theoretical resolution limit at scanning rates of 1 Mpixel/s. One of the first SSM images of a diatom, photographed from the microscope gray scale monitor, is shown in figure 28 and indicates much detail considering the submicron scale. Since spatial resolution, field of view and signal-to-noise ratio are the three most critical parameters in quantitative microscopy, preliminary measurements of these parameters were performed first.

The resolution limit of the SSM was determined using known diatom frustal patterns as was described in Section 3.4. A number of diatoms were acquired and analyzed in order to visually determine the resolution limit. Three of these diatoms (Didymosphenia Geminata, Gyrosigma Attenuatum and Surinella Fastuosa) were transferred to the workstation monitor for display. The smallest frustal spacing of 0.7 μm/lp (Gyrosigma Attenuatum) is seen with a good contrast as is shown in the photograph of figure 29. The preliminary data also indicate that the frustal spacing of the Nitzschia Sigma of 0.43 μm/lp can be detected without using any image enhancement techniques. It should be noted that these diatom patterns represent a far more difficult task for an image acquisition system than the simple two point resolution criteria.

To illustrate the large size of the field of view, an image of a calibration slide at a total magnification of 20X and an effective pixel

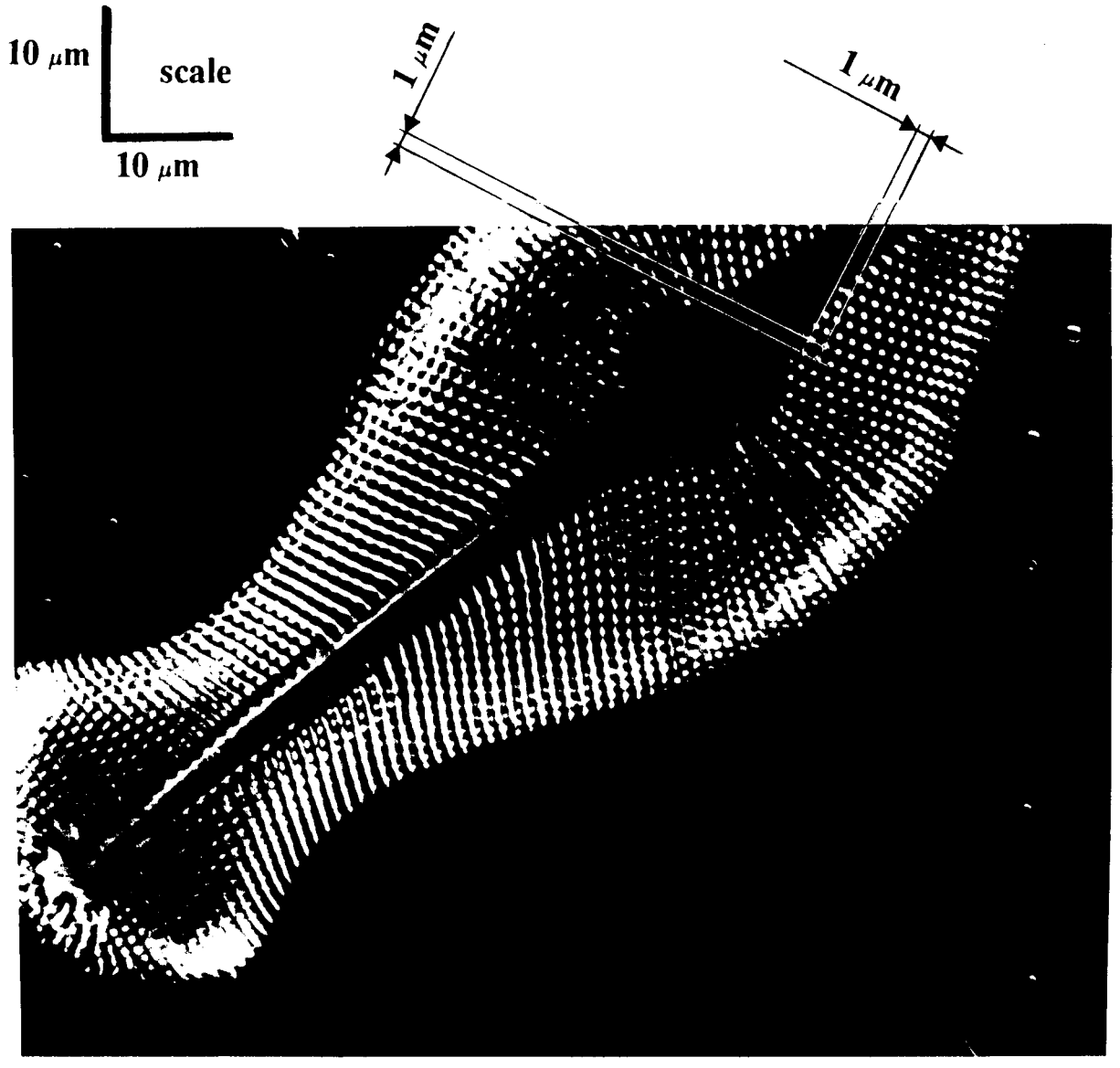

Figure 28: Image of a Didymosphenia Germinata Diatom Acquired by the Solid State Microscope and Displayed on Its 1280 x 1024 Gray Scale Monitor.

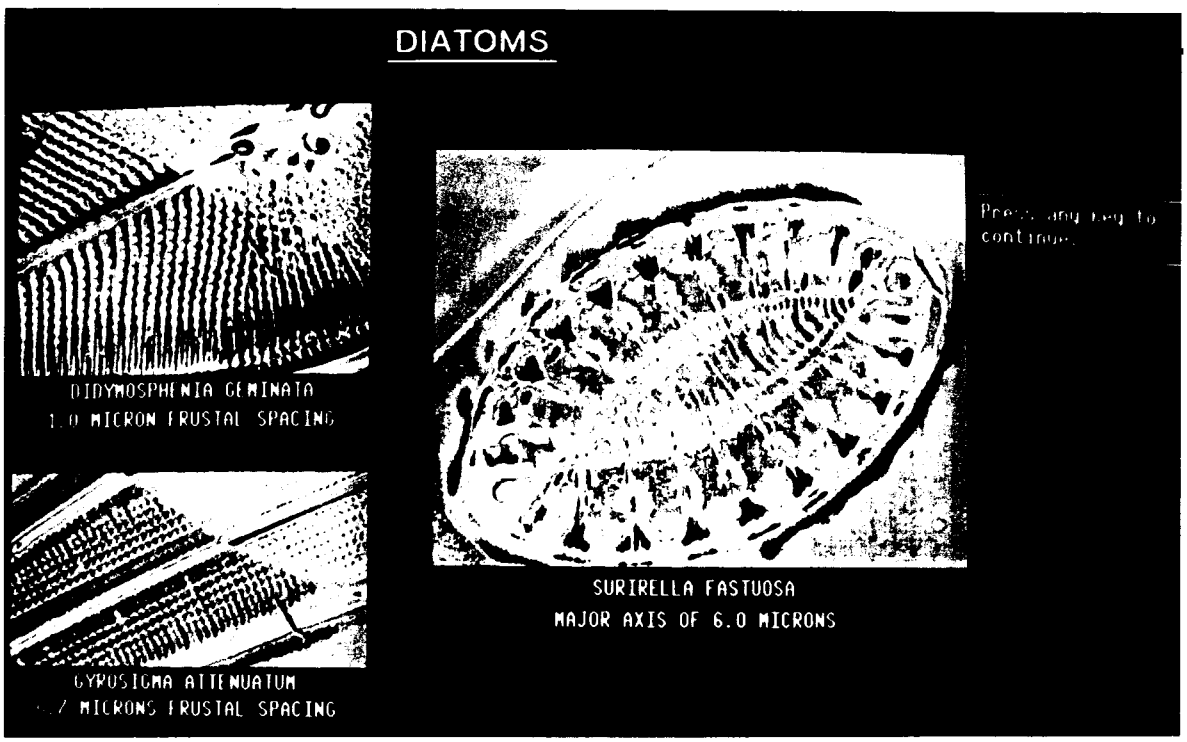

Figure 29: SSM Resolution as Determined by the Frustal Spacings of Diatoms.

size of 0.34 μm was acquired by the SSM prototype. The same image with the same effective pixel size was acquired using a state-of-the-art conventional image cytometry system (Jaggi et al. 1988). The comparison of the two images (figure 30) shows the difference in the information available to the computer. These images are unprocessed and were photographed from the microscope gray scale monitor.

The SSM image in figure 30 represents a 1320 x 1035 x 10 bit array. Also seen is the difference in sharpness and high background uniformity in the SSM images unlike the conventional system. 8 bit gray level histograms of evenly illuminated 128 x 128 pixel areas have been acquired with standard deviations of less than ±1 LSB. Hence the noise levels of the SSM image are within the 9th or 10th bit. A signal-to-noise ratio of 500:1 has been measured using a step function analysis.

5.3 Future Development of SSM

The modular and open architecture of the SSM that has been developed will facilitate the investigations of a number of possible improvements in quantitative microscopy. Of particular interest is the development of the new, specially designed objectives (Young et al. 1982; Shoemaker et al. 1982; Kirk 1987) with an ultra-wide flat field of view. These are essentially diffraction limited and may prove to be the best for digital imaging in microscopy. A number of new developments will further increase the measurement possibilities of a 2nd generation SSM. First, further improvements of the optical field numbers of 28 and 32 are becoming possible (Pluta 1988). Secondly, Eastman Kodak has recently announced a 2033 x 2045 pixel array with 9 μm x 9 μm pixel size (Chang, Tooley and Khosla 1989) and Ford Aerospace is working on a 2048 x 2048 pixel array with 7.5 μm x 7.5 μm pixel size (Bredthauer and

Figure 30: SSM Field of View Compared with a State-of-the-Art Image Cytometry Device at Equal Pixel Size.

Janesick 1989). Third, MegaScan Technology has developed and made commercially available, a 2500 x 2048 pixel gray scale display monitor with appropriate frame memory (Bredthauer and Janesick 1989). Improvements in image acquisition rates and digitization will also make it possible to display real-time 30 frames/s. Therefore, large optical images can be captured so that 4 Mpixel images can be displayed at appropriate sampling rates. With these improvements, a second generation SSM will no doubt benefit from the already advanced microscope technology. To a user, such technology will bring i) higher sampling densities and hence higher resolution at lower objective magnifications, ii) a wider field of view allowing better overview of the microscope slide and ii) a true, real-time solid state microscope.

The flexible optical bench design of the SSM also permits many microscopy modes. The sensing in the optical Fourier plane (Inoue 1986) rather than the intermediate focal plane could provide the frequency spectrum of the image. Inserting a dichroic mirror with appropriate barrier filters between the objective and the CCD will make possible epi-fluorescence measurements. Other modifications of this microscope will facilitate spectral imaging over the full visible spectrum. It has been postulated, for example, that imaging of the mathematical transformation of narrow spectral bands will provide additional information of cellular properties not available by other means. The SSM, as it has been presently developed, is a monochromatic system. However, a 3-CCD chip RGB prism quantitative microscope version for color acquisition can be built and although expensive, should not be a problem. Such a design would mean an additional RGB prism, 3-CCD with associated circuits and 3 framegrabbers with a color, large screen monitor.

It is anticipated that the SSM will be a key component of the analytical cytology device for quantitative pathology. It will also form a key part in the automated prescreening system for detection and classification of exfoliated cervical cells into normal, pre-malignant and malignant classes. For the latter device, most of the key features of the SSM will be required for a clinical system operating in a fully automated mode. The specifications call for spectral imaging composed of two or more spectral lines (Holmquist et al. 1976; Noquichi and Tenjin 1984; MacAulay and Palcic 1989). Coarse features and fine features of recognized cells must be extracted in a single scan in an approximate area of 2 cm^2 in which up to 10,000 cells must be measured within a few minutes (Young 1982; Oud, Zahnier and Harbers-Hendriks 1981; Tucker 1979). Complete cell segmentation into nuclear and cytoplasmic area must be made as well as extraction of nuclear features such as DNA content, nuclear shape and size, and nuclear texture parameters must be performed for discriminant analysis (Holmquist et al. 1978; Pressman 1976; Katzko 1987; MacAulay et al. 1989).

One can envision uses of the SSM in areas other than biology and medicine. Whenever quantitative data of high spatial, photometric, and spectral resolution are required, this apparatus should be considered, particularly as the SSM can be realized in many different configurations and microscopy modes such as dark and bright-field, fluorescence and polarization microscopy.

5.4 Summary of the Author's Contribution

The design of this quantitative microscope for image cytometry is unique and innovative. To design such a device has required a thorough understanding of the theoretical and practical aspects in microscopy and

image cytometry. The knowledge base allowed the author to study the design parameters and apply them to this particular microscope design. The crucial design parameters relate to resolving power and sampling density both of which were analyzed theoretically and experimentally verified. The results have shown that indeed it is now possible to acquire accurate, large images in the primary image plane near the diffraction limit of light.

Under the author's guidance, the engineering group of Cancer Imaging at the B.C. Cancer Research Centre proceeded to develop and build the first prototype device which was completed in April 1989. This allowed the author to validate the design and to show that indeed, by employing the recent advances in the manufacturing of VLSI CCD's and objective lenses, the new design leads to an improvement in quantitative visible light microscopy. It may well be that the author's contribution is what Inoue Shinya and Inoue Ted (April 89, pp. 70) had in mind when they discussed the future of light microscopy: "... the optical principles governing image formation and resolution in the light microscope should be reexamined closely in the light of new applications of electronic imaging".

REFERENCES

Allen, R.D., Travis, J.L., Allen, N.S. and Yilmaz, H.: Video-enhanced contrast polarization (AVEC-POL) Microscopy: A new method applied to the detection of birefringence in the motil reticulopodial network of allogromia laticollaris. Cell Motility. 1:275-289, 1981.

Amos, W.B., White, J.G., Fordham, M.: Use of confocal imaging in the study of biological structures. Appl. Optics 26(16):3239-3243, 1987.

Arndt-Jovin, D.J. and Jovin, T.M.: Analysis and sorting of living cells according to deoxyribonucleic acid content. J. Histochem. Cytochem. 25:585-589, 1977.

Aus, H.M., Harms, H., Haucke, M., Beritova, J., ter Meulen, V., Gunzer, U., Baumann, I. and Abmayr, W.: Leukemia-related morphological features in blast cells. Cytometry 7:365-370, 1986.

Barbe, D.F.: Imaging devices using the charge-coupled concept. IEEE Proc. 63(1):38-67, 1975.

Bengtsson, E., Dahlqvist, B., Eriksson, O., Jarkraus, T., Nordin, B. and Stenkvist, B.: Cervical prescreening using computerized image analysis. Proc. Third Scandinavian Conference on Image Analysis, Copenhagen, 1983.

Betzig, E., Isaacson, M., Barshatsky, A., Lewis, A. and Lin, K.: Near-field scanning optical microscopy. SPIE, Scanning Microscopy Technologies and Applications 897:91-99, 1988.

Binnig, G. and Rohrer, H.: The scanning tunneling microscope. Scientific American, pp. 50-56, Aug. 1985.

Bredthauer, R.: A 2048x2048 Visible Imager. Proc. Electronic Imaging West '89 1:175-176, Pasadena, CA. 1989.

Bradbury, S.: The Microscope Past and Present. Pergamon, Oxford, 1968.

Bradbury, S.: An introduction to the optical microscope. 01: Royal Microscopical Society Microscopy Handbooks, Oxford University Press, ISBN 0-19-856401-5, New York 1984.

Brakenhoff, G.T., Blom, P. and Barends, P.J.: Confocal scanning light microscopy with high aperture immersion lenses. J. Microsc. 117:219, 1979.

Briggs, A.: An introduction to scanning acoustic microscopy. 12: Royal Microscopical Society Microscopy Handbooks, Oxford University Press, ISBN 0-19-856412-0, New York, 1985.

Burkey,B.C. and Chang, W.C.: Accumulation Mode Operation for Reduced Dark Current Generation. Technical Note, Electronics Research Laboratories, Eastman Kodak Company, Rochester, 1989.

Castleman, K.: Digital Image Processing. Prentice-Hall, New York, 1979.

Castleman, K.R.: Spatial and photometric resolution and calibration requirements for cell image analysis instruments. Appl. Optics 26(16):3338-3342, 1987.

Chang, W.C., Toohey, W.E. and Khosla, R.P.: A Prototype: Four Megal Pixel Solid State Camer, Electronic Imaging,1:171-174, Pasadena, CA., 1989.

Chang, W.C., Burkey, B.C., Nichols, D.N., Stevens, E.G. and Khosla, R.P.: A 1.4 million element, full frame CCD image sensor with vertical ovrflow drain for anti-blooming and low color crosstalk. Proc. Electronic Imaging West '88, Anaheim, CA, pp. 158-161, 1988.

Chescoe, D. and Goodhew, P. J. : The Operation of the Transmission Electron Microscope. 02:Royal Microscopical Society Microscopy Handbooks. New York: Oxford University Press, ISBN 0-19-856402-3, New York, 1984.

Gonzalez, R.C. and Wintz, P.: Digital Image Processing, Addison-Wesley, Massachuesetts, 1987.

Green, W.B.: Digital image processing, a systems approach. Van Norstrand Reinhold Comp., ISBN 0-442-28801-8, New York, 1983.

Hansen, E.W.: Modulation transfer function analysis in video microscopy. In: Video Microscopy by S. Inoue, Plenum, pp. 467-475, New York, 1986.

Harms, H.: Letters to the Editor, Cytometry 6:273-275, 1985.

Harms, H., Aus, H.M., Haucke, M., Gunzer, U.: Segmentation of stained blood cells images measured at high scanning density with high magnification and high numerical aperture optics. Cytometry, 7:522-531, 1986.

Harms, H.: Neue verfahren in der Bildverarbeitum, insbesondere in der lichtmikroskopischen Zellbildklassifizierung. Dissertation zur Erlangung des Doktorgrades, Universitaet Bremen, Bremen, West Germany, 1982.

Harms, H. and Aus, H.M.: Estimation of sampling errors in a high-resolution TV microscope image-processing system. Cytometry 5:228-235, 1984.

Harms, H., Boseck, S., Aus, H.M. and Lenz, V.: Untersuchungen der Abtastbedingungen bei Zellbildern mit einem Mikroskop-TV-System. Microscopica Acta 85(1):69-82, 1981.

Haugland, R.P.: Handbook of Fluorescent Probes and Research Chemicals. Molecular Probes, Inc., Eugene, 1989.

Hayakawa, T., Konosheta, K., Miyaki, S., Fuiwake, H., Ohsuka, S.: Ultra low light level camera for photon-counting imaging. Photo Chemistry, Photo Biology 43:95, 1985.

Hiraoka, Y., Sedat, J.W. and Agard, D.A.: Use of a charge-coupled device for quantitative optical microscopy of biological structure. Science, 238:36-41, 1987.

Holmquist, J., Imasato, Y., Bengtsson, E., Olsen, B. and Stenkvist, B.: A microspectrophotometric study of Papanicolaou-stained cervical cells as an aid in computerized image processing. J. Histochem. & Cytochem. 24(12):1218-1224, 1976.

Holmquist, J., Bengtsson, E., Eriksson, O., Nordin, B. and Stenkvist, B.: Computer analysis of cervical cells automatic feature extraction and classification", J. Histochem. & Cytochem. 26(11):1000-1017, 1978.

Inoue, Shinya: Video microscopy of living cells and dynamic molecular assemblies. Applied Optics, 26(16):3219-3225, 1987.

Inoue, S.: Video Microscopy. Plenum, New York, 1986.

Inoue, S. and Inoue, T.: Video enhancement and image processing in light microscopy. American Laboratory 21(4):52-70, 1989.

IEEE: Standard Dictionary of Electrical and Electronics Terms. ed. Frank Jay, John Wiley & Sons, New York, 1984.

Jaggi, B., Poon, S.S.S., MacAulay, C. and Palcic, B.: Imaging system for morphometric assessment of absorption or fluorescence in stained cells. Cytometry 9:566-572, 1988.

Jaggi, B. and Palcic, B.: Implementation and evaluation of the DMIPS Cell Analyzer. IEEE Proc. Eng. Biol. 3:906-911, 1986.

Jaggi, B. and Deen, M.J.: Low temperature operations of silicon charge-coupled devices for imaging applications. Proc. of Symp. on Low Temp. Electronics and High Temp. Superconductors, S.I. Raider, R. Kirschman, H. Hayakawa, and H. Ohta, eds. Electrochemical Soc. 88-9:579-589, 1988.

Jaggi, B. and Palcic, B.: Development of a solid state microscope. SPIE Proc., Medical Imaging III: Image Formation, 1090:48-58, 1989a.

Jaggi, B., Deen, J. and Palcic, B.: Quantitative light microscope using a solid state detector in the primary image plane. U.S. Patent Number 4.845.552, July 4, 1989a.

Jaggi, B., Deen, J., and Palcic, B.: Design of a Solid State Microscope. Optical Engineering 28(6):675-687, June, 1989b.

Jaggi, B. and Palcic, B.: Charge-coupled device requirements in the design of a quantitative microscope for image cytometry. Proc. Electronic Imaging West '89, Pasadena, CA., pp. 177-182, 1989b.

Janesick, J.R., Elliott, T., Collins, S., Marsh, H., Blouke, M.M. and Freeman, J.: "The Future of Scientific CCDs", in State-of-the-Art Imaging Arrays and Their Applications, K.N. Prettyjohns, ed., Proc. SPIE 501:2-31, 1984.

Janesick, James R.: Guest Editorial: Charge-coupled-device manufacture and application. Optical Engineering, 26(8), 26(9), and 26(10), 1987.

Johnson, N.: The art of seeing the very small. New Scientist, pp. 468-472, May, 1983.

Juang, C-B., Finzi, L. and Bustamante, J.: Design and Application of a computer-controlled Confocal Scanning Differential Polarization Microscope. Rev. Sci. Instrum. 59(11): 2399-2408, 1988.

Katzko, M.W., Pahlplatz, M.M.M., Oud, P.S. and Vooijs, G.P.: Carcinoma in situ specimen classification based on intermediate cell measurements. Cytometry 8:9-13, 1987.

Kino, G.S., Corle, T.R. and Xiao, G.Q.: The scanning optical microscope: An overview. SPIE Proc. Scanning Microscopy Technologies and Applications 897:32-41, 1988.

Kirk, Ch.: Aberration effects in an optical measuring microscope. Applied Optics 26(16):3417-3424, 1987.

Kirz, J. and Rarback, H.: Soft x-ray microscopes. Rev. Sci. Instrum. 56(1):1-13, 1985.

Lockwood, D.H., Johnston, D.A., Riccardi, V.M. and Zimmerman, S.O.: The use of subchromosome-length unique band sequences in the analysis of prophase chromosomes. Am. J. Hum. Genet. 43:934-947, 1988.

MacAulay, C. and Palcic, B.: A comparison of some quick and simple threshold selection methods for stained cells. Analyt. Quant. Cyt. Hist. 10:134-138, 1988.

MacAulay, C., Tezcan, H., and Palcic, B.: Adaptive colour basis transformation: A segmentation aid. Analyt. Quant. Cytol. Histol. 11:53-59, 1989.

Marti, O., Drake, B., Gould, S., Hansma, P.K.: Probing surfaces with the atomic force microscope. SPIE Proc. Scanning Microscopy Technologies and Applications 897:22-25, 1988.

Martin, G.J., Womack, K.H. and Fischer, J.H.: A high resolution CCD camera for scientific and industrial imaging applications. High Res. CCD Camera-SPIE, pp. 1-19, 1988.

Mayall, B.H. and Mendelsohn, M.L.: "Errors in Absorption Cytophotometry: Some Theoretical and Practical Considerations", In: Introduction to Quantitative Cytochemistry - II, Wied, G.L. and Bahn, E.F. ed., pp. 171-197, Academic Press, New York, 1970.

Mendelsohn, M.L.: Absorption cytophotometry: Comparative methodology for heterogeneous objects, and the two-wavelength method. Int. to Quant. Cytochem., G.L. Wied, ed., Academic, New York, 1966.

Nikon Canada Inc.: New CF Plan Achromat and Apochromat objectives. Application Note #30, 1985.

Noguchi, Y. and Tenjin, Y.: A scene-segmentation method for multispectral cell images. J. Analyt. Quantit. Cytol. 6(3):212-219, 1984.

Oud, P.S., Zahniser, D.J., Harbers-Hendriks, R.: The development of a cervical smear preparation procedure for the BioPEPR Image Analysis System. J. Analyt. Quantit. Cytol. 3:31-38, 1981.

Ott, H.: Noise Reduction Techniques in Electronic Systems. 2nd Edition, John Wiley & Sons, New York, 1988.

Palcic, B., Jaggi, B.W. and Nordin, J.A.: Dynamic Microscope Image Processing Scanner (DMIPS). United States Patent, #4,700,298, October 13, 1987.

Palcic, B. and Jaggi, B.: Image cytometry system for morphometric measurements of live cells. In: Bioinstrumentation: Developments and Applications, D.L. Wise, ed., Butterworth Publishers, Stoneham, MA. (In press 1989).

Petran, M., Hadravsky, M. and Boyde, A.: The Tandem Scanning Reflected Light Microscope. Scanning 7:97-108, 1985.

Park, S.-I., Nogami, J., Quate, C.F.: Scanning tunneling microscopy: instrument design and application in air and vacuum. SPIE, Scanning Microscopy Technologies and Applications 897:8-15, 1988.

Ploem, J.S.: Laser scanning fluorescence microscopy. Applied Optics, 26(16):3226-3231, 1987.

Ploem, J.S. and Tanke, H.J.: Introduction to Fluorescence Microscopy, 10: Royal Microscopical Society Microscopy Handbooks, Oxford University Press, ISBN 0-19-856408-2, New York, 1987.

Pohl, D.W.: Scanning near-field optical microscopy (SNOM): basic principals and some recent developments. SPIE Proc. Scanning Microscopy Technologies and Applications 897:84-90, 1988.

Pontifex, B.D., Jaggi, B., Deen, M.J., Palcic, B.: Performance of a photodiode array cooled to low temperatures in image cytometry. Proc. IEEE Eng. Med. Biol. Soc. 10:337-379, 1988.

Pool, R.: Near-field microscopes beat the wavelength limit. Research News, July 1988.

Pluta, M.: Advanced Light Microscopy, Princples and Basic Properties. Elsevier, (ISBN 0-444-98939-0), New York, 1988.

Pressman, N.J.: Markovian analysis of cervical cell images. J. Histochem. & Cytochem. 24(1):138-144, 1976.

Preston, K., Duff, M.J.B., Levialdi, S., Norgren, P.E. and Toriwaki, J.I.: Basis of cellular logic with some applications in medical image processing. Proc. IEEE 67(5):826-855, 1979.

Preston, K.: Automation of the analysis of cell images. Analytical and Quantitative Cytology 2(1):1-14, 1980.

Prewitt, J.M.S.: The selection of sampling rate for digital scanning. IEEE Trans. Biomed. Eng., BME-12, 1965.

Register, T.E. and West, W.R.: Diatoms, Carolina Tips, Carolina Biological Supply Company, N. Carolina, 47:1-2, January 1984.

Reynolds, G.O., DeVelis, J.B., Parrent, G.B.Jr. and Thompson, B.J.: The New Physical Optics Notebook: Tutorials in Fourier Optics, SPIE and American Inst. of Physics, ISBN 0-8194-0130-7, New York, 1989.

Royal Microscopal Society: Dictionary of Light Microscopy. Bradbury, S., Evennett, P.J., Haselmann, H. and Piller, eds., Microscopy Handbooks 15, Oxford University Press, ISBN 0-19-856413-9, New York, 1989.

Schnapp, Bruce J.: Viewing Single Microtubules by Video Light Microscopy. Methods in Enzymology, Academic Press, Inc., 53(53):561-573, 1986.

Seib, D.H.: Carrier diffusion degradation of modulation transfer function in charge coupled imagers. IEEE Trans. on Electron Devices, 21(3):210-217, 1974.

Shoemaker, R.L., Bartels, P.H., Hillman, D.W., Jonas, J., Kessler, D., Shack, R.V., Vukobratovich, D.: An ultrafast laser scanner microscope for digital image analysis. IEEE Trans. of Biomed. Eng. BME-29(2):82-91, 1982.

Spadinger, I., Poon, S.S.S. and Palcic, B.: Automated detection and recognition of live cells in tissue culture using image cytometry. Cytometry. (In press, 1989).

Spencer, M.: Fundamentals of Light Microscopy. Cambridge University Press, London, 1982.

Stevens, E.G., Lee, T.-H., Nichols, D.N., Anagnostopoulos, C.A., Burkey, B.N., Chang, W.-C., Kelly, T.M., Khosla, R.P., Losee, D.L. and Tredwell, T.J.: A 1.4-million-element CCD image sensor. ISSCC Technol. Digest 114-155, 1987.

Streetman, B.G.: Solid State Electronic Devices. N. Holonyak, Jr. ed., Prentice-Hall Series in Solid State Physical Electronics, Prentice Hall, ISBN 0-13-822171-5, New York, 1980.

Taylor, D.L., Waggoner, A.S., Lanni, F., Murphy, R.F. and Birge, R.R. (eds), Applications of Fluorescence in the Biomedical Sciences, Alan Liss Inc., New York, 1986.

Teague, E.C. ed.: Scanning Microscopy Technologies and Applications. SPIE Proc. 897, Bellingham, WA., 1988.

Thurston, G., Jaggi, B. and Palcic, B.: Measurement of cell motility and morphology with an automated microscope system. Cytometry 9(5):411-417, 1988.

Trail, J. A. and Byer, R.L.: Scanning soft X-Ray microscopy. SPIE Proc. Scanning Microscopy Technologies and Applications, 897:185-190, 1988.

Tucker, James H., Husain, O.A.N., Watts, Keith, Farrow, Stephen, Bayley, Royston, and Stark, Margaret H.: Automated densitometry of cell populations in a continuous-motion imaging cell scanner. Applied Optics, 26(16):3315-3324, 1987.

Tucker, J.H.: An image analysis system for cervical cytology automation using nuclear DNA content. J. Histochem. & Cytochem. 27(1):613-620, 1979.

Unser, M: Sum and Difference Histograms for Texture Classification. IEEE Trans Pattern Analysis Machine Intelligence PAMI-8(1):118-125, 1988.

Van der Voort, H.T.M., Brakenhoof, G.J., Valkenburg, J.A.C. and Nanninga, N.: Design and use of a computer controlled confocal microscope for biological applications. Scanning 6:66, 1985.

Vidal, D.C.B., Schulter, G. and Moore, G.W.: Cell nucleus pattern recognition: Influence of staining. Acta Cytol. 17:510-515, 1988.

Vinter, D., Nicholls, K.Y., Schwartz, S.M.: Development of a biomedical image processing computer system. IEEE Proc. Eng. Med. Biol. 2:996-1000, 1985.

Vinyard, W.C.: Diatoms of North America. Mad. River Press Inc., Eureka, CA, 1979.

Von dem Borne, A.E.G.Kr., Verheugt, F.W.A., Ossterhof, F., von Riesz, E., Brutel de la Rivere, A. and Engelfriet, C.P.: A simple immunofluorescence test for the detection of platelet antibodies. Br. J. Haematol. 39:195, 1978.

Wakimoto, Z.: Chromatic aberration-free optics for microscopy. Proc. Roy. Micr. Soc. 14(5):327-328, 1979.

Wick, R.A.: Quantum-limited imaging using microchannel plate technology. Applied Optics 26(16):3210-3218, 1987.

Wilke, V.: Optical scanning microscopy - The laser scan microscope. Scanning 7:88, 1985.

Wilson, A.: Technology and trends: what's new - an electronic imaging '87 review., Electronic Design 17(12):17-18, 1987.

Wilson, T. and Sheppard, C.: Theory and Practice of Scanning Optical Microscopy. Academic Press, London, 1984.

Young, I.T., Balasubramarian, D.L. Dunbar, R.L. Peverini, R.P. Bishop: "SSAM: Solid State Automated Microscope", IEEE Trans. on Biomed. Eng. BME-29(2):70-82, 1982.

Young, I.T.: The use of digital image processing techniques for calibration of quantitative microscopes. In: Applications of Digital Image Processing, A. Oosterlinck and A.G. Tescher, eds., SPIE 397:326-335, 1983.